The Uniform California Earthquake Rupture Forecast, Version 3 (UCERF3)—The Time-Independent Model

M ≥ 6.7 Earthquake
Participation Rates (per year)

10^{-6} 10^{-4} 10^{-2}

122°W   120°W   118°W

U.S. Department of the Interior
U.S. Geological Survey

COVER

3D perspective view of California, showing the average long-term rate at which different areas of the state participate in M≥6.7 earthquake ruptures. Black rectangles represent explicitly modeled faults (for UCERF3 Fault Model 3.1). Ruptures associated with the Cascadia megathrust are not shown.

Uniform California Earthquake Rupture Forecast, Version 3 (UCERF3)—The Time-Independent Model

By Edward H. Field, Glenn P. Biasi, Peter Bird, Timothy E. Dawson, Karen R. Felzer, David D. Jackson, Kaj M. Johnson, Thomas H. Jordan, Christopher Madden, Andrew J. Michael, Kevin R. Milner, Morgan T. Page, Tom Parsons, Peter M. Powers, Bruce E. Shaw, Wayne R. Thatcher, Ray J. Weldon, II, and Yuehua Zeng (Working Group on California Earthquake Probabilities)

U.S. Department of the Interior
U.S. Geological Survey

U.S. Department of the Interior
SALLY JEWELL, Secretary

U.S. Geological Survey
Suzette M. Kimball, Acting Director

U.S. Geological Survey, Reston, Virginia 2013

STATE OF CALIFORNIA
EDMUND G. BROWN JR.
GOVERNOR

THE NATURAL RESOURCES AGENCY
JOHN LAIRD
SECRETARY FOR NATURAL RESOURCES

DEPARTMENT OF CONSERVATION
MARK NECHODOM
DIRECTOR

CALIFORNIA GEOLOGICAL SURVEY
JOHN G. PARRISH, Ph.D.
STATE GEOLOGIST

This page intentionally left blank.

Table of Contents

Figures

Tables

Appendixes

List of Abbreviations Used in this Report

Abbreviation	Definition
2in50 PGA	2-percent-in-50-year peak ground acceleration
ABM	Average block model
BSSC	Building Seismic Safety Council
CEA	California Earthquake Authority
CEPEC	California Earthquake Prediction Evaluation Council
CGS	California Geological Survey
COV	Coefficient of variation
EllsworthB	Ellsworth B magnitude-area relationship (WGCEP, 2003)
ERF	Earthquake rupture forecast
ETAS	Epidemic type aftershock sequence
ExCom	Executive Committee
FM	Fault model
GPS	Global Positioning System
GR	Gutenberg-Richter
HanksBakun08	Hanks and Bakun (2008) magnitude-area
InSAR	Interferometric synthetic aperture radar
LA	Los Angeles
MFD	Magnitude-frequency distribution
MOC	Management Oversight Committee
MRI	Mean recurrence interval
MRT	Multidisciplinary Research Team
NEHRP	National Earthquake Hazards Reduction Program
NEPEC	National Earthquake Prediction Evaluation Council
NSHMP	National Seismic Hazard Mapping Program
OEF	Operational earthquake forecasting
Off-fault spatial seis PDF (or SpatialPDF)	Spatial distribution of off-fault gridded seismicity set by choosing one of the spatial probability density maps
OpenSHA	Open-source, Java-based platform for conducting Seismic Hazard Analysis
PGA	Peak ground acceleration
PSHA	Probabilistic seismic hazard analysis
RELM	Regional earthquake likelihood models
SA	Spectral acceleration
SAF	San Andreas Fault
SCEC	Southern California Earthquake Center
SF	San Francisco
Shaw09mod	Modified version of Shaw (2009) magnitude-area relationship, as justified in appendix E (this report)
SpatialPDF (or Off-Fault Spatial Seis PDF)	Spatial distribution of off-fault gridded seismicity set by choosing one of the spatial probability density maps
SRP	Scientific Review Panel
USGS	United States Geological Survey
UCERF	Uniform California Earthquake Rupture Forecast
WGCEP	Working Group on California Earthquake Probabilities

Contributors to UCERF3

The following groups were involved in the development of UCERF3:

Executive Committee (ExCom)

The ExCom is responsible for convening experts, reviewing options, making recommendations, and orchestrating implementation of the model and supporting databases. The role of the ExCom is not to advocate specific model components, but to ensure that a minimum set of models is considered that spans the range of viability.

Edward (Ned) Field (Chair)	U.S. Geological Survey
Timothy Dawson	California Geological Survey
Andrew Michael	U.S. Geological Survey
Tom Parsons	U.S. Geological Survey
Ray Weldon	University of Oregon

Key Contributors

These are individuals who contributed in a major way, either by providing expert opinion or specific model components.

Ramón Arrowsmith	Arizona State University
Glenn Biasi	University of Nevada, Reno
Peter Bird	University of California, Los Angeles
Karen Felzer	U.S. Geological Survey
Jeanne Hardebeck	U.S. Geological Survey
Dave Jackson	University of California, Los Angeles
Kaj Johnson	Indiana University
Christopher Madden	Oregon State University
Kevin Milner	Southern California Earthquake Center
Morgan Page	U.S. Geological Survey
Peter Powers	U.S. Geological Survey
Bruce Shaw	Columbia University (Lamont Doherty)
Wayne Thatcher	U.S. Geological Survey
Yuehua Zeng	U.S. Geological Survey

Management Oversight Committee (MOC)

The MOC is in charge of resource allocation and approving project plans, budgets, and schedules. The MOC is also responsible for seeing that the models are properly reviewed and delivered.

Thomas Jordan (Chair)	Southern California Earthquake Center Director
Tom Brocher	U.S. Geological Survey
Jill McCarthy	U.S. Geological Survey
Chris Wills	California Geological Survey

Scientific Review Panel (SRP)

The SRP is an independent but participatory body of experts who decide whether the WGCEP has considered an adequate range of models, given the forecast duration of interest, and that logic tree branch weights have been set appropriately.

Bill Ellsworth (Chair)	U.S. Geological Survey
Duncan Agnew	Scripps Institution of Oceanography
Ramón Arrowsmith	Arizona State University
Yehuda Ben-Zion	University of Southern California
Greg Beroza	Stanford University
Mike Blanpied	U.S. Geological Survey
Arthur Frankel	U.S. Geological Survey
Sue Hough	U.S. Geological Survey
Warner Marzocchi	Instituto Nazionale di Geofisica e Vulcanologia, Italy
Hamid Haddadi	California Geological Survey
Rick Schoenberg	University of California, Los Angeles
David Schwartz	U.S. Geological Survey

UCERF3 Deformation Model Evaluation Committee

These are individuals are responsible for evaluating the suite of deformation models proposed in UCERF3 and assigning relative weights to each in the final model.

Tom Parsons (Chair)	U.S. Geological Survey
Jack Boatwright	U.S. Geological Survey
Timothy Dawson	California Geological Survey
Arthur Frankel	U.S. Geological Survey
Jim Dieterich	University of California, Riverside
Dave Jackson	University of California, Los Angeles
Wayne Thatcher	U.S. Geological Survey
Ray Weldon	University of Oregon
Chris Wills	California Geological Survey

California Earthquake Authority Multidisciplinary Research Team

Shawna Ackerman	California Earthquake Authority
Bob Anderson	California Seismic Safety Commission
Bruce Patton	California Earthquake Authority
Badie Rowshandel	California Geological Survey

External Evaluation of UCERF3

The National Earthquake Prediction Evaluation Council (NEPEC) and the California Earthquake Prediction Evaluation Council (CEPEC) were asked, upon the conclusion of the project, to evaluate the quality and integrity of the process by which the UCERF3 time-independent earthquake model and forecast had been constructed. Both councils affirmed that the work had been carried out in an appropriate manner taking, into account input from a broad cross-section of the earthquake research community, and that the SRP had managed a thorough review and quality control process throughout the project. Letter reports from the NEPEC and CEPEC are included on the following pages of this report.

As members of the USGS National Seismic Hazard Map Steering Committee, the following also provided comments on the applicability of UCERF3 in the 2014 seismic hazard maps: John Anderson (chair), Norm Abrahamson, Ken Campbell, Michael Hamburger, Bill Lettis, Nilesh Shome, Ray Weldon, Chris Wills, and Martin Chapman.

NEPEC members current and active during the UCERF3 project

Terry Tullis* (Chair)	Brown University
William Leith (Co-chair)	U.S. Geological Survey
Ramón Arrowsmith	Arizona State University
Nick Beeler*	U.S. Geological Survey
David Jackson	University of California, Los Angeles
Bruce Shaw	Columbia University
William Ellsworth	U.S. Geological Survey
Susan Hough	U.S. Geological Survey
Evelyn Roeloffs*	U.S. Geological Survey
John Vidale*	University of Washington
Andrew Michael	U.S. Geological Survey
Allan Rubin*	Princeton University
Roland Bürgmann*	University of California, Berkeley

*Member of UCERF3 final review subcommittee

CEPEC members who participated in the external evaluation of UCERF3

John G. Parrish (Chair)	California Geological Survey
Lucy M. Jones	U.S. Geological Survey
Tom Heaton	California Institute of Technology
Rui Chen	California Geological Survey

Earth and Space Sciences | UNIVERSITY OF WASHINGTON

PROF. JOHN VIDALE, DIRECTOR
Pacific Northwest Seismic Network
E-MAIL: VIDALE@UW.EDU
MONDAY, AUGUST 19, 2013

DR. SUZETTE KIMBALL, ACTING DIRECTOR
U.S. Geological Survey
Reston, Virginia 20192

Dear Dr. Kimball,

This letter conveys the approval by the National Earthquake Prediction Evaluation Council (NEPEC) of the process used by the Scientific Review Panel (SRP) to oversee the time-independent Uniform California Earthquake Rupture Forecast, Version 3 (UCERF3). As you are aware, UCERF3 is a joint undertaking of the U.S. Geological Survey, the California Geological Survey, and the Southern California Earthquake Center, with support from the California Earthquake Authority.

NEPEC was asked by the USGS Earthquake Hazards Program on August 8 to evaluate whether the process by which the UCERF3 forecast was made is sound, such that the model should be of sufficient quality for use in hazard assessments for public policy. This conforms to NEPEC's role defined at the start of the UCERF3 project in 2009. In particular, we were asked to examine the make-up of the SRP, the nature of the SRP reviews, and how the working group responded to those reviews. We were not asked to undertake an independent review of UCERF3 itself, as this was carried out by the SRP over a period of several years.

The six members of NEPEC signing this letter did not have a central role in development of UCERF3; the rest of the NEPEC members did participate significantly in the UCERF3 effort, and were recused from contributing to this letter aside from the chance to comment on it. In response to those comments, we changed some sentences for clarity, but this has not altered the opinion conveyed in this letter.

For this assessment, NEPEC has received annual updates on progress, and we were provided with a letter from the SRP Chair outlining that group's activities, with documentation of SRP reviews and working-group responses to those reviews, and with access to the current draft of the UCERF3 report that is in preparation for publication. Some of us examined portions of that report in the process of our review. The SRP reports document the issues with the UCERF3 components and approaches that arose between June 2010 and April 2013. The May 2013 document from the working group summarizes how UCERF3 was revised in response to the final SRP review with respect to the prior version (3.2).

The new model UCERF3 improves on its predecessor UCERF2 in numerous ways. It has a more complete database of California faults, includes additional geological observations of past earthquake dates and fault configurations, and has incorporated improved and updated "deformation models" to improve estimates of the movement along those faults. The classes of earthquake frequency-magnitude relations considered have been broadened. A numerical inversion algorithm has been used to estimate recurrence rates of a comprehensive suite of possible damaging earthquakes, which is the information needed to estimate the probability of shaking exceeding specific levels. The inversion scheme allows most available geodetic, geological, and seismicity data to be used to develop a self-consistent forecast of future California seismic events based on best-available science. UCERF3 is developed using a more

flexible computational platform than UCERF2 so that additional data can be more easily incorporated. For the long term, the more flexible foundation of UCERF3 provides a better roadmap than did UCERF2 to further refine future hazard assessments as field measurements improve and scientific ideas evolve.

UCERF3 was implemented by leading seismic hazard experts, with broad and extensive participation across the U.S. earthquake mitigation community. UCERF3 was vetted openly and with input from other specialists and users, and their feedback was heeded to test and improve initial models. In a crucial detail, a comprehensive and well-documented logic tree was developed to take account of alternative scientific views on many aspects of the hazard. In response to a question in our charge, we affirm that the SRP is composed of exceedingly well-qualified and appropriate experts.

We are grateful to those involved in the creation of UCERF3 for their diligent and skilled efforts, which will lead to improved guidance for zoning, insurance rates, and public information. In particular we approve of the work and processes used by the SRP to guide the development of UCERF.

John E. Vidale, member, NEPEC, signing also for Nicholas M. Beeler, Roland Bürgmann, Evelyn Roeloffs, Allan M. Rubin, Chair Terry E. Tullis.

E D M U N D G. B R O W N , J R .
GOVERNOR

CALIFORNIA EARTHQUAKE PREDICTION EVALUATION COUNCIL

August 16, 2013

Suzette M. Kimball, Ph. D.   Mark Ghilarducci, Director
Acting Director   Governor's Office of Emergency Services
United States Geological Survey   Cal-OES Headquarters
12201 Sunrise Valley Dr.   3650 Schriever Avenue
Mail Stop 101   Mather, CA 95655
Reston, VA 20192

Re: Evaluation of the Scientific Review Process in Developing UCERF-3

Dear Acting Director Kimball & Director Ghilarducci:

The Working Group on California Earthquake Probabilities (WGCEP) commenced its research and development of the Uniform California Earthquake Rupture Forecast, Version 3 (UCERF-3), early in 2010. Just prior to that, the California Earthquake Prediction Evaluation Council (CEPEC) met jointly with the National Earthquake Prediction Evaluation Council (NEPEC) and concluded that the role of these Councils would be to evaluate the process by which the UCERF-3 Scientific Review Panel (SRP) conducted its technical oversight of the work being done by the WGCEP. In addition, a review of the UCERF-3 development process by CEPEC and NEPEC is required by the California Earthquake Authority as a condition of its providing major funding for the project.

On August 8, 2013 the CEPEC received a formal request from Dr. Michael L. Blanpied, Associate Coordinator for the United States Geological Survey (USGS) Earthquake Hazards Program, to conduct an evaluation of the review process by which the SRP guided and critiqued the work of the WGCEP, and to determine the quality, integrity, and adequacy of that review process. CEPEC undertook this charge following a recommendation from its Chair and concurrence from the Director of the California Office of Emergency Services (Cal-OES). Four of the eight CEPEC members participated in the review; three others excused themselves because of their active participation in the WGCEP and SRP.

Following the CEPEC assessment of the SRP reviews conducted of the WGCEP, CEPEC provides the following comments:

- As reflected in the six SRP review reports, the SRP offered constructive comments and practical recommendations at several stages over the course of the UCERF-3 project. It provided invaluable guidance that spanned a wide range of project matters, including project organization, management, and oversight. The SRP encouraged the WGCEP to engage the potential user groups and stakeholders and to coordinate with the National Seismic Hazard Mapping Program at an early stage in the project. This facilitated the adoption of the UCERF-3 in the 2014 revision of

the National Seismic Hazard Maps and the potential acceptance of the UCERF-3 by the general seismological and engineering community.

- The reviews conducted by the SRP were timely, thorough, and instructive. The SRP reviews have great technical depth and contained considerable details.

The CEPEC concludes that the reviewing process followed by the SRP in its quality control oversight of the work of the WGCEP in developing the UCERF-3 model resulted in an appropriate model to represent the present understanding of the earthquake processes.

Sincerely,

John G. Parrish, Ph. D., PG
Chair – CEPEC

cc: Mike Blanpied, USGS
cc: CEPEC

Uniform California Earthquake Rupture Forecast, Version 3 (UCERF3)—The Time-Independent Model

By Edward H. Field, Glenn P. Biasi, Peter Bird, Timothy E. Dawson, Karen R. Felzer, David D. Jackson, Kaj M. Johnson, Thomas H. Jordan, Christopher Madden, Andrew J. Michael, Kevin R. Milner, Morgan T. Page, Tom Parsons, Peter M. Powers, Bruce E. Shaw, Wayne R. Thatcher, Ray J. Weldon, II, and Yuehua Zeng (Working Group on California Earthquake Probabilities)[1]

Abstract

In this report we present the time-independent component of the Uniform California Earthquake Rupture Forecast, Version 3 (UCERF3), which provides authoritative estimates of the magnitude, location, and time-averaged frequency of potentially damaging earthquakes in California. The primary achievements have been to relax fault segmentation assumptions and to include multifault ruptures, both limitations of the previous model (UCERF2). The rates of all earthquakes are solved for simultaneously, and from a broader range of data, using a system-level "grand inversion" that is both conceptually simple and extensible. The inverse problem is large and underdetermined, so a range of models is sampled using an efficient simulated annealing algorithm. The approach is more derivative than prescriptive (for example, magnitude-frequency distributions are no longer assumed), so new analysis tools were developed for exploring solutions. Epistemic uncertainties were also accounted for using 1,440 alternative logic tree branches, necessitating access to supercomputers. The most influential uncertainties include alternative deformation models (fault slip rates), a new smoothed seismicity algorithm, alternative values for the total rate of M≥5 events, and different scaling relationships, virtually all of which are new. As a notable first, three deformation models are based on kinematically consistent inversions of geodetic and geologic data, also providing slip-rate constraints on faults previously excluded because of lack of geologic data. The grand inversion constitutes a system-level framework for testing hypotheses and balancing the influence of different experts. For example, we demonstrate serious challenges with the Gutenberg-Richter hypothesis for individual faults. UCERF3 is still an approximation of the system, however, and the range of models is limited (for example, constrained to stay close to UCERF2). Nevertheless, UCERF3 removes the apparent UCERF2 overprediction of M6.5–7 earthquake rates and also includes types of multifault ruptures seen in nature. Although UCERF3 fits the data better than UCERF2 overall, there may be areas that warrant further site-specific investigation. Supporting products may be of general interest, and we list key assumptions and avenues for future model improvements.

---

[1]For affiliations of authors, see preceding section, "Contributors to UCERF3."

Introduction

Background

  The 38 million residents of California live among some of the most active earthquake faults in the United States, so efforts to promote public safety and community resilience require credible assessments of the earthquake hazard. The best tool for quantifying the earthquake threat is probabilistic seismic hazard analysis (PSHA; see list of abbreviations in the front matter of the report), which quantifies the likelihood that ground shaking will exceed various levels during a given time period (Cornell, 1968). End-users of PSHA include those charged with land-use planning, building-code revisions, disaster preparation and recovery, emergency response, and the design of lifelines and critical facilities, as well as organizations that promote public education for risk mitigation (National Research Council, 2011).

  One of the two main modeling components of PSHA is an earthquake rupture forecast (ERF), which quantifies the probability of all damaging fault-rupture events in a region, for a given timespan, above some magnitude threshold, and at some level of discretization deemed adequate for hazard assessment. ERFs are also useful for choosing earthquake-planning scenarios (for example, Wald and others, 2005) and for quantifying what events might be unfolding in an earthquake early warning system (for example, Cua and others, 2009).

  Two different entities have traditionally developed official ERFs for California. One is the National Seismic Hazard Mapping Program (NSHMP) of the United States Geological Survey (USGS), which has developed statewide, time-independent (long-term) models for use in the national seismic hazard maps (for example, Algermissen and others, 1982; Frankel and others, 1996, 2002). The other official ERFs were from the Working Groups on California Earthquake Probabilities (WGCEP; 1988, 1990, 1995, and 2003), which developed time-dependent models based on Reid's (1911) elastic-rebound theory (where probabilities drop on a fault after experiencing a rupture and build back up with time as tectonic stresses reaccumulate). These WGCEP models, however, only covered a subset of California; see Field (2007) for a review.

  The 1994 Northridge earthquake led to an insurance-availability crisis, which prompted the California legislature to create the California Earthquake Authority (CEA), a publicly managed provider of residential earthquake insurance that is funded primarily by participating private insurance companies (www.earthquakeauthority.com). CEA currently holds about two-thirds of all such policies in California, making it one of the largest residential earthquake insurance providers in the world. The enabling legislation for CEA states that insurance rates shall be based on the "best available science" and that any statewide variability in insurance rates must reflect actual risk differentials. These requirements created the demand for a time-dependent forecast based on uniform methodologies across the state, which was lacking in the official models developed previously. Consequently, a new WGCEP effort was commissioned in September 2004 and charged with developing a Uniform California Earthquake Rupture Forecast (UCERF). The project was collaborative between the USGS, the California Geological Survey (CGS), and the Southern California Earthquake Center (SCEC), with significant funding from CEA. This working group came to be known as WGCEP 2007.

  The first model developed by WGCEP 2007 was a prototype, UCERF1 (Petersen and others, 2007), assembled from available components without conforming to a consistent time-dependent methodology statewide. The final consensus model, UCERF2, was released to the public in April 2008 as a USGS open-file report including 16 appendixes (Working Group on

California Earthquake Probabilities, 2008), and other supplementary materials, (www.SCEC.org/ucerf2), and was then published in Bulletin of the Seismological Society of America (Field and others, 2009). UCERF2 was the first statewide, time-dependent model that used consistent methodologies, data-handling standards, and uncertainty treatment in all regions. The entire model was implemented in OpenSHA (Field and others, 2003), an open-source, object-oriented computational framework for seismic hazard, which enabled unprecedented flexibility with respect to PSHA calculations for any or all of the alternative time-dependent components. The development was also fully coordinated with the NSHMP, and the time-independent version of UCERF2 was adopted for use in the 2008 USGS national seismic hazard maps (Petersen and others, 2008a).

Although WGCEP 2007 was successful in terms of stated goals, a number of issues were identified in the "Model Limitations and Opportunities for Future Improvements" section of the report. The most salient of these were (1) to relax segmentation assumptions and include multifault ruptures and (2) to incorporate spatiotemporal clustering for the time-dependent forecasting of aftershocks and other triggered earthquake sequences. Both of these issues were subsequently—and dramatically—exemplified following the UCERF2 publication, by events including the 2011 M9 Tohoku earthquake with respect to segmentation (see, for example, Kagan and Jackson, 2013), the 2011 M6.3 Christchurch earthquake in terms of spatiotemporal clustering (for example, Kaiser and others, 2012), and both the 2010 M7.2 El Mayor-Cucapah and 2012 M8.6 Sumatra earthquakes in regard to multifault ruptures (for example, Hauksson and others, 2011; Meng and others, 2012).

A persistent problem in WGCEP and NSHMP studies of California seismicity has been the overprediction, or "bulge," in the modeled event rates between M6.5 and 7.0 (for example, the "earthquake deficit" described by WGCEP 1995). The UCERF2 rates also showed a bulge in this magnitude range, requiring ad hoc adjustments to lower them to within the 95-percent confidence bounds of observed rates. WGCEP 2007 speculated that the relaxation of strict segmentation would provide a better solution to the bulge problem, and they noted that the multifault ruptures observed in the 1992 Landers, California, and 2002 Denali, Alaska, earthquakes supported this hypothesis.

In addition to the 2011 M6.3 Christchurch earthquake, which demonstrated that aftershocks could be more damaging than their main shock (Kaiser and others, 2012), the 2009 L'Aquila, Italy, earthquake also exemplified the potentially dire effects of earthquake triggering (van Stiphout and others, 2010). In fact, an international commission convened in the aftermath of the latter earthquake (Jordan and others, 2011) concluded that we need to move more aggressively toward Operational Earthquake Forecasting (OEF), which, by definition, would include both authoritative, real-time forecasts, as well as official protocols for communicating implications to the public (Jordan and others, 2011). Furthermore, OEF is now listed as one of the strategic-action priorities of the USGS, with a goal of providing "effective situational awareness" during hazardous events, with core responsibilities including issuing warnings and providing timely information to emergency managers, the media, and the public (Holmes and others, 2013, p. 32–33).

Recognizing the limitations of UCERF2 and the rapid pace of earthquake forecasting research, the USGS, CGS, and SCEC reconstituted WGCEP in 2010 and, with support from CEA, charged it with developing a new model, UCERF3. This report presents the resultant time-independent component of UCERF3, in which we have relaxed segmentation and included multifault ruptures via a generalized inversion approach. A number of other issues have been addressed as well, and virtually all datasets have been revised and updated. Four different

UCERF3 models were developed, evaluated, and formally reviewed during the course of this project: versions 3.0, 3.1, 3.2, and 3.3, where the latter is the final time-independent model presented here (abbreviated as "UCERF3" below). Although a detailed version history is not provided in this report, the more important changes are discussed in the context of lessons learned.

The spatial domain of UCERF3 is the same as that used for UCERF2, shown by the polygon surrounding California in *figure 1*. This is sometimes referred to as the "RELM" region, because it was first adopted for the purpose of developing and testing alternative forecasts in the Regional Earthquake Likelihood Models (RELM) project (Field, 2007; Schorlemmer and others, 2007). RELM has since expanded into the Collaboratory for the Study of Earthquake Predictability (Zechar and others, 2010), and the continued use of this evaluation region will greatly facilitate formal, independent testing of UCERF3.

As with its predecessor, UCERF3 development has been coordinated with the NSHMP, and the time-independent component presented here has been formally recommended for use in the 2014 revisions to national seismic hazard maps. The model for the Cascadia subduction zone, which extends partway into northern California from Oregon and Washington, was developed by a separate NSHMP working group. Coordination with UCERF3 was achieved via joint participation in workshops (*table 2*). Because the Cascadia model is largely decoupled from UCERF3 and is described in appendix P (this report), we do not discuss it here.

A number of key products were developed for UCERF3, most of which are represented in the various appendixes listed in *table 1*. Each appendix was reviewed by the UCERF3 Scientific Review Panel (SRP) and often by additional experts selected by the SRP. Although some of these appendixes have also been published as peer-reviewed journal papers, we refer to these appendixes here by the corresponding letter given in *table 1*. All are noteworthy achievements in and of themselves, and many will be of broader interest. For example, the UCERF3 deformation models (appendix C, this report) can be used in developing physics-based earthquake simulators (for example, Tullis and others, 2012).

The time-dependent components of UCERF3 will be the topic of future reports. For instance, we are attempting to include spatiotemporal earthquake clustering by merging a point-process Epidemic Type Aftershocks Sequence model (ETAS; Ogata, 1988) into our finite-fault-based framework. Our ultimate aim is to deploy UCERF3 as part of an operational earthquake forecast, although doing so will require additional work with respect to real-time network interoperability. Other goals for the time-dependent model include addressing self-consistency issues with respect to elastic-rebound probability calculations in unsegmented models (Field and others, 2009) and further investigating the implications of apparent seismicity rate changes with respect to the likelihood of large damaging earthquakes (the "empirical" model of WGCEP 2003 and in UCERF2; see, for example, Reasenberg and others, 2003). Prototypes of all these components have been developed and reviewed, but final implementation awaits the necessary completion of the long-term model presented here.

The different approach taken in developing UCERF3 necessitated an extensive set of PSHA calculations, both for logic-tree sensitivity tests and for determining adequacy with respect to averaging over stochastic elements of the long-term model. This unanticipated requirement delayed the project, but the fact that we include hazard calculations is a notable first among WGCEPs. Although the UCERF3 platform now lends itself to continual updates and improvements, the features and options included here were dictated by deadlines of the Building Seismic Safety Council (BSSC).
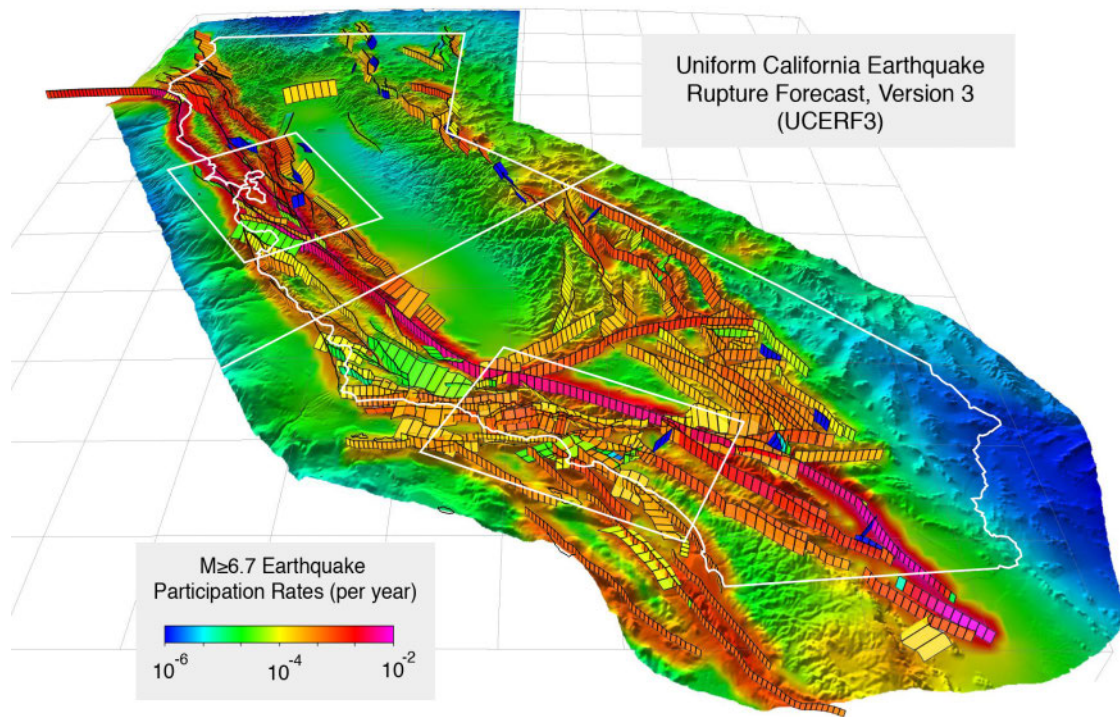
Figure 1.   3D perspective view of California, showing the 2,606 fault sections (black rectangles) of UCERF Fault Model 3.1 (FM 3.1). Colors indicate the long-term rate at which each area participates in M≥6.7 earthquakes, averaged over all 720 UCERF3 logic tree branches for FM 3.1, and including aftershocks. The entire colored area represents the UCERF model region, which comprises California and a buffer zone. The white boxes define the San Francisco Bay area and Los Angeles regions used in various calculations, and the white line crossing the state is our definition of northern versus southern California. The Cascadia megathrust is not shown on this map; it and the Mendocino transform fault (which is shown) extend beyond the UCERF model region.

Model Framework

The UCERF3 framework, like that of UCERF2, has been constructed from the four main model components shown in *figure 2*. The fault model gives the physical geometry of the larger, known, and more active faults; the deformation model gives slip-rate and creep estimates for each fault section, as well as deformation rates of the modeled faults (if available); the earthquake rate model gives the long-term rate of all earthquakes throughout the region (at some level of discretization); and the earthquake probability model gives the likelihood that each event will occur during a specified time span, perhaps conditioned on additional information such as date of last event. The first three of these model components are discussed here (in subsequent sections below). These are sufficient for time-independent PSHA, as the assumed Poisson probability model depends only on long-term rates. Truly time-dependent probability models, based on renewal and clustering processes, will be the topic of future publications.

Table 1.   List of appendixes to this report.

Appendix	Title	Authors
A	Updates to the California Reference Fault Parameter Database—Uniform California Earthquake Rupture Forecast, Version 3 Fault Models 3.1 and 3.2	Dawson, T.E.
B	Geologic-Slip-Rate Data and Geologic Deformation Model	Dawson, T.E., and Weldon, R.J., II
C	Deformation Models for UCERF3	Parsons, T., Johnson, K.M., Bird, P., Bormann, J.M., Dawson, T.E., Field, E.H., Hammond, W.C., Herring, T.A., McCaffrey, R., Shen, Z.-K., Thatcher, W.R., Weldon R.J., II, and Zeng, Y.
D	Compilation of Creep Rate Data for California Faults and Calculation of Moment Reduction Due to Creep	Weldon, R.J., II, Schmidt, D.A., Austin, L.J., Weldon, E.M., and Dawson, T.E.
E	Evaluation of Magnitude-Scaling Relationships and Depth of Rupture	Shaw, B.E.
F	Distribution of Slip in Ruptures	Biasi, G.P., Weldon, R.J., II, and Dawson, T.E.
G	Paleoseismic Sites Recurrence Database	Weldon R.J., II, Dawson, T.E., Biasi, G.P., Madden, C., and Streig, A.R.
H	Maximum Likelihood Recurrence Intervals for California Paleoseismic Sites	Biasi, G.P.
I	Probability of Detection of Ground Rupture at Paleoseismic Sites	Weldon, R.J., II, and Biasi, G.P.
J	Fault-to-Fault Rupture Probabilities	Biasi, G.P., Parsons, T., Weldon R.J., II, and Dawson, T.E.
K	The UCERF3 Earthquake Catalog	Felzer, K.R.
L	Estimate of the Seismicity Rate and Magnitude-Frequency Distribution in California from 1850–2011	Felzer, K.R.
M	Adaptive Smoothed Seismicity Model	Felzer, K.R.
N	Grand Inversion Implementation and Testing	Page, M.T., Field, E.H., Milner, K.R., and Powers, P.M.
O	Gridded Seismicity Sources	Powers, P.M., and Field, E.H.
P	Models of Earthquake Recurrence and Down-Dip Edge of Rupture for the Cascadia Subduction Zone	Frankel, A.D., and Petersen, M.D.
Q	The Empirical Model	Felzer, K.R.
R	Compilation of Slip-in-the-Last-Event Data and Analysis of Last Event, Repeated Slip, and Average Displacement for Recent and Prehistoric Ruptures	Madden, C., Haddad, D.E., Salisbury, J.B., Zielke, O., Arrowsmith, J.R., Weldon R.J., II, and Colunga, J.
S	Constraining Epidemic Type Aftershock Sequence (ETAS) Parameters from the Uniform California Earthquake Rupture Forecast, Version 3 Catalog and Validating the ETAS Model for Magnitude 6.5 or Greater Earthquakes	Hardebeck, J.L.
T	Defining the Inversion Rupture Set Using Plausibility Filters	Milner, K.R., Page, M.T., Field, E.H., Parsons, T., Biasi, G.P., and Shaw, B.E.

*All appendixes can be cited as independent elements of the USGS Open File Report on UCERF3.

We acknowledge there are situations where the distinction in figure 2 can break down, such as when differentiating a "multifault rupture" (in the earthquake rate model) from the case where one fault very quickly triggers another (in the earthquake probability model). The distinction nevertheless remains both a modeling convenience and a practical necessity to the extent that building codes remain based on long-term rates of events.

Fault Models		**Deformation Models**		**Earthquake-Rate Models**		**Probability Models**
Specifies the spatial geometry of larger, more active faults.	→	Provides fault slip rates used to calculate seismic moment release.	→	Gives the long-term rate of all possible damaging earthquakes throughout a region.	→	Gives the probability that each earthquake in the given Earthquake Rate Model will occur during a specified time span.

Figure 2.   Diagram of the four main model components of the UCERF3 framework.

This modularization also aids in the implementation of alternative models (for example, logic-tree branches discussed below) and in the replacement of model elements with new components. Building on OpenSHA, WGCEP 2007 put considerable effort into developing an open-source, object-oriented, and extensible "UCERF cyberinfrastructure," including the use of distributed data resources and flexible analysis tools. UCERF3 represents a dividend on these investments, which we have augmented with new computational capabilities, including the harnessing of supercomputers to solve for earthquake rates and generate large numbers of hazard curves.

Model Uncertainties

Because of a lack of consensus on how to forecast earthquakes, it is important that our model adequately portray epistemic uncertainties, which represent our incomplete understanding of how the earthquake system works, as well as the aleatory uncertainties, which represent the inherent randomness assumed in any given model of the system (Senior Seismic Hazard Analysis Committee, 1997). The history of WGCEPs can be viewed as a progression of including more and more epistemic uncertainties. For example, WGCEP 1988 did not consider a possible recurrence of the two largest historical events (the great 1857 and 1906 earthquakes), whereas WGCEP 2003 represented a quantum leap in having 10,000 different models for the Bay Area alone.

As in UCERF2, we represent epistemic uncertainties using a logic tree structured according to the four main model components. Our final branch options and associated weights for the UCERF3 time-independent model are shown in *figure 3*. Note that some branch options are given zero weight but are shown nonetheless, in case practitioners want to reconsider their applicability in special (for example, site-specific) studies. The set of nonzero-weighted branches gives rise to 1,440 different UCERF3 models.

UCERF3 represents an important step in the WGCEP quest for a more complete representation of epistemic uncertainty. For example, rather than assuming or prescribing earthquake-generating attributes of the various seismic sources, as in previous NSHMP and WGCEP models, we take a more derivative approach to system-level behavior by solving for a much wider range of models that are consistent with the data. Of course UCERF3 is still a crude approximation of the actual system (for example, imposing strict separation between "on-fault" and "off-fault" earthquakes). Because "all models are wrong, but some are useful" (Box, 1979),

the relevant question for practitioners is whether UCERF3 is a better representation of future earthquake activity than UCERF2 for the purpose of managing seismic risk.

Participants, Review, and Consensus Building

The organizational structure used in this study is similar to WGCEP 2007, comprising an Executive Committee (ExCom), a Management Oversight Committee (MOC), a Scientific Review Panel (SRP), and a large group of contributing experts. The ExCom was responsible for convening experts, reviewing options, and making decisions about model components. The MOC allocated resources and approved project plans, budgets, and schedules; it also oversaw the model review and delivery processes. The SRP is an independent, participatory body of experts that reviewed the project plans, research results, and model elements. In particular, the SRP provided WGCEP with guidance regarding model viability and the range of models needed to adequately represent epistemic uncertainties. Other WGCEP contributors include research scientists, resource experts, model advocates, and information technology professionals. Members of these groups are listed in the "Contributors to UCERF3" section. We also note that CEA's Multidisciplinary Research Team (MRT) participated in UCERF3 reviews, but they were not directly involved in the model development nor any decisions about branch options.

The discussion of model options and consensus building has been achieved through a series of community workshops (*table 2*), which included participants from the broader community. Some workshops focused on the scientific ingredients going into UCERF3, while others were aimed at informing user communities and getting their feedback. Numerous smaller working group meetings are not listed in *table 2*.

Though all participants influenced decisions with respect to logic-tree branches and their weights, including the SRP, the ExCom had responsibility for the final decisions. In the case of deformation models, where the ExCom felt that special expertise was needed, an ad hoc evaluation committee was convened to advise on branch weights (discussed in the "Logic Tree Branch Weights" section). The entire UCERF3 process was monitored by representatives of the National Earthquake Prediction Evaluation Council (NEPEC), which formally advises the USGS Director, and the California Earthquake Prediction Evaluation Council (CEPEC), which formally advises the California Office of Emergency Services.

UCERF3.3 Logic-tree Branches
(for long-term model)
Bold elements represent the reference branch (used for sensitivity tests) and values in parentheses represent branch weights.

Fault Models:

FM3.1
(0.5)

FM3.2
(0.5)

Deformation Models:

Geologic	*AveBlockMod*	*NeoKinema*	**Zeng**
(0.3)	*(0.1)*	*(0.3)*	*(0.3)*

Earthquake Rate Models:

Scaling Relationships

$\begin{pmatrix} mag\text{-}area\ \& \\ slip\text{-}length \\ relationships \end{pmatrix}$

Shaw09mod for both (Shaw, 2013a, 2013b) **(0.20)**	*EllsworthB for both* (Ellsworth, WGCEP-2002) *(0.20)*	*HanksBakun08 for both* (Hanks & Bakun, 2008) *(0.20)*	*EllsworthB w/ SqrtLength* (Shaw, 2012) *(0.20)*	*Shaw09mod w/ Const Stress Drop* (Shaw, 2012) *(0.20)*

Slip Along Rupture (Dsr)

Tapered (Sin$^{1/2}$) **(0.5)**	*Boxcar* *(0.5)*	*Slip-Rate proportional* *(0.0)*

Total M ≥ 5 Event Rate (yr^{-1})

6.5 *(0.1)*	**7.9** **(0.6)**	*9.6* *(0.3)*

Inversion Model

Characteristic UCERF2 Constrained **(1.0)**	*Characteristic Unconstrained* *(0.0)*	*Gutenberg-Richter Constrained* *(0.0)*	*Gutenberg-Richter Unconstrained* *(0.0)*

M$_{max}^{off\text{-}fault}$

7.3 *(0.1)*	**7.6** **(0.8)**	*7.9* *(0.1)*

Off-Fault Spatial Seis PDF (aka SpatialPDF)

UCERF2 Smoothed Seis *(0.5)*	**UCERF3 Smoothed Seis** **(0.5)**	*Deformation Model Based* *(0.0)*

Fault Moment Rate Fix

Apply Implied Coupling Coefficient *(0.0)*	*Relax MFD Constraint* *(0.0)*	*Apply Both Options* *(0.0)*	**Do Nothing** **(1.0)**

Figure 3. Diagram of UCERF3 long-term model logic-tree branches with weights given in parentheses. The branches are organized by the basic model components in *figure 2*: fault models (green), deformation models (purple), and earthquake rate models (blue). The branches and weighting decisions, as well as reference branch values for sensitivity tests (bold typeface), are described in the sections for each component. UCERF3 has a total of 1,440 nonzero branches.

Table 2. Working Group on California Earthquake Probabilities consensus-building activities, 2009–2013.

Date		Activity Description
2013	June 21	UCERF3 Time-Independent Model (report #9) submitted
	Feb. 21	Workshop on use of UCERF3 in the USGS National Seismic Hazard Map
	Feb. 13–14	UCERF3 fault-by-fault evaluation meeting #3
	Jan. 25	UCERF3 fault-by-fault evaluation meeting #2
	Jan. 24	UCERF3 fault-by-fault evaluation meeting #1
2012	Oct. 17–18	California workshop of the National Seismic Hazard Mapping Project (NSHMP)
	July 9	UCERF3 Model Framework (report #8) submitted
	May 8–9	Scientific Review Panel meeting
	Apr. 30	Review of Preliminary UCERF3 Model (report #7) submitted
	Mar. 31	Preliminary UCERF3 Model (report #6) submitted
	Mar. 21–22	Cascadia subduction zone workshop
	Jan. 26	UCERF3 deformation model meeting
	Jan. 24-25	Earthquake Hazards Program northern California workshop
	Jan. 5-6	WGCEP all-hands meeting
2011	Dec. 15	Cascadia subduction zone workshop
	Oct. 25	Joint UCERF3 and NGA-W2 workshop on common issues
	Oct. 24	UCERF3 plan overview (emphasizing the grand inversion for users)
	Sept. 30	Final UCERF3 Plan (report #5) submitted
	Sept. 11–14	SCEC annual meeting
	June 30	SRP Review of Proposed UCERF3 Plan (report #4) submitted
	June 13–14	Scientific Review Panel meeting
	June 11	Workshop on distribution of slip in large earthquakes
	June 10	Workshop on instrumental and historical seismicity
	June 9	Workshop on the use of physics-based simulators
	June 8	Workshop on time-dependent models
	June 4–5	Workshop on UCERF3 deformation models
	May 31	Proposed UCERF3 Plan (report #3) submitted
	Apr. 8	Statewide fault model and paleoseismic data workshop (in southern California)
	Apr. 6	Statewide fault model and paleoseismic data workshop (in northern California)
	Mar. 2–3	Distribution of slip in large earthquakes meeting
	Jan. 12	WGCEP all-hands meeting
2010	Dec. 31	UCERF3 Methodology Assessment—Proposed Solutions to Issues (report #2) submitted
	Nov. 18–19	Cascadia subduction zone workshop
	Nov. 10–12	Scientific Review Panel meeting
	Nov. 3–4	CEPEC/NEPEC meeting
	Sept. 12–15	SCEC annual meeting
	Aug. 2	Fault-to-fault jumps task meeting
	June 30	UCERF3 Methodology Assessment—Issues and Research Plan (report #1) submitted
	Apr. 1–2	Workshop on incorporating geodetic surface deformation data in UCERF3
	Feb 17–18	WGCEP all-hands meeting
2009	Dec. 1–2	UCERF3 kick-off and planning meeting

Fault Models

The UCERFs are primarily fault-based earthquake rupture forecasts, in that most large earthquakes (~80 percent) occur on the possible rupture surfaces defined by a fault model (*fig. 2*). The fault database developed for UCERF2 has been updated with both revisions and additions, with special consideration being given to fault endpoints for the purpose of defining multifault rupture possibilities. Full details are given in appendix A (this report), and a summary of the more important changes is presented here.

Definition

A fault model gives the spatial geometry of the larger, active faults throughout the region, with alternative models representing epistemic uncertainties in the fault system geometry. By definition, a fault model is composed of a list of fault sections, where each fault section is represented by:

- Fault section name (for example, "San Andreas (Parkfield)")
- Fault trace (list of latitudes, longitudes, and depths for the upper fault edge)
- Upper and lower seismogenic depth estimates
- Average dip estimate
- Average rake estimate (although this can be modified by a deformation model)
- Fault zone polygon (an areal representation of a fault zone)

Because distinct fault sections are defined only to the extent that one or more of these attributes vary along strike, some sections can be quite long (for example, the northern San Andreas Fault has only four sections). The complete master list of fault sections for California is given in the Fault Section Database, which is part of the California Reference Geologic Fault Parameter Database. Some fault section entries in this database are mutually exclusive (for example, representing alternative representations). The list of fault sections in a given fault model is therefore considered to be a complete, viable representation of the large, known, and active faults throughout the region.

Fault Zone Polygons

The fault zone polygon attribute, described in appendix O (this report), is new to UCERF3, and is intended for specifying:

- Whether the fault section represents a simple surface or a broader, braided system of faults;
- The area over which the deformation-model slip rate applies;
- The faults to which observed microseismicity is attributed;
- The area over which elastic-rebound-based probability reductions are applied after an earthquake; and
- Whether a future large earthquake is identified as a rupture of a UCERF3 modeled fault.

A retrospective example of the identification problem is whether the 2010 El Mayor-Cucapah earthquake (Hauksson and others, 2011) was an event on the UCERF2 Laguna Salada Fault source, or whether it was part of the background seismicity. With the addition of fault zone polygons in UCERF3 this distinction is not ambiguous, or at least a lot less so.

In UCERF3, each fault section represents a proxy for all events that nucleate inside its fault zone polygon. Polygons based on geologic considerations (*fig. 4A*) were assigned to each fault section in appendix A (this report), thereby satisfying the first bullet above. However, for some faults such as the San Andreas, this zone gets as narrow as 1 km on each side of the fault, which is too thin for the other intended uses listed above. This reflects the fact that there is no single polygon definition that will perfectly satisfy all intended uses.

A fault zone width was effectively defined in UCERF2 based on standards established previously by the NSHMP in distinguishing fault-based sources from gridded, off-fault seismicity. Specifically, the maximum magnitudes for gridded seismicity were previously reduced in the vicinity of fault-based sources to avoid overlap with the minimum magnitude of fault sources (for example, Petersen and others, 2008b). Although this led to a checkerboard pattern for the zones around faults (according to the grid cells assigned to each fault), the average width of their zones was about 12 km on either side of vertically dipping faults.

WGCEP has therefore adopted a default width of 12 km on both sides of vertically dipping faults, with this tapering to the surface projection for faults dipping less than 50 degrees. More specifically, fault zone polygons are the combination (or union) of three independently defined polygons (*fig. 4B*): the geologically defined polygon for the fault; the surface projection of the fault if dipping; and a buffer on either side of the fault trace. The width of the buffer polygon on either side of a fault trace scales linearly from 0 km at 50° dip to 12 km at 90° dip (*fig. 4C*). This provides vertical faults with a broad zone of influence that scales down as dip decreases and the area of the surface projection polygon increases. Figure 4*B* demonstrates how the three polygons are combined. This fault zone definition is both consistent with past NSHMP practice and avoids the checkerboard pattern. It is still somewhat arbitrary, however, so potential hazard implications of this choice need to be considered carefully in any given application, as we will illustrate below.

Logic Tree Branches

UCERF3 comprises two alternative fault models: FM 3.1 and FM 3.2, which are analogous to the fault model alternatives FM 2.1 and FM 2.2 used in UCERF2. These two new models, shown in figure 5, represent alternative representations of several fault groups. Reducing all possible combinations to just two models introduces artificial correlation between the alternatives for different faults; however, the groupings are judicious choices for minimizing the number of logic-tree branches (every additional fault model requires 720 new logic-tree branches), and the PSHA calculations discussed below indicate adequacy for at least the most common hazard metrics.

Development Process

Fault models FM 3.1 and 3.2 were developed in coordination with the Statewide Community Fault Model project, which builds on SCEC's Community Fault Model development (Plesch and others, 2007). Two workshops were held to solicit feedback from the broader community in April of 2011 (*table 2*). Relative to UCERF2, the primary modifications are (1) 153 new faults sections were added, mostly in northern California, and about 95 fault sections were revised (the numbers are not exact because some are a bit of both); (2) fault endpoints were reexamined by reviewing more detailed geologic maps, to enable better quantification of multifault rupture probabilities; and (3) connector fault sections were added between larger faults where deemed appropriate, to enable multifault ruptures or, where needed, to define block boundaries for the deformation models. Figure 5 shows the fault sections that were added, modified, or left unchanged from UCERF2. Further details on how these fault models were constructed are given by in appendix A (this report).
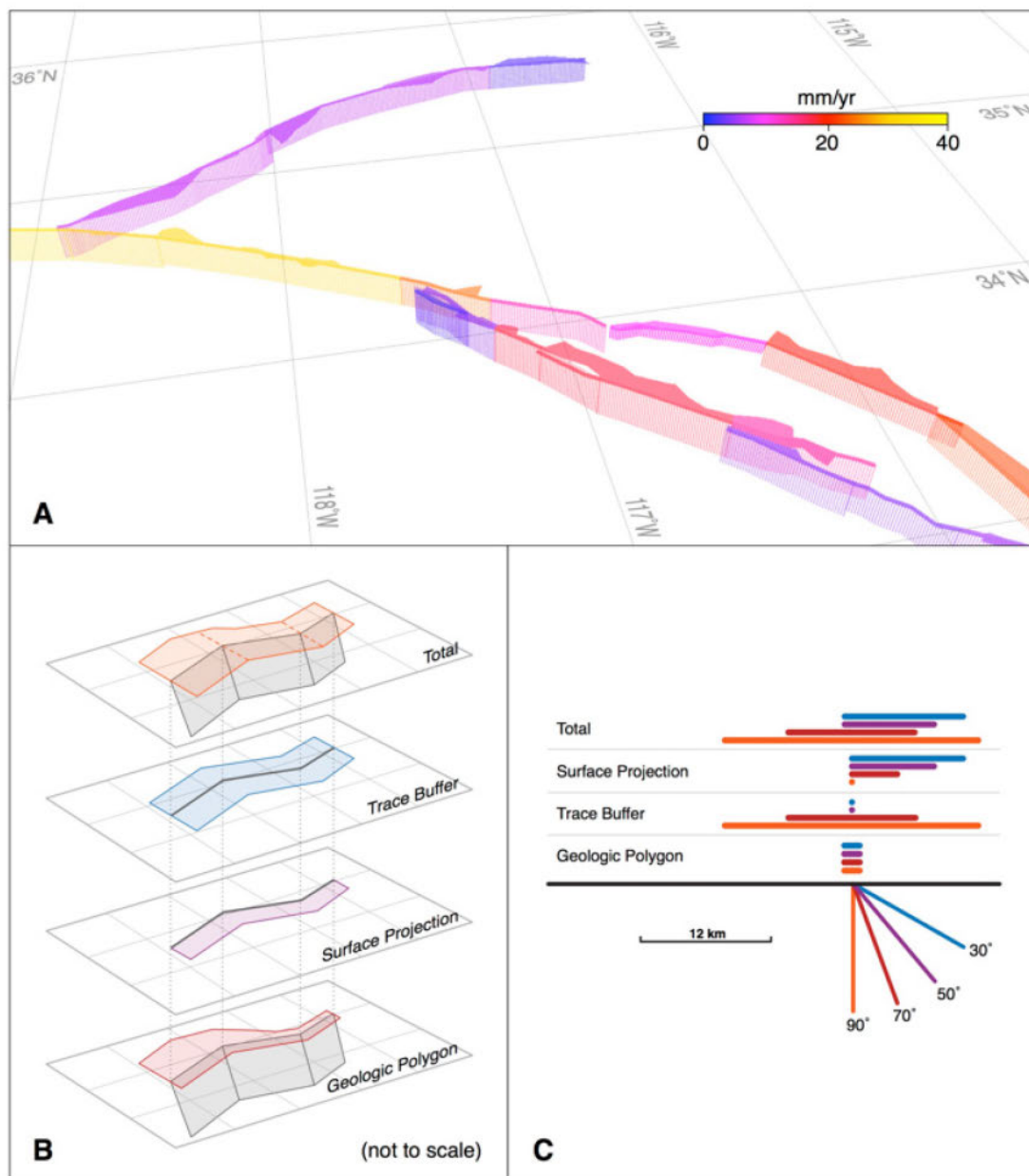
Figure 4. Diagrams illustrating the definition and creation of fault zone polygons. *A,* Perspective view of the Garlock, southern San Andreas, and San Jacinto fault systems, color coded by slip rate (other faults in this region are not shown). Downdip projections of the faults are stippled, and the geologically defined surface polygons are solid. The geologic polygons typically extend to 1 km on either side of the fault traces, but in many places are much broader to accommodate additional mapped surface features. *B,* Schematic diagram of the union of geologic, surface projection, and trace buffer polygons to form the "complete" fault zone polygon used in UCERF3. The exemplified fault dips at ~70°, so the buffer polygon extends to 6 km on either side of the fault trace. The dashed orange lines in the complete polygon mark the subdivisions used to define polygons for the individual fault sections. *C,* Strike-perpendicular cross section of a fault showing how dip variations influence the widths of the trace buffer, the surface projection, and the complete fault zone polygon used in UCERF3.
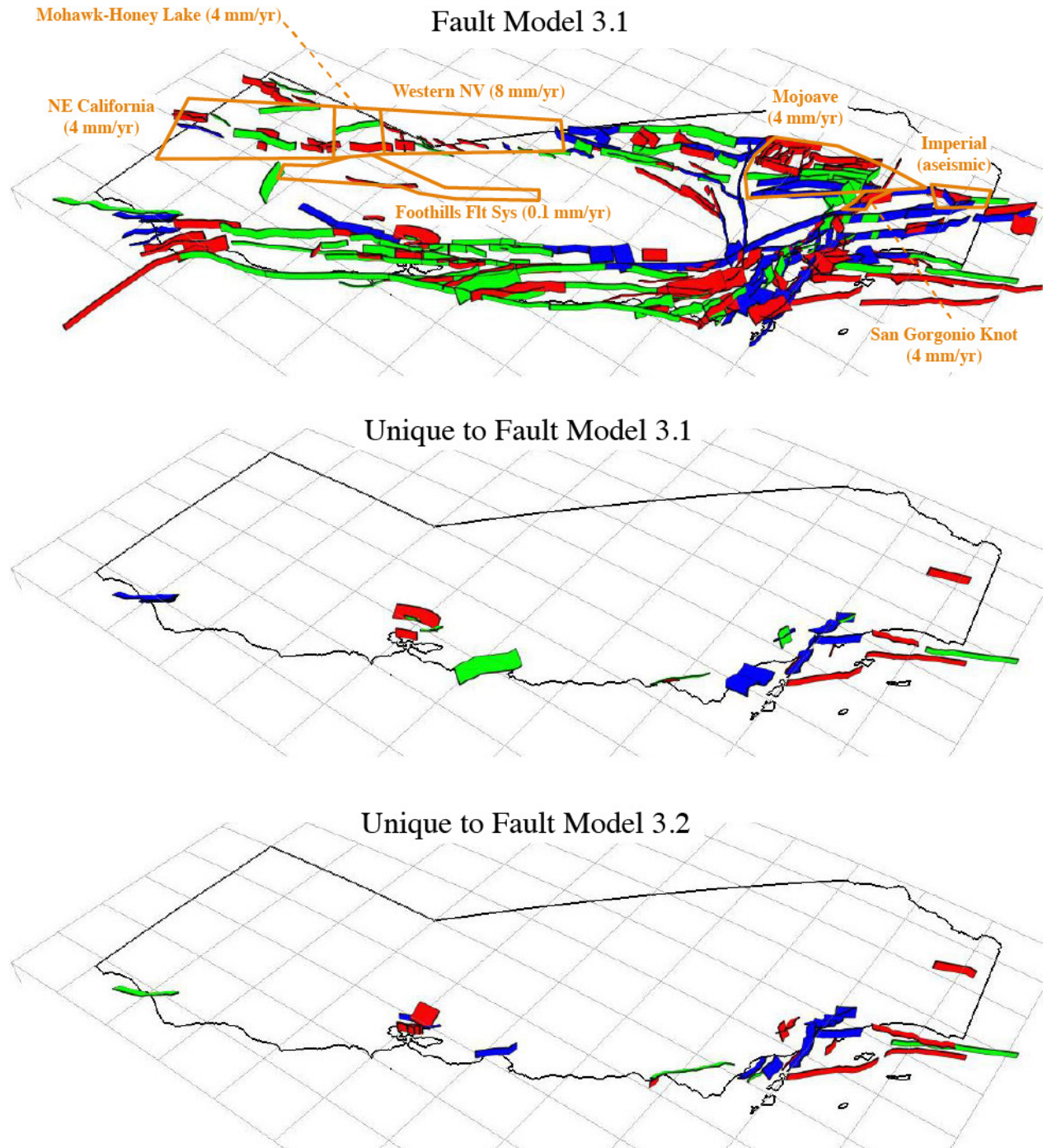
Figure 5.   Perspective map diagrams of California showing UCERF3 Fault Model (FM) 3.1 (top), and fault sections unique to FM 3.1 (middle) and FM 3.2 (bottom). Fault sections are colored to identify those that were added (red), modified (green), and unchanged (blue) since UCERF2. Some of the modifications are relatively trivial (for example, name change only); see appendix A (this report) for precise details. Type C zones applied in UCERF2 (orange polygons) are labeled with their modeled deformation rates. The Cascadia subduction zone is not shown here, but is given in appendix P (this report).

Deformation Models

The rate of large events in fault-based ERFs depends directly on fault slip rates, which can be derived from measured and dated geologic offsets and perhaps interpolated or extrapolated along faults. Slip rates can also be obtained by modeling geodetic measurements such as Global Positioning System (GPS) observations (*fig. 6*). Because it is impossible to identify all faults, another contribution to hazard can be "off-fault" deformation (in quotes here because this deformation is at least partially occurring on unmodeled faults), which can be inferred from observed seismicity and (or) GPS observations.

Only about 30 percent of UCERF2 faults had measured slip-rate estimates, and most others had an estimate from only a single location. UCERF2 deformation models were therefore based on expert-opinion evaluation of geologic and geodetic data. In addition to on-fault slip rates, off-fault deformation was represented by a set of geographic polygons, referred to as "type C zones," each of which was assigned an effective slip rate (*fig. 5, top panel*). As an a posteriori check, UCERF2 deformation models were summed across various transects to confirm that total plate tectonic rates were well matched.

For UCERF3, we have developed four different deformation models. One is a geologically "pure" model (uninfluenced by GPS observations), while the other three are kinematically consistent models that directly include both geologic and geodetic constraints. By using these models, we minimize relying on expert opinion to broker discrepancies between geodetic and geologic data, as was done in UCERF2. Importantly, this approach has provided data-driven slip rate estimates for faults with no prior assigned rates (which were excluded from UCERF2) and has filled in slip rates along faults with sparse observations. The latter three models also provide off-fault strain rate maps, allowing us to abandon the UCERF2 type C zones.

Geologic Slip Rate Constraints

Because UCERF2 expert-opinion slip rates were influenced by both geologic and geodetic data, an effort was made in UCERF3 to extract and compile the geologic-only constraints at points on faults where such data exist (appendix B, this report). In addition to geologic slip rates, appendix B also includes the supporting data, such as information about the site location, offset features, dating constraints, number of events, reported uncertainties, comments—and separate qualitative ratings of the offset features, dating constraints, and overall slip rate. In the majority of cases, these data were compiled from the original sources, although extensive use was also made of the written summaries included in the USGS Quaternary Fault and Fold Database (U.S. Geological Survey, 2013; *earthquake.usgs.gov/hazards/qfaults;* Machette and others, 2004).

Given the number of Quaternary active faults in California, the dataset of geologic slip rates is somewhat sparse. The compilation includes ~230 reported slip rates, of which about 150 reported rates are ranked as moderately to well constrained. Of the ~350 fault sections in the UCERF3 fault model, only about 150 fault sections are directly constrained by slip rate data (*fig. 7B*). This emphasizes the fact that slip rates in previous models, as well as in the pure geologic model here, are often extrapolated over long distances and that values for most fault sections are not directly constrained by geologic data.

Geologic Deformation Model

One of the new UCERF3 deformation models is a purely geologic model that includes no constraints from geodesy or plate motion models (appendix B, this report). As with the other deformation models, the output is an estimated slip rate at all points on the model faults. Where available, these slip rates were assigned using the revised geologic data in appendix B; elsewhere, best-estimate values were taken from UCERF2, except where the latter included hybrid slip rates (from both geology and geodesy) or where the old slip rates were inconsistent with other types of data, such as the USGS rate category and published slip rates.

A number of fault sections had no previously assigned slip rate, and these were simply excluded from UCERF2. Such sections have been assigned to a rate category in UCERF3, based primarily on recency of activity, but also on geomorphic expression and comparison to similar, nearby faults with slip rate constraints. The following criteria were applied when using recency of activity to assign slip rate bounds:

- Active in Quaternary (<1.6 million years) 0.0 to 0.2 mm/yr
- Active in Late Pleistocene (< ~130,000 years) 0.2 to 1.0 mm/yr
- Active in Holocene (< ~11,000 years) 1.0 to 5.0 mm/yr

Very few faults were placed into the last category, primarily because the fastest slipping faults are already well characterized throughout California. The exceptions to this are offshore faults, which are difficult to study. In the absence of other data, the best estimate for each category was selected using a relationship between the number of UCERF fault sections and known slip rates. This weighted mean approach is described in appendix B (this report). The Geologic deformation model is displayed in *figure 7C*. *Table 3* lists the moment rate contributions from the various types of sources in UCERF2, and *table 4* lists the implied moment rates for the new deformation models. Of particular note is that the new faults (UCERF2 faults that lacked slip rates plus the new faults added to UCERF3) constitute a collective moment rate of 0.27×10^{19} N·m/yr (for FM 3.1), which is more than half of the total off-fault moment rate in UCERF2 (0.47×10^{19} N·m/yr). The latter represents the off-fault background and type C zone contributions in *table 3*. Discounting the added faults, the moment rate of the UCERF3 Geologic deformation model is about 1 percent above that of the UCERF2 model.
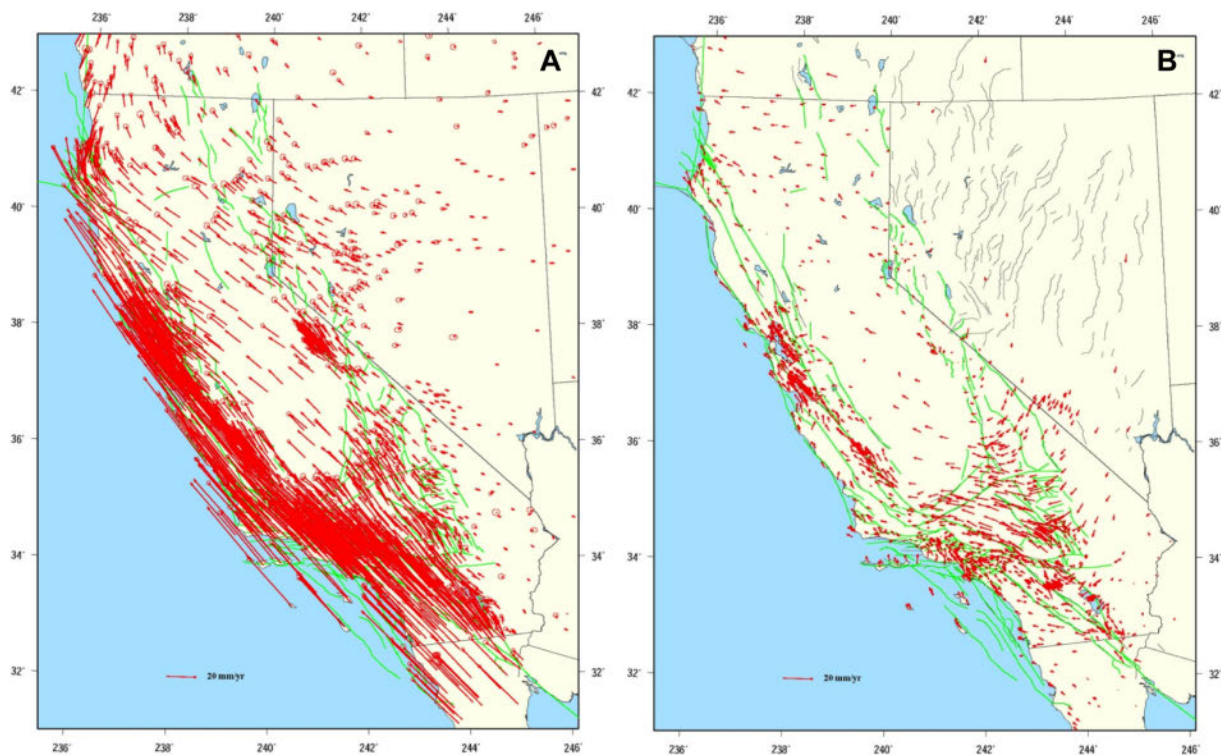
Figure 6.   Maps showing GPS velocity vectors for California. *A*, Distribution of UCERF3 GPS velocity vectors for California, referenced to the North America Plate (from appendix C, this report). *B*, The residual velocities computed as the difference between observed GPS velocities and those predicted by the UCERF2 Deformation Model 2.1. The velocity scales of the two plots are the same. The residual vectors indicate that UCERF2 generally underestimates the average statewide deformation rate, particularly in the most populated parts of the state.

Deformation Models from Joint Inversion of Geodetic and Geologic Data

Several workshops and meetings were convened to address the UCERF3 goal of deriving slip rates and off-fault strain maps from kinematically consistent inversions of GPS and geologic data (*table 2*). Appendix C (this report) describes both the GPS database, shown here in *figure 6*, as well the three UCERF3 deformation models developed by inverting those data together with the geologic constraints:

- **NeoKinema.** A model obtained by inverting geologic, geodetic, and principal stress data using the finite element method of Bird (2009) to estimate the long-term velocity field both on and off faults. It is not based on a block geometry.

- **Zeng.** A model by Zeng and Shen (unpublished work) representing faults as buried dislocations in a homogeneous elastic half space. Each fault segment slips at a solved-for slip rate beneath a locking depth, except at a few segments where shallow creep is allowed. A continuity constraint allows adjustment between more and less block-like deformation. The model here is on the less-block-like end of that spectrum.

- **Averaged Block Model (ABM).** A model constructed by averaging five different block models using a kinematically consistent method. The input models were updates of McCaffrey's DefNode (McCaffrey, 2002; 2005), Hammond's block model (Hammond and

others, 2011), Johnson's quasi-block model (Johnson and Fukuda, 2010), and special (more block-like) versions of NeoKinema and Zeng's model. The averaging used the slip rates from all five block-model inversions as "data" in a unified block model inversion. Residual in-block strain that results from slip on block boundaries is mapped onto identified faults using a buried-dislocation approach as described above for the Zeng model (for details, see appendix C, this report). The leftover strain that cannot be reasonably accommodated on faults is the "off-fault" portion.
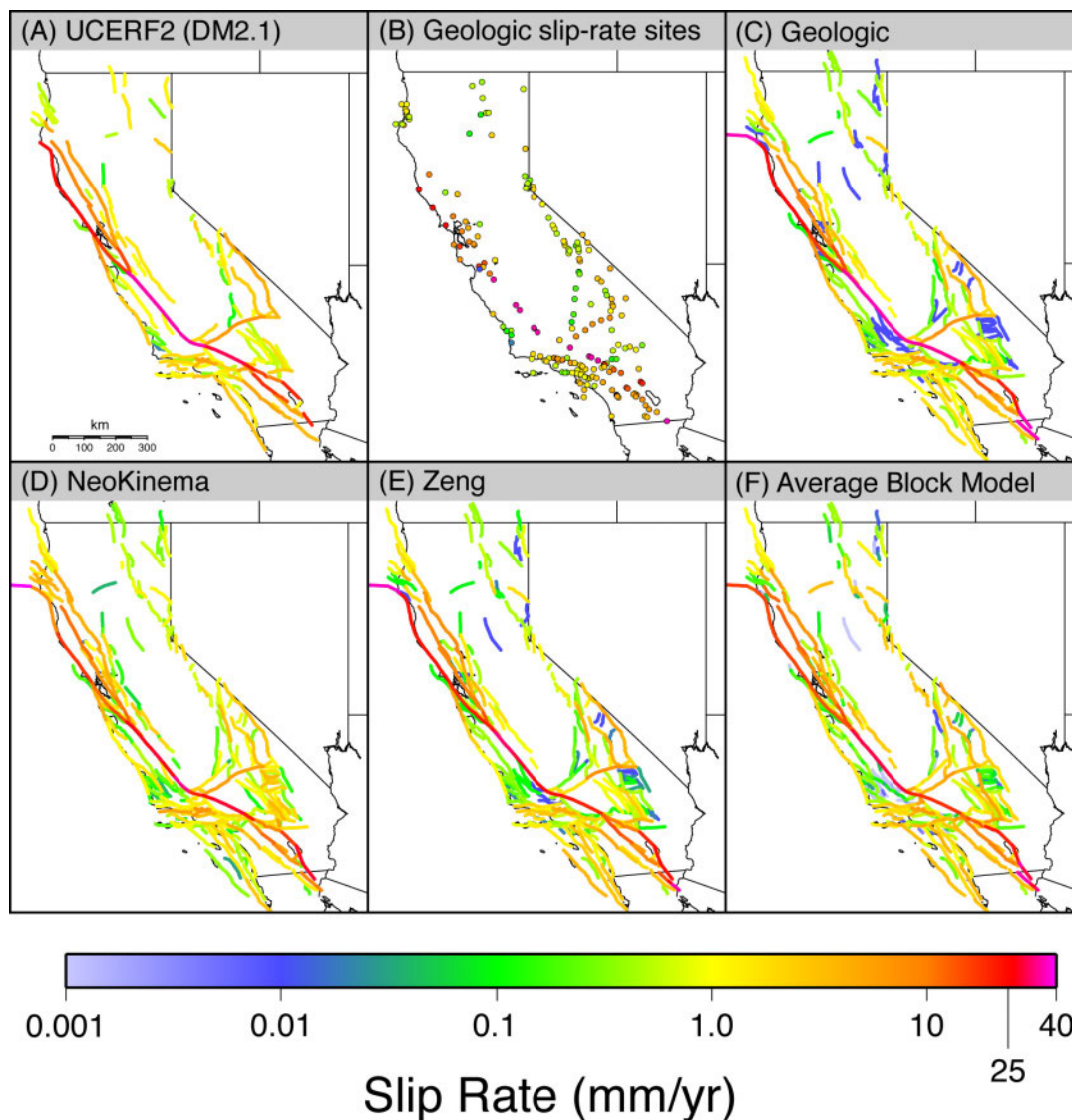
Figure 7.   Maps of California showing slip-rate models. *A,* Fault slip rates for the UCERF2 Deformation Model 2.1. *B,* Sites of geologic slip-rate constraints. *C–F,* Fault slip rates for the four UCERF3 deformation models for Fault Model 3.1.

Each deformation model provides slip-rate estimates for every UCERF3 fault section. Each also provides off-fault deformation in the form of strain rate tensors on a 0.1°×0.1° grid covering California, which is converted to an off-fault moment rate grid as described in appendix

C (this report). All three models were constrained by a consensus GPS velocity field constructed for this purpose (appendix C), as well as by the geologic slip rate constraints from appendix B (this report). The slip rates for these deformation models are shown in *figure 7*. The new fault zone polygons described above were not used in the deformation modeling process here.

Table 3.   Moment rates for the various types of sources in UCERF2.

[$\dot{M}_0$, given in units of 10^{19} N·m/yr or 10^{26} dyne·cm/yr][5]

Source Type	Moment Rate ($\dot{M}_0$)	Percent of Total Seismic	Percent of Total
CA faults [1]	1.73	76%	73%
Non-CA faults [2]	0.07	3%	3%
Off-faults background [3]	0.37	16%	16%
C Zones (seismic) [4]	0.10	5%	4%
C Zones (aseismic) [4]	0.10		4%
Total (seismic)	2.27	100%	
Total (including aseismic)	2.37		100%

[1]Value reflects the 10 percent reduction for smaller earthquakes (generally <6.5, which are treated as background seismicity) and aftershocks. The UCERF2 faults are only a subset of UCERF3 fault model, to which about 160 new fault sections have been added.

[2]Faults outside of California (in Nevada and Oregon), but within the UCERF model region.

[3]Value does not include type C zones or deep seismicity near Cascadia (in the NSHMP file agrd_deeps_out) but does include aftershocks and the special areas for Brawley (1.6×1016 N·m/yr), Mendocino (3.7×1017 N·m/yr), and Creeping San Andreas Fault (1.9×1016 N·m/yr).

[4]Half the moment rate in type C zones was assumed aseismic in UCERF2.

[5]Values in this table were compiled by running the OpenSHA method UCERF3.utils.UCERF2_MFD_ConstraintFetcher.computeMomentRates().

Creep and Aseismicity

In this report, the term "creep" refers to interseismic creep, which operates over decadal and longer time periods, rather than the postseismic creep that follows most earthquakes. Appendix D (this report) documents observations of creep on California faults and develops a new methodology to estimate seismic moment rate reductions due to creep. It approximately doubles the number of creep estimates that were available in UCERF2, primarily by utilizing interferometric synthetic aperture radar (InSAR) and dense geodetic network data. Appendix D also applies a model developed by Savage and Lisowski (1993) to infer how creep extends to depth, and it examines observations of microrepeating earthquakes (recognized as repeatedly rupturing asperities embedded within a creeping fault surface) to see if they are consistent with the model-predicted creep reduction with depth.

Table 4. Moment rates $\dot{M}_0$ (in units of 10^{19} N·m/yr) for the UCERF3 deformation models, plus implied values of maximum magnitude (M_{max}) and mean recurrence interval (MRI) of $M{\geq}8$ events[8].

[ABM, average block model; %, percent. Also listed are UCERF2 values, and the notes give important comparison details]

Fault Model	Deformation Model	On-fault $\dot{M}_0$[1]	On-fault $\dot{M}_0$ increase from UCERF2[2]	On-fault $\dot{M}_0$ for new faults[3]	% from new faults	$\dot{M}_0$ change on UCERF2 faults[4]	Off-fault $\dot{M}_0$[5]	Off-fault $\dot{M}_0$ change from UCERF2	Total $\dot{M}_0$ (including off-fault aseismic)	Total $\dot{M}_0$ increase over UCERF2[6]	% of total off faults	M_{max}[7]	MRI $M{\geq}8$ (years)[8]
3.1	ABM	1.93	11%	0.35	18%	-9%	0.92	44%	2.85	20%	32%	8.41	207
	Geologic	2.02	17%	0.27	13%	1%							
	NeoKinema	1.76	1%	0.32	18%	-17%	1.02	60%	2.78	17%	37%	8.39	214
	Zeng	1.88	9%	0.28	15%	-8%	0.88	37%	2.76	16%	32%	8.38	216
3.2	ABM	1.92	11%	0.37	19%	-10%	0.92	44%	2.84	20%	33%	8.41	207
	Geologic	2.02	17%	0.28	14%	1%							
	NeoKinema	1.75	1%	0.32	18%	-17%	1.04	63%	2.79	18%	37%	8.39	213
	Zeng	1.88	9%	0.29	16%	-8%	0.88	37%	2.76	16%	32%	8.38	216
2.1	UCERF2	1.73	0%	0.00	0%	0%	0.64	0%	2.37	0%	27%	8.15	385

[1]Value includes fault-specific downdip widths and creep-based moment-rate reductions; default is 0.1 where no creep data exist. For reference, the average lower seismogenic depth is ~12 km in the UCERF3 Fault Models; with surface creep the average seismogenic thickness is ~11 km. Note that UCERF3 does not include most of the UCERF2 "Non-CA Faults" listed in table 30, so contributions from these are included "off fault" here. The value of 1.73 listed for UCERF2 includes a 10-percent reduction for small earthquakes and aftershocks (table 30), but this is compensated by UCERF3 applying the default aseismicity of 0.1 (which was zero in UCERF2).

[2]These are the on-fault values divided by the value of 1.73 for UCERF2.

[3]Moment-rate contributions from only the more than 150 new fault sections added in UCERF3 (not included in UCERF2). For the geologic model with Fault Model 3.1, 49 percent percent of the increase (0.28×10^{19} N·m/yr) is from the following two new faults: Cerro Prieto (0.083×10^{19} N·m/yr) and Mendocino (0.054×10^{19} N·m/yr).

[4]Change in on-fault moment rate for the same faults as used in the UCERF2 model.

[5]Values from off-fault strain rates given in appendix C, which assume a seismogenic thickness of 11 km. The UCERF2 value includes contributions from both "C-Zones (aseismic)" and "Non-CA Faults" (table 30), the latter because most of the "Non-CA Faults" have been excluded in UCERF3.

[6]Relative to the UCERF2 total value of 2.37×10^{19} N·m/yr (table 30), which includes contributions from "C-Zones (aseismic)" in table 30. The UCERF3 on-fault values have aseismic contributions removed, but there may be aseismic contributions in the UCERF3 off-fault values.

[7]Implied values computed assuming a truncated Gutenberg-Richter distribution constrained to have the observed rate of 7.9 $M{\geq}5$ events per year (appendix L, this report) and a *b*-value of 1.0.

[8]Values in this table compiled by running the following OpenSHA method on 04/24/13:UCERF3.analysis.DeformatioN-modelsCalc.calcMoRateAndMmaxDataForDefModels().

As in UCERF2, the aseismicity factor is defined as the fraction of rupture area, between the upper and lower seismogenic depths, that is reduced by creep, while the coupling coefficient defines what fraction of the slip rate is fully seismic (not due to creep). Nonzero aseismicity factors primarily reduce rupture magnitudes (due to area reduction), whereas coupling coefficients less than 1.0 reduce event rates (due to the slip-rate reduction). Both reduce moment rates.

Only aseismicity factors were applied in UCERF2, and only about 20 percent of UCERF2 fault sections had nonzero values. Furthermore, UCERF2 aseismicity factors were computed as the surface creep rate divided by the total average slip rate, a ratio hereafter referred to as the "creep fraction." It is now understood, however, that most creep is shallow and decreases rapidly with depth. By integrating over a depth-dependent creep model, we have developed a new relationship for moment rate reduction versus creep fraction (appendix D, this report). The result, plotted in figure 8, shows that the moment rate reduction increases less rapidly with creep fraction than in UCERF2; the latter is a straight line with a slope of 1.0. For each fault section, the partitioning between aseismicity factor and coupling coefficient depends on the creep fraction. For creep fractions less than 0.9:

aseismicity factor = creep fraction

coupling coefficient = 1.0

For creep fractions between 0.9 and 0.95, or for creep fractions between 0.9 and 1.0 on the San Andreas creeping section:

aseismicity factor = 0.9

coupling coefficient = 1.0 – 10 × (creep fraction – 0.9)

That is, coupling coefficient varies linearly from 0.0 to 0.5 for creep fractions between 0.9 and 0.95, with the relatively complicated functional form being needed to avoid double counting (*fig. 8B*). Values are capped for creep fractions above 0.95 according to:

aseismicity factor = 0.9

coupling coefficient = 0.5

As discussed in appendix N (this report), the transition threshold at 0.9 was chosen to ensure that the Parkfield segment of the San Andreas gets an area reduction consistent with the magnitude 6.0 events that have historically occurred on that fault section. Slip rate reductions on highly creeping faults act to limit the rate of throughgoing ruptures (for example, see appendix N for discussion of the San Andreas creeping section). The dependence on long-term slip rates (*fig. 8A*) implies that the moment rate reductions vary among the deformation models (average aseismicity factor and coupling coefficient values are listed for each fault section on the "OrigSlipRatesEtc" sheet of the *U3_FaultSectionData* file given in the Data and Resources section).
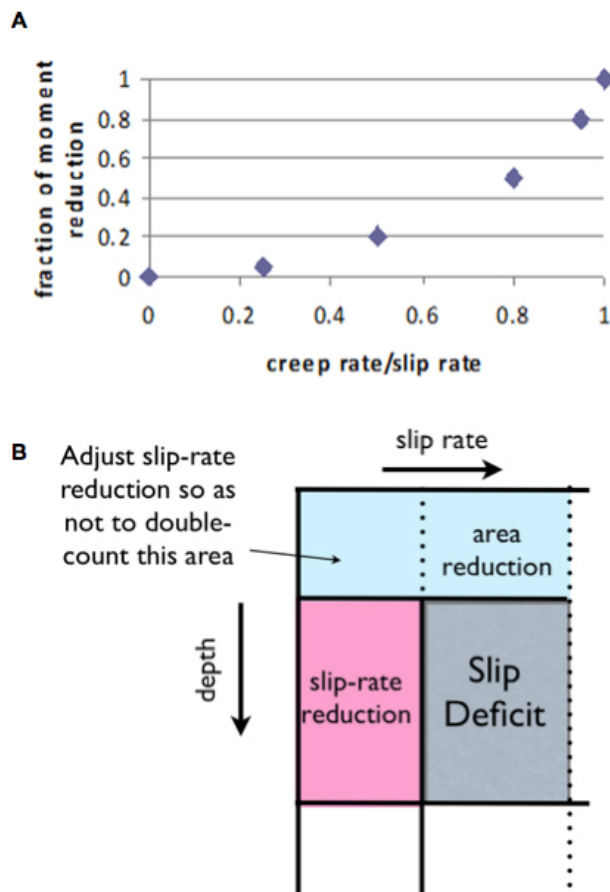
Figure 8.   Diagrams illustrating the adjustments to moment rate and slip rate due to creep. A, The UCERF3 creep model, which specifies moment rate reduction as a function of the ratio of creep rate to slip rate. B, The moment rate reductions in the UCERF3 creep model are applied in two ways— as an aseismicity factor, which reduces seismogenic area, and as a coupling coefficient, which reduces the slip rate. Details are discussed in the "Creep and Aseismicity" section.

In UCERF2, the moment rate reduction was set to zero for faults with no creep data. However, it is very difficult to recognize creep on most California faults where slip rates are on the order of a few mm/yr, especially for low creep fractions. To account for this observational bias, UCERF3 applies a default aseismicity factor of 0.1 where data are lacking, which is the approximate average over all fault sections that have data, including those that are known not to creep. This implies a default 10 percent reduction in area and, consequently, in moment rate.

Implied Moment Rates

Moment rate statistics for the UCERF3 deformation models are compared with UCERF2 in _table 4_. The total moment rates for the UCERF3 deformation models range from $2.76{\times}10^{19}$ N·m/yr to $2.85{\times}10^{19}$ N·m/yr, which is a 16 to 20 percent increase over the UCERF2 value of $2.37{\times}10^{19}$ N·m/yr; the latter includes both the seismic and aseismic contributions listed in _table 4_. This increase is consistent with the residuals shown in _figure 6B_, which are independent of the UCERF3 models. Also listed are the implied M_{max} and mean recurrence intervals for $M{\geq}8$ events

(assuming a truncated Gutenberg-Richter [GR] distribution), none of which appear to be unreasonable from a total moment rate perspective.

The on-fault moment rates for the UCERF3 models imply an increase between 1 and 17 percent relative to UCERF2, all of which is the result of adding new faults (total moment rate changes considering only the same faults vary between +1 and -17 percent). For the geologic deformation model, 49 percent of the new-fault increase comes from just two fault section additions: Cerro Prieto (0.083×10^{19} N·m/yr) and Mendocino (0.054×10^{19} N·m/yr).

Compared to UCERF2, off-fault moment rates increased from 37 to 60 percent among the new models. However, these total off-fault moment rates are not used as a direct constraint in UCERF3 (total moment rates are actually implied by other logic tree choices, as discussed below). In terms of the percentage of the total moment rate that is off-fault, the new deformation models have values between 32 and 37 percent, a bit higher than the UCERF2-implied value of 27 percent.

Figure 9 shows the spatial distribution of the off-fault and total moment rates given by the three GPS-based models (the geologic deformation model does not provide off-fault deformation), as well as total moment rate ratios with respect to UCERF2 and the UCERF3 average. In general, the UCERF3 models are in better agreement with each other than with UCERF2, at least for off-fault moment rates. The ratios with UCERF2 show biggest differences near the edges of the RELM region.

The total deformation model moment-rate distributions can be compared to smoothed seismicity, which was used in UCERF2 for setting off-fault earthquakes rates. As discussed in more detail below, two smoothed seismicity models are used in UCERF3, one from UCERF2, based on a 50-km Gaussian smoothing function, and a new model based on an adaptive smoothing approach given in appendix M (this report). Figure 10 compares the moment rate maps implied by these two smoothed seismicity models with that of the average UCERF3 deformation model (see figure caption for some important assumptions). The differences can be explained by one or more of the following: problems with the deformation models; temporal seismicity rate changes not reflected in the earthquake catalog; inadequate aftershock declustering in the smoothed seismicity maps; spatially dependent aseismicity; catalog completeness issues in some areas; the existence of characteristic magnitude-frequency distributions on faults; Gutenberg-Richter *b*-value and (or) maximum magnitude variability; or that there is no significant difference given overall uncertainties. We had originally hoped to set off-fault event rates using smoothed seismicity, and to then set maximum magnitudes to match the spatial variability of off-fault moment rates from the deformation models. This does not work, however, because some areas would need magnitudes greater than 10 to satisfy both the seismicity and deformation model moment rates.
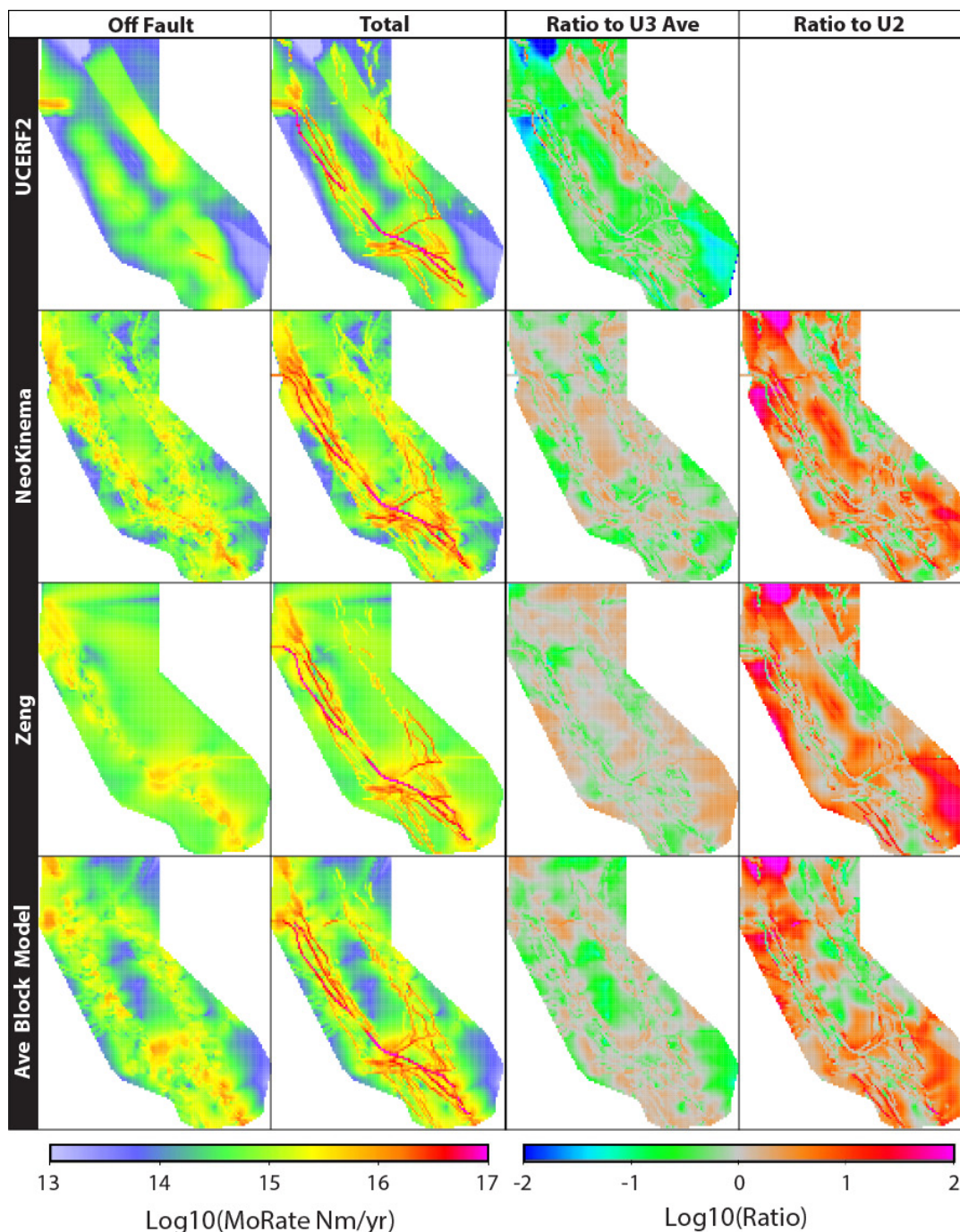
Figure 9. Maps showing spatial distribution of off-fault moment rates (first column) for the three UCERF3 deformation models that provide such estimates (for Fault Model 3.1 only), together with that implied by the UCERF2 forecast model (including both gridded sources and type C zones). Total moment rates (that is, including faults) are shown in the second column, and ratios with respect to the average UCERF3 results are shown in the third column (giving equal weight to each model, rather than the branch weights shown in figure 3). Ratios with respect to UCERF2 are shown in the fourth column. Details on how UCERF3 off-fault moment rate maps were computed, such as an assumed seismogenic thickness of 11 km, are given in appendix C (this report).
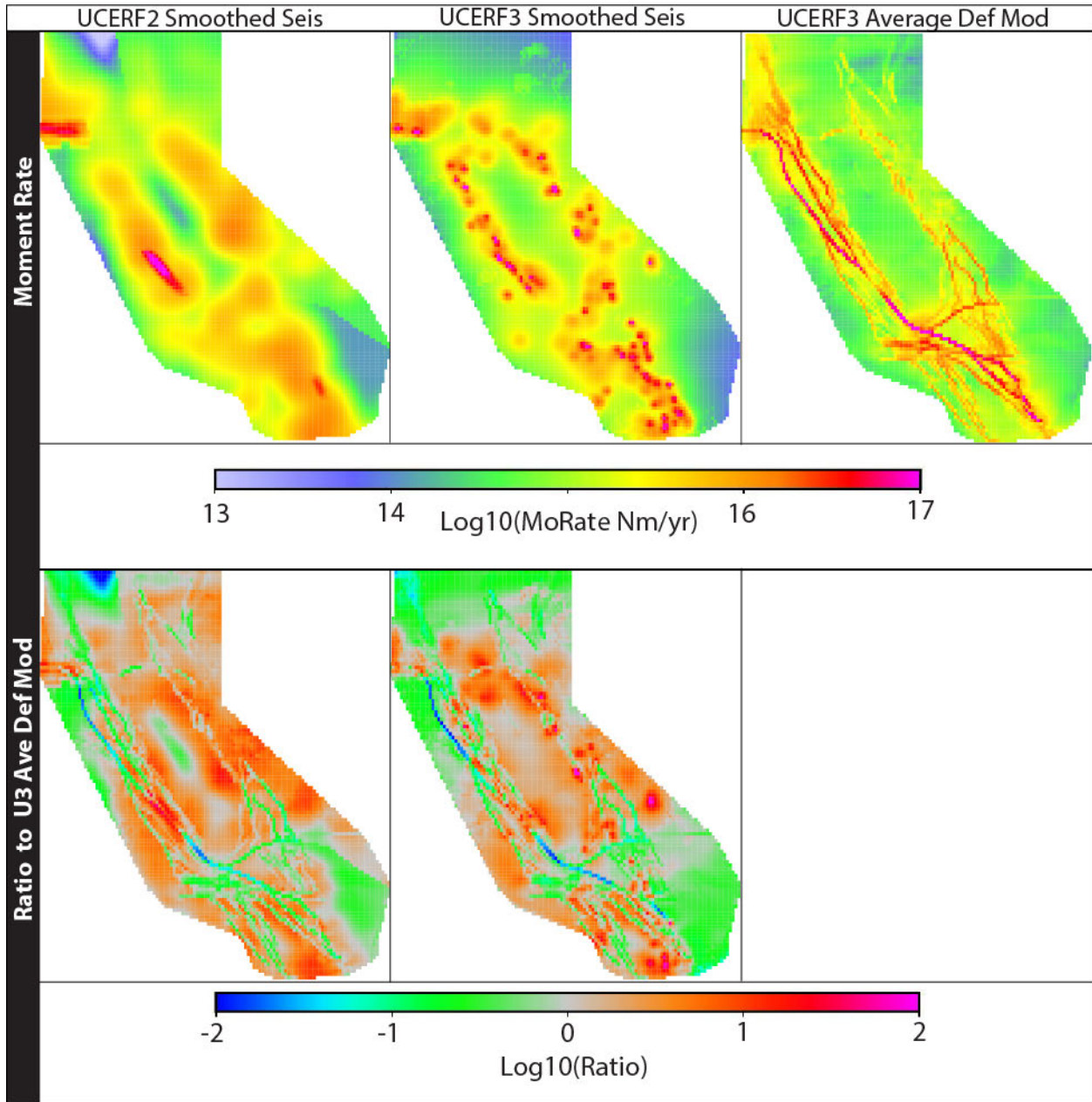
Figure 10. Maps showing the spatial distribution of moment rates implied by the UCERF2 smoothed seismicity model (Petersen and others, 2008b) and the new UCERF3 smoothed seismicity model (appendix M, this report), compared to the average UCERF3 deformation model (described in figure 9). The smoothed seismicity maps have the same total moment rate as the UCERF3 average, and they essentially assume a Gutenberg-Richter distribution with the same maximum magnitude everywhere. Also shown are ratios of the smoothed seismicity maps to the UCERF3 average (bottom row).

Logic Tree Branch Weights

A complete description of deformation-model weighting is given in appendix C (this report), only a brief summary of which is provided here. All the UCERF3 deformation models fit their input datasets within overall observational uncertainties. The models generally fit the geologic observations better than the geodetic data, mostly because the former were given higher weight to avoid strong along-fault slip rate variations that can occur when overfitting geodetic data. By design, the geologic deformation model fits the geologic data averages exactly. However, the geologic constraints on a significant fraction of California faults (~30 percent) are very weak to nonexistent, which was the primary reason to commission geodetic models in the first place. NeoKinema represents the best fit to GPS data, with average misfits three times lower than for the ABM and Zeng deformation models. The Zeng deformation model applies the minimum possible changes to geologic constraints in fitting GPS data and is explicitly constrained to stay within geologic bounds on most faults.

In addition to consistency with geologic and geodetic data, appendix C (this report) also ranks the models in terms of overall moment rate, fit to plate-tectonic rates and directions, and the amount of off-fault deformation. All information was given to an ad hoc expert committee for evaluation and weighting. Members had varying opinions with respect to the value of each evaluation metric, which led to a wide range of suggested branch weights, but most members gave more credence to geologic observations.

The models underwent further evaluation, review, and fine tuning following the ad hoc committee's deliberations, with three fault-by-fault review meetings being particularly influential (*table 2*). The final UCERF3 weights are (also shown in *figure 3*): NeoKinema (30 percent), Zeng (30 percent), ABM (10 percent), and geologic (30 percent).

The ABM deformation model has the lowest weight because it tends to have relatively high slip rates at its block boundaries, which might be an artifact of the approach. The Zeng deformation model reflects minimal changes to geologic constraints; therefore the collective weight for the "more geologic" models is 0.6, and that for the "more geodetic" models (ABM and NeoKinema) is 0.4. This balance reflects our perspective on the applicability of short-term geodetic signals versus relatively long-term geologic slip rates in determining earthquake likelihoods in California. Whether the optimum balance should vary with forecast duration is a question for further study. We also note that final UCERF3 models do not necessarily match all slip rates exactly, because these constraints are weighed against others in the inversion described below. These deformation models' weights are therefore a priori, and subject to effective modification.

Earthquake Rate Models and the "Grand Inversion"

The earthquake rate component of the UCERF3 model framework (*fig. 2*) defines the long-term rate of all possible earthquake ruptures above the magnitude threshold, $M{\geq}5$, and with a discretization sufficient to represent hazard. Each earthquake rate model comprises two types of sources: ruptures with dimensions larger than the seismogenic depth occurring on explicitly modeled faults (supraseismogenic on-fault ruptures); and other earthquakes, modeled as seismicity on a 0.1°×0.1° geographic grid with each cell assigned a magnitude-frequency distribution (MFD) of earthquake nucleation rates. The gridded seismicity is separated into events inside a fault zone polygon (subseismogenic on-fault ruptures), and those outside all fault

zone polygons (off-fault ruptures). Cells partly inside and partly outside a fault zone polygon are fractionally apportioned. The complete bookkeeping details are given in appendix O (this report).

In UCERF2, the models for each fault were constructed separately, and background seismicity was then added. The UCERF3 procedure solves for the rates of all events simultaneously using the inversion method of Field and Page (2011), which builds on the work of Andrews and Schwerer (2000). This unified, system-level approach enables the relaxation of fault segmentation and the inclusion of multifault ruptures, two major goals of UCERF3. Its implementation has been dubbed the "grand inversion." Aftershocks are included in the UCERF3 long-term rate model. To facilitate certain applications, we provide a procedure for removing aftershocks that is consistent with previous NSHMP practice.

Methodology

We first consider only those ruptures that occur on the faults included in the UCERF3 fault and deformation models and only model events that have rupture lengths greater than or equal to the local seismogenic thickness. To relax segmentation, we subdivide each fault section into S equal-length subsections with lengths that are about half the seismogenic thickness, resulting in S=2606 for FM 3.1 (*fig. 11*) and 2664 for FM 3.2. The surfaces of possible ruptures are taken to be the complete set of two or more contiguous fault subsections. Requiring at least two subsections ensures that the minimum rupture lengths are approximately equal to the seismogenic thickness. The rupture set is filtered by retaining only ruptures that pass all of the following "plausibility" criteria, as detailed in appendix T (this report):

- All fault sections connect within 5 km or less, as assessed in appendix J (this report).
- Ruptures cannot include a subsection more than once.
- Ruptures must contain at least two subsections of any main fault section, unless the only way two fault sections can connect is through a single-subsection connector, as described in appendix T (this report).
- Ruptures can only jump between fault sections at their closest points (in 3D).
- The maximum azimuth change between neighboring subsections is 60º, except for left-lateral to right-lateral connections such as Garlock to the San Andreas.
- The maximum azimuth change between the first and last subsection is 60º, except for left-lateral to right-lateral connections such as Garlock to the San Andreas.
- The maximum cumulative rake change (summing over each neighboring subsection pair) is 180º, based on rakes of the geologic deformation model to ensure rupture-set consistency.
- The maximum cumulative azimuth change, computed by summing absolute values over each neighboring subsection pair, is less than 560º (a filter that reduces "squirreliness"; that is, many changes of azimuth).
- Branch points (potential connections between main fault sections) must pass a Coulomb criterion that earthquake triggering between the two fault sections is physically reasonable, as described in appendix T (this report).
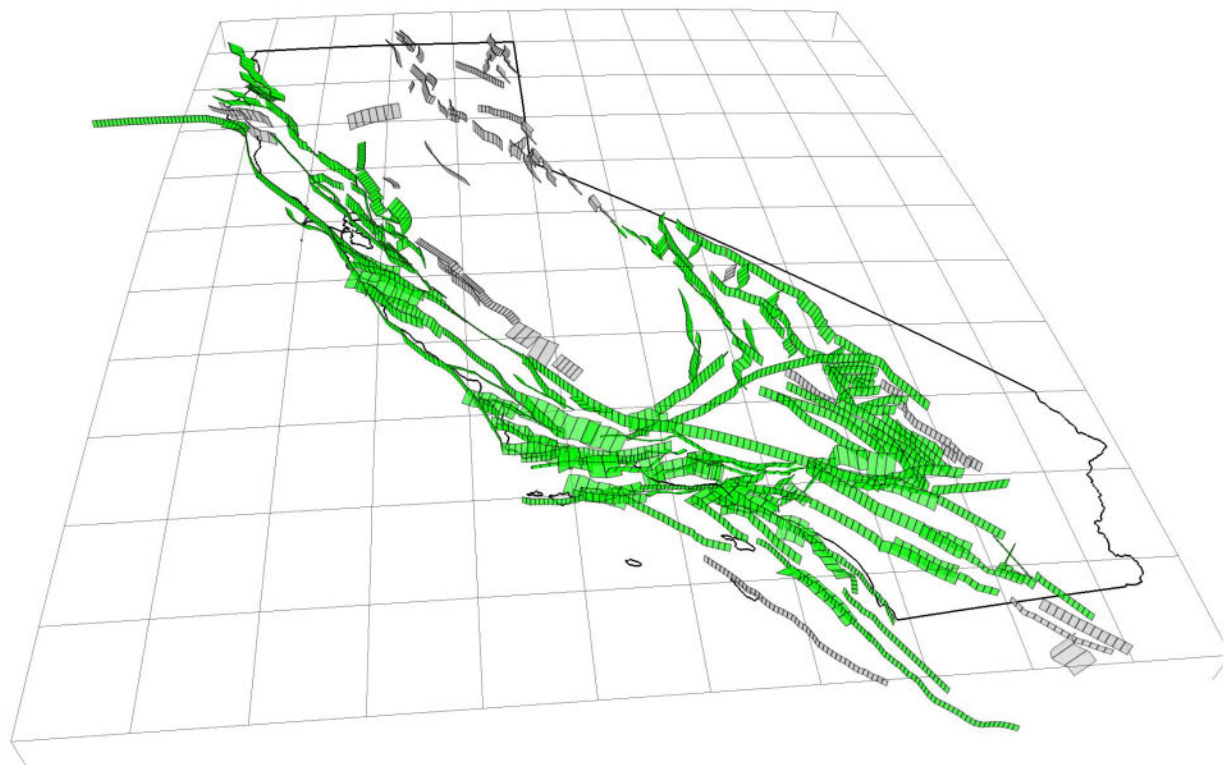
Figure 11.   Map showing UCERF3 Fault Model 3.1 sections divided into an integral number of equal length subsections (lengths equal to, or just less than, half the section's seismogenic thickness). All subsections shown in green are connected to all others in green without jumping more than 5 km between faults.

This filtering produces 253,706 and 305,709 unique "viable" ruptures for FM 3.1 and FM 3.2, respectively. In comparison, mapping the UCERF2 ruptures onto their nearest equivalents in the FM 3.1 yields only 7,773 ruptures. The much larger UCERF3 rupture set reflects the high connectivity of California's fault system—nearly all the fault sections connect to each other without jumping more than 5 km (green subset in *figure 11*). Again, it is believed that ignoring this connectivity in UCERF2 may have contributed to an overprediction of moderate sized earthquake rates. In any case, UCERF2 generally lacks types of multifault ruptures that have been seen in nature.

It is important to note, however, that UCERF3 rupture sets are still an approximation of the system. For example, the 5-km fault separation cutoff, which is based on both theoretical and empirical studies (Harris and Day, 1993; Wesnousky, 2006), presumes knowledge of fault connectivity at depth that we do not have. Of the "viable" ruptures that pass the above test, one could almost certainly identify at least a few that are in some ways less likely than ruptures that have been filtered out. The relevant question is whether the current approach is a better approximation than largely ignoring multifault ruptures (as in UCERF2). Moreover, seismic hazard is more sensitive to the combined magnitude-frequency distribution of nearby faults, rather than to the details of individual ruptures, as will be discussed below.

The inversion method estimates the long-term rates of the R viable ruptures $\{f_r : r = 1, 2, \ldots, R\}$ by solving the system of equations described in *table 5*. The equations can be weighted by

the uncertainties in the data and (or) by the degree of belief in the importance of a particular constraint. Conceptually, this approach is simpler, more objective, and more reproducible than that adopted in UCERF2. For example, the (largely artificial) distinction between type A and type B faults has been dropped, and type C zones have been merged into off-fault seismicity.

In addition to setting equation-set weights, subjectivity is also involved in assigning weights to alternative logic tree branches. Both of these, however, can be guided by how well the models fit the data. What the grand inversion really represents is a system-level framework for both incorporating expert opinion and for identifying a more complete range of models that are consistent with all available data. The framework is also extensible, in that other equations-set constraints could easily be added to the list in table 5; as we said repeatedly during development and review—tell us what you don't like about a result and you have given us a new inversion constraint.

In an exploratory study, Field and Page (2011) solved the inverse problem by the nonnegative least squares algorithm of Lawson and Hanson (1974). This algorithm is not computationally feasible for an inversion using the statewide system of faults. Therefore, we have developed a parallelized code that can efficiently solve very large equation sets by simulated annealing, as described in appendix N (this report). Owing to the stochastic nature of the algorithm, simulated annealing can also provide a range of models that sample the solution space of the inverse problem, which generally is underdetermined, or mixed-determined at best. This sampling can be used to represent the epistemic uncertainty associated with model nonuniqueness.

Appendix N also discusses a number of important inversion implementation details, including the tuning of equation-set weights, the sensitivity of the results to those weights, final misfits with respect to the various data constraints, reproducibility tests based on synthetic datasets, and alternative simulated annealing algorithms.

Implementation Ingredients

This section describes the various data and models used in the grand inversion, organized according to the equation sets of *table 5*.

Slip Rate Balancing (Equation Set 1)

Equation set 1 of table 5 involves satisfying the fault section slip rates (v_s) defined by the given deformation model. Doing so requires knowledge of the average slip on the sth subsection in the rth rupture (D_{sr}), where the average is over multiple occurrences of the event, and where the slip value is that at midseismogenic depths. Using such slip rate matching, rather than the moment rate balancing of previous WGCEPS, avoids potential depth-of-rupture ambiguities. We first compute the average slip for a given rupture, D_r, and then partition this among the subsections to get D_{sr}.

Table 5. The grand inversion system of equations used in solving for the long-term rate of fault-based ruptures, where f_r represents the frequency or rate of the rth rupture.

[Important implementation details, such as equation-set weighting, are given in appendix N (this report)]

Equation set		Description
$$\sum_{r=1}^{R} D_{sr} f_r = v_s$$	(1)	**Slip Rate Balancing**: v_s is the subsection slip rate (from a deformation model) and D_{sr} is the slip on the sth subsection in the rth event, averaged over multiple occurrences of the rupture and as measured at mid-seismogenic depth.
$$\sum_{r=1}^{R} G_{sr} P_r^{paleo} f_r = f_s^{paleo}$$	(2)	**Paleoseismic Event Rate Matching**: f_s^{paleo} is a paleoseismically inferred event rate estimate, G_{sr} specifies whether the rth rupture utilizes the sth subsection (0 or 1), and P_r^{paleo} is the probability that the rth rupture would be seen in a paleoseismic trench.
$$R_s^m = \frac{R_{s-1}^m + R_{s+1}^m}{2}$$	(3)	**Fault Section Smoothness Constraint**: This enables forcing the nucleation rate, R, in the mth magnitude bin to vary smoothly along a fault section, where the s-1 and s+1 subsections are adjacent to the sth subsection.
$$\lambda_r f_r = 0$$	(4)	**Improbability Constraint**: This allows us to force relatively improbable events to have a lower rate (for example, based on multi-fault rupture likelihoods). A higher value of adds more misfit for a given rupture rate, forcing the inversion to minimize that rupture rate further.
$$f_r = f_r^{a-priori}$$	(5)	**A Priori Constraint**: This constrains the rates of particular ruptures to target values, either on an individual basis (for example, make Parkfield occur every ~25 years) or for a complete rupture set (for example, as close as possible to those in UCERF2).
$$\sum_{r=1}^{R} M_{gr}^m f_r = R_g^m$$	(6)	**Regional MFD Constraint**: This enables forcing a geographic region, g, to have a specified magnitude-frequency distribution (MFD), such as Gutenberg-Richter. R_g^m represents the nucleation rate for the mth magnitude bin in the gth region. Matrix $M_{gr}^m f_r$ contains the product of whether the rth rupture falls in the mth magnitude bin (0 or 1) multiplied by the fraction of that rupture that nucleates in the gth region.
$$\sum_{r=1}^{R} M_{sr}^m f_r = R_s^m$$	(7)	**Fault Section MFD Constraint**: This enables forcing subsections to have specific nucleation MFDs. R_s^m is the nucleation rate for the mth magnitude bin on the sth subsection. Matrix $M_{sr}^m f_r$ contains the product of whether the rth rupture falls in the mth magnitude bin (0 or 1) multiplied by the fraction of that rupture that nucleates on the sth subsection.

The magnitude of each rupture is computed from a magnitude-area relationship, $M(A_r)$. In UCERF2 the Hanks and Bakun (2008) and Ellsworth B (Working Group on California Earthquake Probabilities, 2003) relationships were used with equal weights. For UCERF3, we have also included a slightly modified version of the Shaw (2009) relationship, as justified in Shaw (2013) and appendix E (this report). These three relationships, referred to hereafter as HanksBakun08, EllsworthB, and Shaw09mod, are plotted in figure 12, and their functional forms are as follows:

$$M = 3.98 + \log(A) \qquad if\ A \leq 537\ km^2 \ \ (M \leq 6.71) \qquad\qquad \text{HankBakun08}$$
$$M = 3.07 + (4/3)\log(A) \quad if\ A > 537\ km^2 \qquad\qquad\qquad \text{(Hanks and Bakun, 2008)}$$

$$M = 4.2 + \log(A) \qquad\qquad\qquad\qquad\qquad\qquad\qquad\qquad \text{EllsworthB}$$
$$\text{(WGCEP, 2003)}$$

$$M = 3.98 + \log(A) + (2/3)\log\left(\frac{2\,Max\left(1.0, \sqrt{A/W_o^2}\right)}{1 + Max\left(1.0, \left(\frac{A}{7.4W_o^2}\right)\right)}\right) \qquad\qquad \text{Shaw09mod}$$
$$\text{(Shaw, 2009, 2013)}$$

where M is magnitude, A is area (km), and W_o is the original downdip width (unreduced by aseismicity).

Two different approaches are used to get D_r for each rupture. One, used in UCERF2, involves converting the magnitude from the $M(A_r)$ relationship to moment and then dividing by the rupture area A_r and shear modulus μ to get D_r:

$$D_r = \frac{Mo_r}{\mu A_r} = \frac{10^{1.5*M(A_r)+9.05}}{\mu A_r}$$

where Mo_r is the moment of the rth rupture. The shear modulus (μ) is assumed to be 3.0×10^{10} Pa throughout this report.

Because A_r is based on the depth of microseismicity, D_r might be an overestimate if slip extends below such depths in larger ruptures. Therefore, an alternative is to obtain D_r using one of two viable slip-length scaling relationships, which have been derived from surface-slip observations (Shaw, 2013) and updated here in appendix E (this report) using the enhanced UCERF3 surface slip database in appendix F (this report). The first, which assumes slip scales as the square root of length, is given as:

$$D_r = 0.22\sqrt{L_r} \qquad\qquad\qquad\qquad\qquad \text{SqrtLength}$$

The second, which assumes constant stress drop, is given as:

$$D_r = 0.151\left[\frac{7}{3L_r} + \frac{1}{30}\right]^{-1} \qquad\qquad\qquad \text{ConstStressDrop}$$

where D_r is average slip in meters and L_r is length in km. Appendix E (this report) gives the full functional forms in terms of physical parameters. Neither of these relationships is applicable

when the average aseismicity factor is ≥0.2; in such cases, D_r is obtained from magnitude and area, as described above.

Examples obtained using these two slip-length models, as well as using the three magnitude-area relationships above, are given in *figure 12* (bottom). The slip-length models generally give a smaller D_r for longer ruptures, which could be real (for example, due to slip penetrating below the depth of microseismicity) or it could represent a bias in slip measurements (for example, surface values being lower than those at seismogenic depths). Adding these slip-length relationships therefore provides an element of epistemic uncertainty not included in UCERF2.
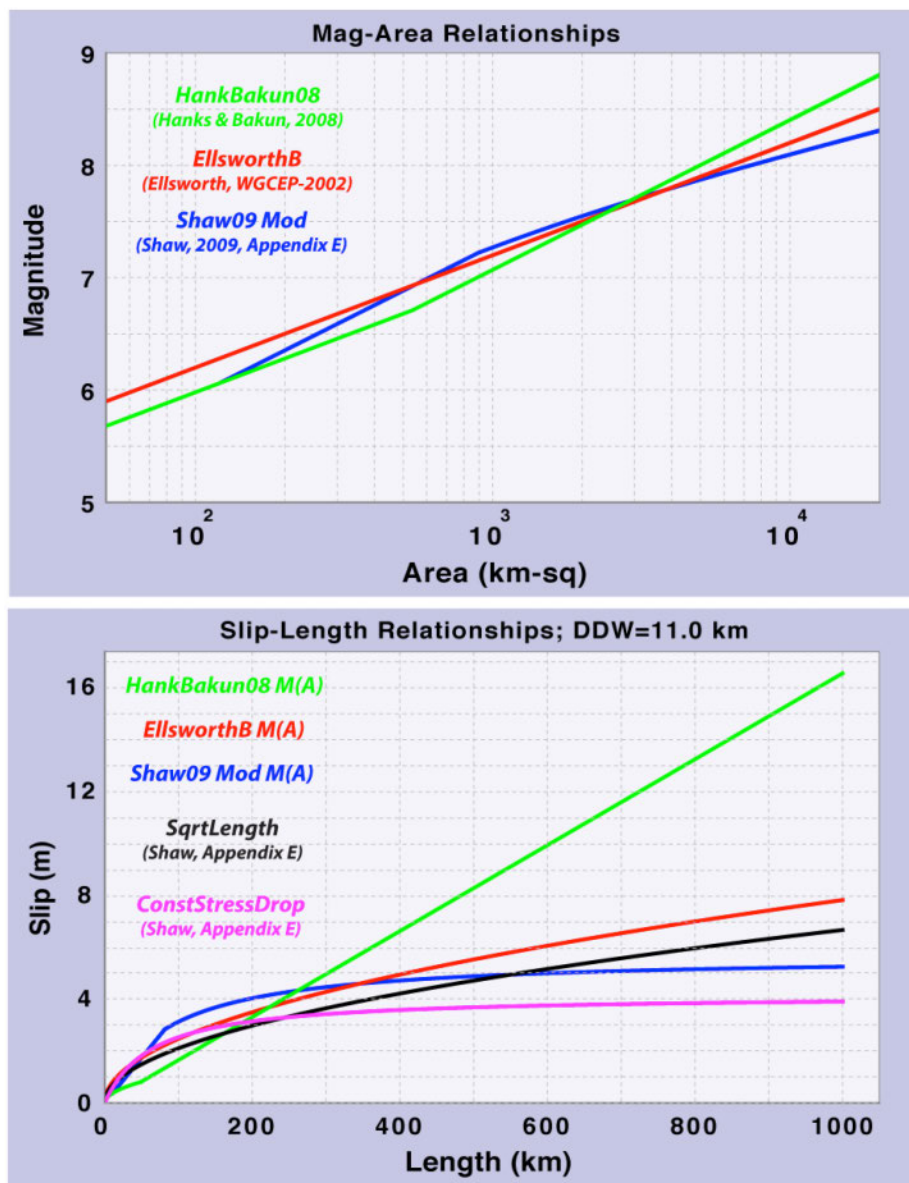
Figure 12. Graphs showing the magnitude-area (top) and slip-length (bottom) relationships used in UCERF3, which are documented in appendix E (this report). The *M(A)*-derived slip-length curves at the bottom assume an average seismogenic thickness of 11 km in converting area to length.

As discussed in appendix E (this report), some magnitude-area and slip-length relationship combinations are incompatible with the underlying assumptions. For example, using HanksBakun08 to get magnitude from area and then using ConstStressDrop to get slip from length can lead to unreasonably large widths for long ruptures..

Table 6 lists the combinations allowed in UCERF3, together with their associated weights, which are also shown in figure 3. All branches are given equal weight in UCERF3.

Table 6.   Magnitude-area and slip-length model combinations used in UCERF3*

Magnitude-Area Relationship	Slip-length Relationship	Branch Weight
EllsworthB	EllsworthB	20%
HanksBakun08	HanksBakun08	20%
Shaw09mod	Shaw09mod	20%
EllsworthB	SqrtLength	20%
Shaw09mod	ConstStressDrop	20%

*See appendix E (this report) for equations and explanations.

We need to partition D_r among the subsections used by each rupture to get D_{sr}, which again represents the average over multiple occurrences of the rupture. As discussed in appendix F (this report), the preferred choice is the observationally based "tapered-slip" (square-root-sine) model of Weldon and others (2008), which is shown in *figure 13*. This tapered-slip model was applied in UCERF2 when solving for the rate of ruptures on type A faults. The assumption here is that intraevent, along-strike slip variability averages out over multiple occurrences to yield the tapered shape. In UCERF3 this tapered-slip model is also applied to multifault ruptures, implying that there is no pinching out of the average slip at fault stepovers.
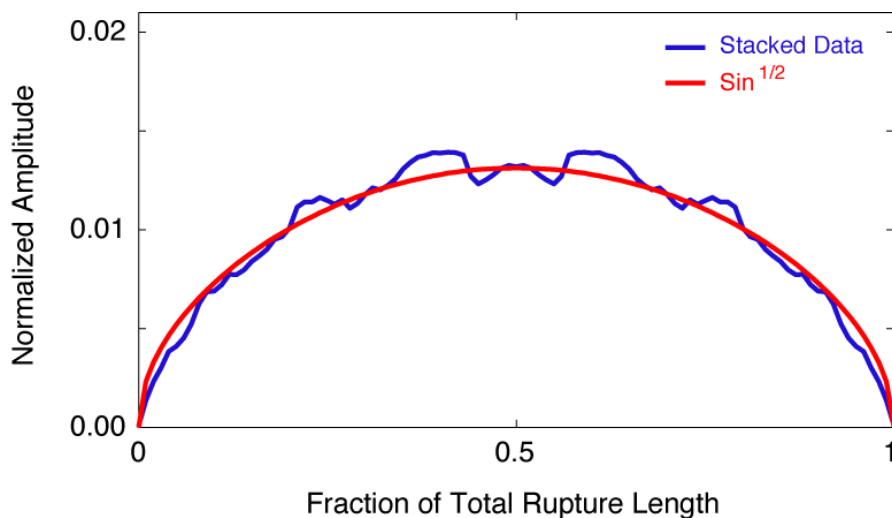
Figure 13.   Graph of mean rupture profile based on a stack of 13 mapped surface ruptures. The stack was obtained by normalizing the observed profiles to unit length and averaging them with their reflections about the midpoint. The details of this analysis are presented in UCERF2, appendix E (Weldon and others, 2008).

The choice of D_{sr} model should be consistent with how slip rates vary in the deformation model; for example, if slip is persistently low at fault stepovers, then the slip rates should be

33

lower there too. Because the deformation models do not resolve such along-strike slip rate variations, applying a multi-rainbow shape is not warranted, especially given the epistemic uncertainty about what is happening at seismogenic depths. However, because the deformation model slip rates do not ramp down toward the ends of faults that terminate (that is, where there are no connections to other faults), applying the tapered slip might artificially introduce a higher rate of smaller earthquakes to satisfy slip rates at these endpoints. To minimize this potential problem, UCERF3 also uses use a uniform (boxcar) slip distribution ($D_{sr} = D_r$) as an alternative logic tree branch, and the two options are given equal weight. A more correct solution may be to taper both the slip and the slip rates at fault terminations or intersections. Better observations are needed to constrain how the multifault slip functions actually vary in nature.

The UCERF3 framework is capable of applying the WGCEP (2003) D_{sr} model, in which the slip is proportional to the slip rate of each subsection. However, this option is given zero weight for the same reasons it was excluded in UCERF2—lack of observational support and implications that some ruptures cannot happen. There is some evidence to support a characteristic slip model where the amount of slip on a subsection is similar for all ruptures (Hecker and others, 2013), but applying this would be difficult because of very limited observational constraints, which would require the propagation of large epistemic uncertainties that have unknown spatial correlations. Instead, we compare the slip-per-event implications of UCERF3 with the results from Hecker and others (2013).

Because the inversion is solving for the rate of seismogenic thickness and larger ruptures, the slip rates in equation set 1 need be reduced to account for the moment released in subseismogenic events. This correction differs between Characteristic and Gutenberg-Richter logic tree branches (listed under Inversion Model in _figure 3_), details of which are given in the "Inversion Setup and Associated Gridded Seismicity" section.

Paleoseismic Event Rate Matching (Equation Set 2)

Equation set 2 matches event rates derived from paleoseismic trench studies. Not all ruptures that occur beneath a site are paleoseismicially observable, so we use the factor P_r^{paleo} to specify the probability that the rth rupture will be seen in a trench study. In UCERF3, there are two types of event rate constraints: direct event rates derived from paleoseismically observed dates of events; and proxy event rates obtained from average slip-per-event data, where the proxy rate equals slip rate divided by the average slip. We distinguish f_r^{paleo} and P_r^{paleo} for these two data types as $f_r^{paleo-event-rate}$ and $P_r^{paleo-event-rate}$ versus $f_r^{paleo-slip-proxy}$ and $P_r^{paleo-slip-proxy}$, respectively.

Appendix G (this report) provides an updated compilation of event dates for various paleoseismic studies in California, and appendix H (this report) provides estimates of the mean paleoseismic event rates, $f_r^{paleo-event-rate}$, implied by these data. The updated rates are compared with values used in UCERF2 in _table 7_, where we now have 31 constraints (9 more than in UCERF2).

A new model for the probability of seeing a given rupture in a trench, $P_r^{paleo-event-rate}$, is given in appendix I (this report). The probability depends on both the average slip of the rupture, D_r, and the position of the site relative to the nearest end of the rupture, implying that one is less likely to observe surface offsets near the ends of a rupture, consistent with the tapered slip model. _Table 8_ lists representative values for $P_r^{paleo-event-rate}$. In principle, this could be

done on a trench-by-trench basis to account for the unique depositional environment at each site. The probability model adopted in UCERF3, however, is generic.

Appendix R (this report) provides a compilation of average slip-per-event data, derived from either offset features or paleoseismic trench studies where available for California faults. These are reproduced here in *table 9*, which also lists the associated proxy event rates, $f_r^{paleo-slip-proxy}$, implied by each deformation model. Although measurement uncertainties are given for the average slips in appendix R, the associated confidence bounds are not listed in *table 9* because they do not reflect the additional uncertainty due to the limited sampling of events. Appendix R also provides a model for $P_r^{paleo-slip-proxy}$, which represents a simple linear interpolation between the values listed here in *table 10*.

Fault Section Smoothness Constraint (Equation Set 3)

A problem we encountered in an earlier version of the model (UCERF3.0) was that, in satisfying the above paleoseismic event rates, the inversion would simply put a high (or low) rate of events right at the paleoseismic sites. This produced artificially sharp peaks and troughs in the rate of events along strike. Equation set 3 mitigates this behavior by providing an along-fault smoothing constraint that minimizes curvature in the along-fault rate of events. We apply this smoothing only to fault sections that have one or more paleoseismic event-rate constraints, and confine it to the internal subsections of that section. That is, we do not apply this smoothing beyond the ends of fault sections, because this would require additional assumptions and careful bookkeeping at fault branches.

Improbability Constraint (Equation Set 4)

Improbability constraints can force a lower rate on any designated event or event type, such as multifault ruptures involving large jumps. Appendix J (this report) summarizes the various observational and theoretical studies that can guide the assignment of improbability constraints. However, the Coulomb stress-transfer calculations given in appendix T (this report) were used to cull the total UCERF3 rupture set down to a subset deemed viable. Furthermore, the rates of multifault ruptures are already constrained in the inversion by both slip rate balancing (larger ruptures consume more slip) and by the regional GR constraint (larger events have lower collective rates), rendering an improbability constraint somewhat redundant. We therefore have not applied any improbability constraints in UCERF3, and this choice is supported by results presented below.

Table 7. Event rate estimates and mean recurrence intervals (MRIs) at paleoseismic sites from appendix H (this report), based on the data compilation in appendix G (this report).

[Comparisons to UCERF2 MRIs are also listed for sites that had data in that study. The "16%" and "84%" columns represent the 68-percent confidence bounds for the mean estimates]

Site	Lat	Lon	Mean Rate (per yr)	16%	84%	MRI (yr)	16%	84%	UCERF2
Calaveras fault - North	37.5104	-121.8346	1.62E-03	1.16E-03	2.24E-03	618	446	859	445
Compton	33.9660	-118.2629	3.76E-04	2.46E-04	5.72E-04	2658	1748	4059	
Elsinore - Glen Ivy	33.7701	-117.4909	5.58E-03	4.63E-03	6.77E-03	179	148	216	291
Elsinore Fault - Julian	33.2071	-116.7273	3.08E-04	5.35E-05	5.62E-04	3251	1779	18702	1193
Elsinore - Temecula	33.4100	-117.0400	9.81E-04	5.23E-04	1.88E-03	1019	533	1914	741
Elsinore - Whittier	33.9303	-117.8437	3.13E-04	5.45E-05	5.73E-04	3197	1747	18358	1256
Frazier Mountian, SSAF	34.8122	-118.9034	6.73E-03	4.97E-03	9.09E-03	149	110	201	
Garlock Central (all events)	35.4441	-117.6815	6.97E-04	4.59E-04	1.06E-03	1435	941	2178	729
Garlock - Western (all events)	34.9868	-118.5080	8.13E-04	5.29E-04	1.25E-03	1230	798	1889	711
Green Valley - Mason Road	38.2341	-122.1619	3.41E-03	2.50E-03	4.66E-03	293	215	399	
Hayward fault - North	37.9306	-122.2977	3.14E-03	2.52E-03	3.92E-03	318	255	396	363
Hayward fault - South	37.5563	-121.9739	5.97E-03	5.24E-03	6.80E-03	168	147	191	210
N. San Andreas - Alder Creek	38.9813	-123.6770	1.15E-03	2.01E-04	2.11E-03	870	474	4984	
N. San Andreas - Santa Cruz	36.9626	-121.6981	9.10E-03	7.04E-03	1.18E-02	110	85	142	115
N. San Andreas - Fort Ross	38.5200	-123.2400	3.27E-03	2.74E-03	3.88E-03	306	258	366	360
N. San Andreas - North Coast	38.0320	-122.7891	3.79E-03	3.03E-03	4.73E-03	264	211	330	248
N. San Andreas -Offshore Noyo	39.5167	-124.3333	5.33E-03	4.63E-03	6.14E-03	188	163	216	
Puente Hills	33.9053	-118.1104	2.85E-04	2.32E-04	3.52E-04	3506	2842	4313	
San Gregorio - North	37.5207	-122.5135	9.81E-04	1.72E-04	1.80E-03	1019	554	5824	480
Rodgers Creek	38.2623	-122.5334	3.07E-03	1.99E-03	4.79E-03	325	209	503	
San Jacinto - Hog Lake	33.6153	-116.7091	3.21E-03	2.41E-03	4.28E-03	312	234	416	233
San Jacinto - Superstition	32.9975	-115.9436	1.97E-03	1.07E-03	3.65E-03	508	274	938	402
S. SAF- Carrizo Bidart	35.2343	-119.7887	8.72E-03	6.49E-03	1.17E-02	115	86	154	
S. San Andreas – Burro Flats	33.9730	-116.8170	4.87E-03	3.68E-03	6.41E-03	205	156	272	234
S. San Andreas - Coachella	33.7274	-116.1701	5.60E-03	4.16E-03	7.55E-03	179	132	241	
S. San Andreas - Indio	33.7414	-116.1870	3.61E-03	2.81E-03	4.61E-03	277	217	357	358
S. San Andreas - Pallett Creek	34.4556	-117.8870	6.70E-03	5.45E-03	8.26E-03	149	121	184	136
S. San Andreas - Pitman Canyon	34.2544	-117.4340	5.76E-03	4.47E-03	7.41E-03	174	135	224	261
S. San Andreas - Plunge Creek	34.1158	-117.1370	4.87E-03	3.67E-03	6.28E-03	205	159	272	361
S. SAF M. Creek - 1000 Palms	33.8200	-116.3010	3.83E-03	3.07E-03	4.80E-03	261	208	326	303
S. San Andreas - Wrightwood	34.3697	-117.6680	9.43E-03	7.97E-03	1.12E-02	106	90	125	98

Table 8.   Example values from the probability of paleoseismic detection model (P_r^{paleo}) used in equation set 2 of the inversion, from appendix I (this report).

Average Slip (D$_r$, meters)	Magnitude (approximate)	Probability of Detection ("Dist" is fractional distances from end of rupture)		
		Dist = 0.05	Dist = 0.25	Dist = 0.5
0.08	5.5	0.01	0.02	0.02
0.16	6.0	0.06	0.11	0.14
0.88	6.5	0.53	0.62	0.64
2.04	7.0	0.80	0.82	0.83
3.20	7.5	0.95	0.96	0.97
4.36	8.0	0.98	0.99	0.99

Table 9.   Average slip data from appendix R (this report), where the first 17 rows are from table 5 therein (average slip from offset features), and the last 6 rows (shaded) are from table 6 therein (based on paleoseismic trench studies).

[Also listed are the proxy mean event rates and proxy mean recurrence intervals implied by each deformation model]

Fault Section, Subsection #	Lat[2]	Lon[2]	Average Slip (m)	ABM		Geologic		NeoKinema		Zeng	
				Proxy Rate	Proxy MRI	Proxy Rate	Proxy MRI	Proxy Rate	Proxy MRI	Proxy Rate	Proxy MRI
San Andreas (Carrizo) rev, 1	35.24	-119.79	3.52	7.57E-03	132	9.11E-03	110	8.52E-03	117	6.79E-03	147
San Andreas (Carrizo) rev, 5	35.05	-119.56	4.06	6.47E-03	155	7.89E-03	127	7.38E-03	135	5.88E-03	170
San Andreas (Carrizo) rev, 6	35.01	-119.50	4.61	5.66E-03	177	6.95E-03	144	6.50E-03	154	5.18E-03	193
San Andreas (Cholame) rev, 8	35.65	-120.20	2.50	1.06E-02	94	1.28E-02	78	9.47E-03	106	1.02E-02	98
San Andreas (Coachella) rev, 4	33.64	-116.06	2.99	6.12E-03	163	6.29E-03	159	5.16E-03	194	6.21E-03	161
San Andreas (Coachella) rev, 10	33.44	-115.82	3.20	5.73E-03	174	5.89E-03	170	4.83E-03	207	5.82E-03	172
San Andreas (Mojave S), 2	34.64	-118.35	2.87	6.05E-03	165	1.07E-02	94	8.87E-03	113	6.56E-03	152
San Andreas (Mojave S), 3	34.62	-118.28	2.85	6.08E-03	164	1.07E-02	93	8.92E-03	112	6.60E-03	152
Elsinore (Julian), 5	33.24	-116.78	1.12	2.99E-03	334	2.52E-03	396	1.23E-03	815	2.18E-03	458
Garlock (West), 10	35.13	-118.22	4.68	8.66E-04	1155	1.53E-03	654	1.15E-03	873	3.37E-04	2971
Garlock (West), 12	35.20	-118.09	3.46	1.23E-03	813	2.07E-03	484	1.55E-03	646	4.55E-04	2199

Fault Section, Subsection #[1]	Lat[2]	Lon[2]	Average Slip (m)	ABM		Geologic		NeoKinema		Zeng	
				Proxy Rate	Proxy MRI	Proxy Rate	Proxy MRI	Proxy Rate	Proxy MRI	Proxy Rate	Proxy MRI
Garlock (Central), 15	35.57	-117.15	3.11	1.12E-03	892	2.12E-03	472	1.68E-03	595	2.27E-03	441
San Jacinto (Anza) rev, 1	33.68	-116.82	1.87	4.61E-03	217	7.05E-03	142	5.97E-03	168	6.46E-03	155
San Jacinto (Anza) rev, 5	33.51	-116.55	1.44	5.99E-03	167	9.15E-03	109	7.74E-03	129	8.38E-03	119
San Jacinto (Clark) rev, 0	33.47	-116.48	2.94	1.92E-03	521	2.57E-03	390	1.56E-03	641	1.99E-03	504
San Jacinto (Clark) rev, 1	33.43	-116.41	2.50	2.25E-03	444	3.01E-03	332	1.83E-03	546	2.33E-03	429
San Jacinto (Clark) rev, 4	33.31	-116.21	1.30	2.48E-03	404	3.52E-03	284	3.52E-03	284	4.49E-03	223
Compton, 2	33.97	-118.26	2.80	2.85E-04	3510	3.03E-04	3303	2.89E-04	3456	3.97E-04	2516
Puente Hills, 2	33.91	-118.11	2.77	2.05E-04	4872	3.06E-04	3264	4.02E-04	2485	4.34E-04	2304
Puente Hills, 2	33.91	-118.11	2.93	1.94E-04	5166	2.89E-04	3461	3.80E-04	2634	4.09E-04	2443
San Andreas (Carrizo) rev, 0	35.27	-119.83	5.42	4.91E-03	204	5.91E-03	169	5.53E-03	181	4.40E-03	227
San Andreas (Mojave S), 13	34.37	-117.67	3.15	5.51E-03	181	9.72E-03	103	8.08E-03	124	5.98E-03	167
San Andreas (Mojave S), 9	34.46	-117.89	6.00	2.89E-03	346	5.10E-03	196	4.24E-03	236	3.14E-03	319

[1]Sections, subsections correspond to Fault Model 3.1.

[2]Location (Lat, Lon) is approximately halfway down the trace of fault subsection listed in column 1.

Table 10.   Probability of observing surface slip ($P_r^{paleo-slip-proxy}$) as given in appendix R (this report).

[Values are linearly interpolated between those listed]

Slip (D_{sr}, meters)	Probability of Detection
0.0	0.0
0.25	0.1
≥2.0	0.95

Total Regional Rate of M≥5 Events

A fundamental parameter and logic-tree branch choice is the total rate of M≥5 events per year, denoted $R_{M \geq 5}^{total}$, that occur within the UCERF3 model region (shown in _figure 1_). The

seismicity analysis in appendix L (this report) determines seismicity rates using data for the time periods 1850–2011 (historical and instrumental) and 1984–2011 (modern instrumental catalog). We use the UCERF2 catalog completeness thresholds calculated by Felzer (2008) for eight different regions and over a variety of different eras based on changes in data availability with time. One modification is a drop in the 1850–1865 completeness threshold from M8.0 to M7.4, based on the determination that an M>7.4 earthquake would probably have been felt over a sufficiently wide area to have been noted, despite the sparse population. The lower magnitude cutoff has also been reduced from M4 in UCERF2 to M2.5 here, and all rate calculations include the UCERF2 corrections for magnitude uncertainties and rounding errors (Felzer, 2008).

The rates for each era have been averaged together, weighted linearly by era duration. This differs from the Weichert (1980) method applied by the NSHMP and used in the UCERF2 smoothed seismicity model, where each era is weighted by the number of earthquakes contained. The Weichert (1980) method produces a more accurate result if the underlying rates are the same in each era. However, if the seismicity rate changes with time, as implied by the empirical models of WGCEP 2003 and 2007, the Weichert (1980) method produces a result that is heavily skewed towards the instrumental era. When computing an observed seismicity rate for UCERF2, the Weichert method was applied in three long time periods, and the results from those three time periods were averaged. This somewhat minimizes the effect of the weighting by the number of events in the Weichert method. By using more and smaller time periods in UCERF3, we have completely eliminated the assumptions of constant rate.

The 1850–2011 rate averages for each region were summed to obtain the total regional rate. A new global analogue model has also been used to account for possible temporal rate variations, leading to the following branch options for $R_{M\geq5}^{total}$: 6.5 events/yr (10 percent weight), 7.9 events/yr (60 percent weight), 9.6 events/yr (30 percent weight). The preferred value (7.9) is 5 percent greater than the value of 7.5 given in UCERF2 (see Felzer, 2008), and the branch-averaged UCERF3 value (8.3) is 11 percent greater than the UCERF2 value. In addition to dropping the Weichert method completely, part of this difference comes from 5 years of additional data and from decreasing the lower magnitude cutoff. Asymmetric weights are used here because the post-1850 era is more likely to be below, rather than above, the true average rate, especially given the lack of any $M\geq8$ events during this time period.

It is important to note that the UCERF2 observed value of 7.5 was not used as an explicit constraint in that model, with the final implied UCERF2 value (~5.8 $M\geq5$ events per year) being determined primarily by the smoothed seismicity model (see Petersen and others, 2008b). Therefore, the gridded seismicity component of UCERF2 is more consistent with recent seismicity rates, and thereby effectively includes the empirical time-dependent models of WGCEP 2003 and 2007. We believe the long-term rates are more appropriate for the UCERF3 earthquake rate model, especially given that users will be able to apply any empirical model correction that makes it into the forthcoming time-dependent components. As a consequence, the preferred UCERF3 rate (7.9) is 36 percent greater than the effective UCERF2 model rate (5.8), and the UCERF3 branch-averaged rate (8.3) is 43 percent greater.

Off-Fault Spatial Seis PDF

The spatial distribution of off-fault gridded seismicity is set by choosing one of the spatial probability density maps shown in *figure 14* (referred to as the Off-Fault Spatial Seis PDF logic-tree branch in *figure 3*, sometimes abbreviated as SpatialPDF here). One option is the UCERF2 smoothed seismicity map (*fig. 14A*) from the UCERF2, appendix J (Petersen and

others, 2008b)*,* which is based on the Frankel (1995) methodology. This represents $M{\geq}4$ events smoothed using 2D Gaussian kernel with a sigma of 50 km, and a somewhat narrower, anisotropic smoothing near a few active faults.
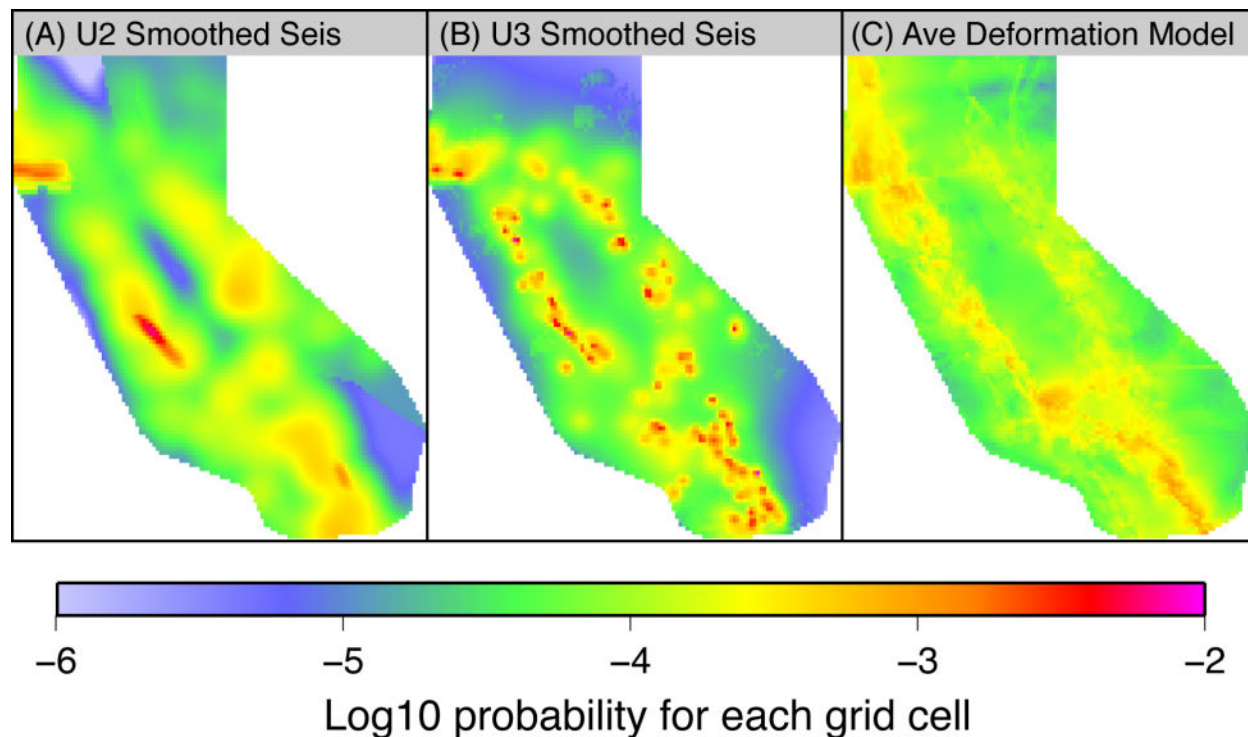
Figure 14. Maps showing the various off-fault spatial seismicity probability density functions (SpatialPDF) used in UCERF3 for setting gridded seismicity (referred to as the Off-Fault Spatial Seis PDF logic tree branch in figure 3). Values in each map sum to unity. *A*, The UCERF2 Smoothed Seismicity model. *B*, The UCERF3 Smoothed Seismicity model of Felzer (appendix M, this report), which has a higher resolution, adaptive smoothing kernel. *C*, SpatialPDF implied by the average of the off-fault moment rate maps from appendix C (this report), which includes the Average Block Model, NeoKinema, and Zeng deformation models, and averages over maps for both Fault Models 3.1 and 3.2.

Another SpatialPDF option is the "UCERF3 Smoothed Seismicity" map shown in figure 14*B*, which was developed by Felzer (appendix M, this report) using the adaptive smoothing algorithm of Helmstetter and others (2007). Specifically, this considers $M{\geq}2.5$ events, and the sigma of a 2D Gaussian smoothing kernel is determined by the distance to the nth closest earthquake, where $n{=}8$ was chosen here based on optimization tests given in appendix M. Such higher resolution smoothing has had superior performance in the formal RELM tests (for example, Zechar and others, 2013) and is more consistent with surveys of precariously balanced rocks (for example, Brune and others, 2006). Nevertheless, UCERF2 smoothing may be more appropriate for the larger events that dominate hazard ($M{>}6$), and (or) for the longer term forecasts of interest for building codes.

A third SpatialPDF option is to use the off-fault moment-rate map associated with the chosen deformation model (appendix C, this report), which was shown previously in figure 9, or the average of the three models that provide off-fault estimates (*fig. 14C*). The specification of

SpatialPDF branch weights differs between the Characteristic and Gutenberg-Richter Inversion Model options (*fig. 3*) and will therefore be discussed in the section on "Inversion Setup and Associated Gridded Seismicity".

Fraction of Seismicity On Versus Off Faults

Like previous WGCEP and NSHMP models, the UCERF3 framework explicitly differentiates between fault-based sources and off-fault (gridded) seismicity, starting with the deformation model. The fraction of observed seismicity attributable to on-fault versus off-fault events is implied by both the choice of SpatialPDF (*fig. 14*) and the fault zone polygons (as a proxy for all events within). Summing the PDF values inside all fault zones implies the following percentage of on-fault seismicity:

- 53 percent for UCERF2 smoothed seismicity paired with Fault Model 3.1
- 58 percent for UCERF2 smoothed seismicity paired with Fault Model 3.2
- 53 percent for UCERF3 smoothed seismicity paired with Fault Model 3.1
- 59 percent for UCERF3 smoothed seismicity paired with Fault Model 3.2

None of the deformation models are used to calculate the percentage of on-fault seismicity because doing so requires assuming the MFD at each location, as well as the fraction of moment that is released aseismically, both on- and off-fault.

Maximum Off-Fault Magnitude ($M_{max}^{off-fault}$)

Another logic tree choice is the assumed maximum magnitude of off-fault seismicity, $M_{max}^{off-fault}$. The three branch options applied in UCERF3 are 7.3, 7.6, and 7.9, with weights of 10, 80, and 10 percent, respectively (*fig. 3*). For UCERF2, $M_{max}^{off-fault}$ was spatially variable, being 7.6 in the type C zones and 7.0 for gridded seismicity elsewhere, with a custom reduction near faults to avoid double counting with fault-based sources. As such, $M_{max}^{off-fault}$ has increased in UCERF3 for areas away from faults and outside type C zones, driven in part by the 2010 M7.2 El Mayor-Cucapah earthquake exceeding the UCERF2 background-seismicity value of 7.0 (although whether this event was on- or off-fault is ambiguous in UCERF2, as noted above). Branch weights were based on expert-opinion consensus, with the low weight at M7.3 being driven by high, implied off-fault aseismicity (when comparing consequent moment rates to the deformation model values in *table 4*), and the low weight at M7.9 reflecting a lack of evidence for such events (even though they are rare). The fact that three $M_{max}^{off-fault}$ options are provided is an improvement over UCERF2, which only had a single branch for off-fault seismicity.

Inversion Setup and Associated Gridded Seismicity

Here we describe the "Characteristic" versus "Gutenberg-Richter" branch options for the Inversion Model (*fig. 3*), including their conceptual motivation, how the remaining inversion constraints are constructed, and how the gridded seismicity is specified for each option. A supplementary file *U3_PreInversionAnalysisTable,* given in the "Data and Resources" section, lists many of the metrics discussed here for each potential logic tree branch.

Characteristic Branches

These branches represent the possibility that faulting is governed by "characteristic behavior," which has come to mean one or more of the following: segmentation of faulting, in

which ruptures persistently terminate at certain locations; an increased rate of events at higher magnitudes compared to an extrapolation of the Gutenberg-Richter magnitude frequency distribution from smaller magnitudes; and a narrow range of slip from event to event at a point on a fault. In principle, these attributes could be implemented as direct constraints in the grand inversion. However, distilling the essence of a characteristic model into independent inversion constraints has proven difficult.

For the UCERF3 model presented here, the Characteristic branch is defined by forcing, via *equation set 7*, each fault subsection to stay as close as possible to an a priori characteristic nucleation MFD, in which there is an increased rate of higher magnitude events. For both the new faults and those designated as type B in UCERF2, the total nucleation MFD for each fault section was constructed by putting one-third of the moment rate into a Gutenberg-Richter distribution and two-thirds into a characteristic distribution. For the Gutenberg-Richter component the minimum magnitude was set by the smallest supraseismogenic rupture on that section; maximum magnitude was set by the total fault section area and the chosen magnitude-area relationship; *b*-value was set as 1.0 (aftershocks are included); and *a*-value was set to satisfy one-third of the section slip rate, reduced for subseismogenic ruptures as quantified below.

The characteristic component is represented with a single magnitude at the Gutenberg-Richter maximum magnitude, with an event rate that satisfies two-thirds of the slip rate (also reduced for subseismogenic ruptures). No aleatory variability in magnitude is given for the characteristic portion, although such variability can be added later for hazard calculations, as was done in UCERF2. The total characteristic nucleation MFD (the sum of both the Gutenberg-Richter and characteristic portions) is generally consistent with past NSHMP models. However, it is not exactly the same as that for type B faults in UCERF2, because the latter had branches both for connecting more type B faults (into megafaults) and for setting *b*-value to zero on the Gutenberg-Richter portion. These latter options were introduced in UCERF2 only to mitigate an overprediction of event rates near *M*6.7 (the bulge problem), which is handled directly in the UCERF3 grand inversion.

For fault sections that were designated as type A in UCERF2, the characteristic nucleation MFD constraint is defined as that implied by UCERF2, averaged over all branches. This approach preserves the extra attention given to type A faults in UCERF2. The resultant characteristic nucleation MFD derived for each fault section is then divided evenly among the associated subsections (for use in *equation set 7*), which provides some along-fault smoothness in event rates along the main fault sections. Depending on the weight assigned to *equation set 7*, the grand inversion tries to stay as close as possible to these characteristic nucleation MFDs.

For the regional MFD constraint in *equation set 6*, a target MFD for the entire region is first constructed from the chosen regional rate, $R_{M \geq 5}^{total}$, and the implied regional maximum magnitude, M_{max}. The latter is computed from the largest area rupture in the fault system (given the chosen deformation model and magnitude-area relationship). The target MFD is further assumed to be a perfect truncated Gutenberg-Richter distribution with a *b*-value of 1.0. This total MFD, an example of which is shown as the black curve in *figure 15*, is then partitioned into a supraseismogenic on-fault MFD for use in the regional MFD constraint of *equation set 6*, as well as MFDs for the subseismogenic on-fault seismicity and the truly off-fault seismicity.

Because a fault section is a proxy for all ruptures that nucleate within its fault zone polygon, the total rate of events for each fault section is determined by multiplying $R_{M \geq 5}^{total}$ by the sum of SpatialPDF values inside the section's fault zone polygon. Summing these rates over all fault sections gives the total rate of on-fault events (listed above, and illustrated on left side of

orange curve in *figure 15A*). Following UCERF2, the MFD for subseismogenic, on-fault ruptures is assumed to be Gutenberg-Richter up to the minimum magnitude of supraseismogenic ruptures. In UCERF2 this supraseismogenic transition was *M*6.5, except where the characteristic magnitude was less, whereas in UCERF3 the transition is fault-section dependent, owing to variations in seismogenic widths. Below the minimum supraseismogenic magnitudes, the total on-fault target MFD (orange curve in *figure 15A*) must be parallel to the total target (black curve) and offset by the difference between $R_{M \geq 5}^{total}$ and the total off-fault rate. Above the maximum magnitude of the off-fault events, $M_{max}^{off-fault}$, the total target on-fault MFD (orange curve) must match the total regional target (black curve). In other words, the total on-fault target MFD has a *b*-value of 1.0 above and below these two transition points and assumes a straight-line interpolation in between (in log-rate space), meaning a constant, lower *b*-value at intermediate magnitudes (*fig. 15A*).

The truly off-fault MFD (green curve in *figure 15A*) is simply the difference between the total target MFD (black curve) and the total on-fault target MFD (orange curve). The supraseismogenic, on-fault MFD, shown as the blue line in *figure 15B*, is the total on-fault target (orange curve) minus the total subseismogenic on-fault MFD (cyan curve, which represents the sum of all subseismogenic, on-fault MFDs described above).

The supraseismogenic, on-fault MFD (blue curve in *figure 15B*) summarizes the total of all regional MFD constraints represented by *equation set 6*. In principle, this total could be broken into arbitrarily small subregions, but uncertainties on the rates in smaller areas impose practical limits. For UCERF3, the total MFD was divided into just two regional constraints, one for northern and one for southern California. Furthermore, *equation set 6* is applied as an equality constraint below magnitude 7.85, and as an inequality constraint at higher magnitudes (appendix N, this report). The latter allows the final solution MFD to roll off more quickly than the target if allowed or required by the other data constraints.

The total gridded seismicity for UCERF3 (gray line in *figure 15B*) is the sum of the off-fault MFD (green) and the total subseismogenic on-fault MFD (cyan). This result is generally consistent with the total UCERF2 gridded seismicity (magenta line in *figure 15B*), though smoother in shape and exhibiting lower rates at some magnitudes (consistent with the added UCERF3 faults taking moment rate from the gridded seismicity). The red line in *figure 15B* shows the total MFD for fault-based sources in UCERF2, which by itself exceeds the total regional target around *M*7.0—the "bulge" described in the UCERF2 report—which is eliminated in the grand inversion by imposing the constraints of equation set 6. The brown line in *figure 15B* is the total MFD for UCERF2 (which equals magenta plus red).

Up to this point, the deformation-model moment rates (*table 4*) have not been used in constructing the various target MFDs. A useful pre-inversion diagnostic is to compute implied coupling coefficients, defined here as the moment rate of the target MFD divided by the deformation model moment rate from *table 4*. These diagnostics are listed separately for the total on-fault and off-fault model components, and for all logic tree branches, in the *U3_PreInversionAnalysisTable*. These implied coupling coefficients can exceed 1.0 if the target MFD implies more moment rate than exists in the deformation model.
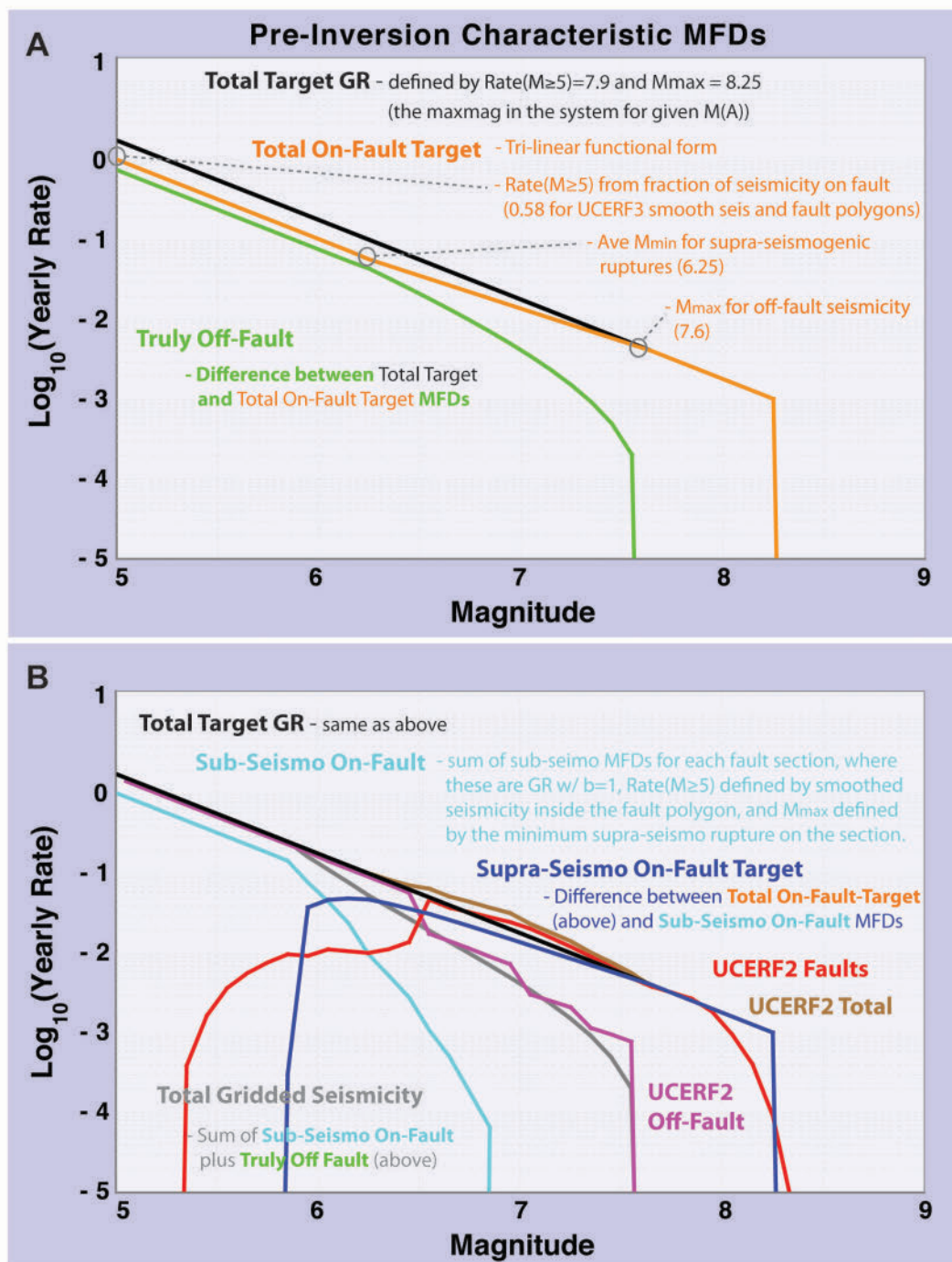
Figure 15.   Graphs showing examples of the various regional magnitude-frequency distributions (MFDs) considered in setting up the Characteristic Inversion Model branches. See labels and main text for an explanation of each curve. This example is for the reference branch, which is shown with bold elements in *figure 3. A*, Illustration of the total target Gutenberg-Richter, total on-fault target, and truly off-fault MFDs. *B*, Illustration of the subseismogenic on-fault, supraseismogenic on-fault target, total gridded seismicity, and equivalent MFDs from UCERF2.

The off-fault coupling coefficients implied for a given deformation model depend primarily on the choice of $R_{M \geq 5}^{total}$ and $M_{max}^{off-fault}$, and to a lesser extent on the SpatialPDF. The values implied from UCERF3 range from 0.17 (for NeoKinema deformation model with $R_{M \geq 5}^{total}$ = 7.6, $M_{max}^{off-fault}$ = 7.3, UCERF3 Smoothed Seismicity, and the Shaw09mod magnitude-area relationship) to 0.62 (for Geologic deformation model with $R_{M \geq 5}^{total}$ = 9.6, $M_{max}^{off-fault}$ = 7.9, $UCERF2$ Smoothed Seismicity, and the EllsworthB magnitude-area relationship); values for all braches are given in the *U3_PreInversionAnalysisTable*. These coupling coefficients imply off-fault moment rate reductions of 38 to 83 percent (relative to that predicted by the deformation models). One could alternatively tune $M_{max}^{off-fault}$ to some desired coupling coefficient. However, off-fault coupling coefficients are essentially unconstrained, and the parameterization in terms of $M_{max}^{off-fault}$ is more intuitive for most hazard analysts. The possibility of using the implied off-fault coupling coefficients in deciding a posteriori branch weights is not pursued here, although as noted above, it was a consideration in assigning the lower $M_{max}^{off-fault}$ value of 7.3 a relatively small weight (10 percent).

The on-fault coupling coefficients implied by the deformation models are more potentially useful to modify the model. Values greater than 1.0 are remedied by the inversion rolling off the final MFD more rapidly at highest magnitudes relative to the target. Values less than 1.0 imply the slip rates are higher than can be accommodated by the target MFD, and the UCERF3 logic tree consequently has four Fault Moment Rate Fix options for this:

- *Apply Implied Coupling Coefficient*—reduce the slip rates on all fault sections by the implied coupling coefficient.

- *Relax MFD Constraint*—permit an overprediction "bulge" in the final MFD if needed to satisfy slip rates.

- *Apply Both Options*—apply both of the above.

- *Do Nothing*—let the inversion decide where to reduce slip rates in matching the target MFD.

For UCERF3, only the Do Nothing option is given nonzero weight, because fault moment rate reductions are not an important issue for the characteristic models (the majority of implied on-fault coupling coefficient values are greater than 1.0, with the lowest being 0.86; *U3_PreInversionAnalysisTable*). This means the inversion will decide whether and where to reduce slip rates (balancing this against the other constraints in the inversion). An alternative approach might be to target specific faults with site-specific coupling coefficients. Indeed, the exclusion of the Mendocino, Cerro Prieto, and Brawley Faults from previous NSHMP models was apparently done for this reason. However, we presently lack any basis for applying fault-specific coupling coefficients (beyond those already applied), and we want to avoid excluding any major faults from consideration.

The Relax MFD Constraint might still be appealing in order to relax the regional GR constraint (because there is some chance the UCERF2 bulge is real, even though there is no supporting evidence for it). The result of doing so, however, is quite consistent with keeping the GR constraint, but applying the highest branch option for $R_{M \geq 5}^{total}$ (9.6 events per year); that is, the Relax MFD Constraint tends to increase rates at all magnitudes equally (appendix N, this report), so we effectively have this option in the model.

The logic tree in *figure 3* gives the following two branches for the characteristic Inversion Model:

- *Characteristic UCERF2 Constrained*—This applies the fault-section nucleation MFD constraints described above for *equation set 7*. Note that rupture rates are prevented from going to zero by enforcing a minimum "water-level" rate, which is the rupture rate for a GR starting-model multiplied by 0.01 (see appendix N, this report).
- *Characteristic Unconstrained*—No fault section MFD constraints are applied here. This model is more underdetermined, so a larger set of inversion runs are needed to sample the solution space; results can either be averaged or used to sprout additional subbranches of the logic tree.

Currently only the first of these options is given non-zero weight for two reasons: to stay as close as possible to UCERF2, and because the second option requires much more extensive exploration of the solution space, which we did not have time to conduct.

The fault slip rates are reduced in the inversion according to the moment rate implied by subseismogenic, on-fault ruptures. This reduction was originally done on a fault section basis, but high rates of observed seismicity in some areas produced subseismogenic MFDs that had moment rates greater than those assigned to the fault section, leading to negative corrected moments. Therefore, only a systemwide average is applied to reduce slip rates for subseismogenic ruptures in UCERF3. The reduction for each logic tree branch is derived by dividing the moment rate of the subseismogenic MFD (cyan curve *figure 15B*) by the total on-fault moment rate from the deformation model (*table 4*); the values among branches here vary from 4.1 to 10 percent (*U3_PreInversionAnalysisTable*).

The off-fault gridded seismicity sources are defined by partitioning the associated MFD (green curve *figure 15A*) among the regional grid cells that are outside fault zone polygons, weighted by the relative spatialPDF value in each grid cell. The Characteristic branches use either the UCERF2 or UCERF3 smoothed seismicity model (*figure 14A* or *B*), with equal weight being given to each. While there was some preference for the UCERF3 smoothed seismicity model, for reasons discussed above, preliminary hazard calculations showed it to imply significant hazard changes (discussed below). And so, given the remaining uncertainties on which smoothed seismicity map is most applicable for large damaging events in a long-term model, we ended up giving each equal weight. While there was also interest in applying the deformation-model based spatialPDF options (model-specific maps shown *figure 9*, or the average shown in *figure 14C*), we did not have time to do so.

The subseismogenic MFD for each fault section is distributed among the grid cells that fall within the associated fault zone polygon, consistent with the smoothed seismicity rates used to derive the subseismogenic MFDs. Given the ad hoc choices used to construct fault zone polygons (*fig. 4*), the hazard implications of this methodology need to be understood. The primary influence of fault zone width is on the maximum magnitude for gridded seismicity near faults. Inside the polygons this maximum magnitude is defined by the minimum magnitude of supraseismogenic on-fault ruptures (6.3 on average), whereas outside the polygons it is specified by $M_{max}^{off-fault}$, with UCERF3 logic-tree options of 7.3, 7.6, or 7.9. Therefore, changing the fault zone widths primarily changes the gridded seismicity maximum magnitudes near the outer edges of the polygon, which should have only a very small effect on UCERF3 hazard estimates because the hazard near faults is generally dominated by supraseismogenic, on-fault ruptures.

Gutenberg-Richter Branches

These branches represent the possibility that earthquakes on individual faults are governed by a Gutenberg-Richter magnitude-frequency distribution. This GR hypothesis conflicts with all previous WGCEP and NSHMP models, which assumed that ruptures on large, well-developed faults exhibit characteristic behavior. Imposing GR behavior on faults in the UCERF2 framework exacerbates the MFD "bulge" near $M6.7$, whereas the UCERF3 grand inversion reduces this problem by allowing multifault ruptures. Given the support the GR hypothesis has received in recent analyses (for example, Parsons and Geist, 2009), we tried to accommodate such a branch on the UCERF3 logic tree.
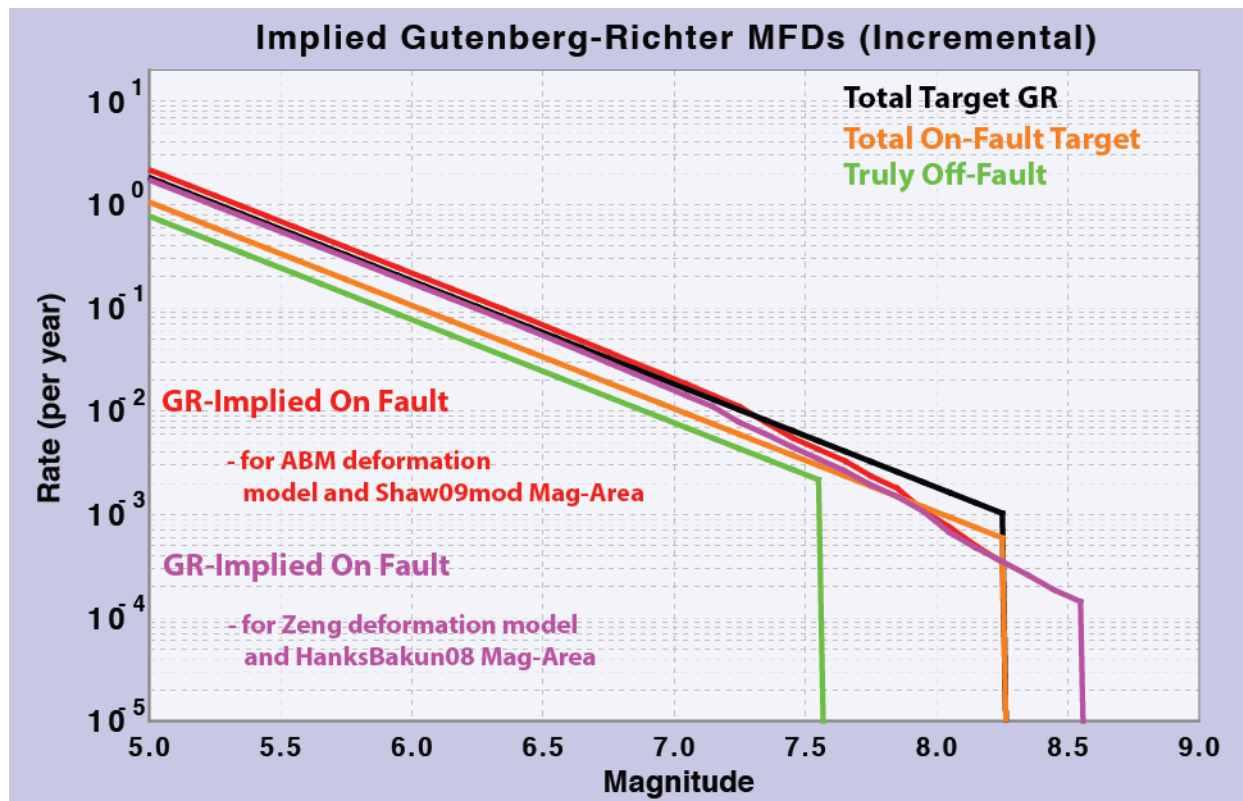
Figure 16. Graph showing magnitude-frequency distributions implied by the Gutenberg-Richter (GR) hypothesis. Total target GR (black line) satisfies the total regional rate (7.9 events/year for UCERF3) and the M_{max} implied by the largest event in the fault system (8.25 for Shaw09mod magnitude-area relationship here). The total on-fault target (orange line) is the total target GR multiplied by the fraction of on-fault seismicity (58 percent here), and the truly off-fault (green line) MFD is the total target minus the total on-fault target, and then truncated at $M_{max}^{off-fault}$=7.6. The GR-implied on-fault curves (red and magenta lines) represent the MFDs implied by the GR hypothesis for two extreme branches (and with no off-fault seismicity being added), both of which fall well above the total on-fault target; results for all other GR branches with $R_{M \geq 5}^{total}$ = 7.6 fall between these end-members. The GR-implied curves roll off at the highest magnitudes because not all fault sections participate in the largest events.

The target MFDs for the GR case are simple to construct (fig. 16). The total regional target (black line in figure 16) is again specified by the choice of $R_{M\geq5}^{total}$ and M_{max}, and partitioned according to the fraction of seismicity that is on-fault (for example, 58 percent for UCERF3 smoothing), yielding the orange on-fault target MFD shown figure 16. The off-fault MFD (green line) is the different, truncated at the specified value of $M_{max}^{off-fault}$.

The GR hypothesis states that each fault section nucleates a GR distribution of earthquakes, with a *b*-value of 1.0 and a maximum magnitude defined by the largest rupture in which the section participates, including multifault ruptures. The rate of events, or the GR *a*-value, for each fault section can then be found by satisfying the section moment rate. Even before any inversion, we can sum all the consequent fault-section MFDs to obtain a total GR-implied on-fault MFD. Two examples are shown figure 16. The red curve, which represents the ABM Deformation Model paired with the Shaw09mod magnitude-area relationship, exceeds not only the on-fault target (orange) but also the total regional target (black). The magenta curve, which represents the Zeng Deformation Model pared with the HanksBakun08 magnitude-area relationship, is just below the total target, and well above the on-fault target. Results for all other GR branches fall between these two cases.

This discrepancy can be quantified as an on-fault coupling coefficient, defined as the ratio of the total rate of the target on-fault MFD (orange line in *figure 16*) to the total rate of the GR-implied on-fault MFD (red or magenta curve figure 16). The implied coupling coefficients, listed in the *U3_PreInversionAnalysisTable,* range from 0.37 to 0.75 among all the GR branches *figure 3* (slip rate reductions of 63 to 25 percent). One option for matching the target MFDs is to apply these implied coupling coefficients, which can be done via two of the "Fault Moment Rate Fix" options in the UCERF3 logic tree (*fig. 3*):

- *Apply Implied Coupling Coefficient*—reduce the slip rates on all fault sections by the implied coupling coefficient (same reduction on all faults).
- *Do Nothing*—let the inversion decide where to reduce slip rates in matching the target MFD.

The other two "Fault Moment Rate Fix" options listed *figure 3*, which include relaxing the regional MFD constraint all together, cannot be applied, because both violate the GR hypothesis.

Not all fault sections participate in the largest events, causing the on-fault GR MFDs to roll off at high magnitudes (red and magenta curves figure 16). Hence, more moment has to be taken up by smaller earthquakes, which increases overall rate of events. The discrepancy would be reduced if all sections shared the same maximum magnitude, but this would require including many of the ruptures filtered out by our plausibility criteria, or adding many more faults throughout the region to increase connectivity (which would add moment as well).

There is some evidence that faults might have a lower *b*-value than surrounding regions (Page and others, 2011). Assuming *b*=0.95 on faults reduces the discrepancy a little, but not enough to satisfy regional rates. The definition of fault zone polygons also has some influence in terms of the target on-fault rate, such that increasing their collective area would lessen the discrepancy. However, reasonable adjustments are not adequate. In fact, figure 16 implies that the fault zone polygons would have to encompass the entire region (because the red and magenta curves essentially match the total target). Doing so would also worsen existing problems with the implied off-fault coupling coefficients (*U3_PreInversionAnalysisTable*).

Other possible explanations are that the true total regional rate ($R_{M\geq5}^{total}$) is significantly higher than our existing branch options, that shear rigidity is considerably less than that assumed

$(3.0\times10^{10}$ Pa), or some combination of the possibilities discussed here. Any one of these GR corrections would have significant implications. For example, applying the implied coupling coefficients of 0.37 to 0.75 would reduce fault-based hazard by about 25 to 63 percent, whereas increasing the total regional rate would increase hazard by a similar amount.

An alternative is that the hypothesis is wrong; faults do not honor a GR nucleation MFD. In fact, this may be one of the most important UCERF3 findings. Either way, these branches would get very low relative weight given the extraordinary corrections needed to satisfy all data, leading us to abandon further pursuit for UCERF3, which was the advice of our SRP as well. Further details are therefore not provided here, although these branches remain fully implemented for those wishing to explore viability and (or) practical implications further.

Gardner-Knopoff Aftershock Filter

The UCERF3 earthquake rate model includes aftershocks, whereas previous NSHMP models have removed such events using the Gardner-Knopoff declustering algorithm (Gardner and Knopoff, 1974). The definition of aftershocks implied by this type of declustering is out of date. For example, it implies that the fraction of aftershocks relative to main shocks is magnitude dependent, whereas recent aftershock studies do not support such dependence (for example, Felzer and others, 2004).

Nevertheless, the Gardner-Knopoff definition is still used in formulating and applying hazard policies; for example, in current building codes that rely on the NSHMP models. To facilitate comparison and consistency with other earthquake hazard models, a procedure for removing Gardner-Knopoff aftershocks has been implemented in the UCERF3 framework.

Gardner-Knopoff declustering typically reduces the *b*-value from about 1.0 (full catalog) to about 0.8 (declustered catalog). For this reason, the NSHMP has generally used a *b*-value of 0.8 for modeling smaller events as gridded seismicity. The *b*-value difference can be combined with the fraction of $M{\geq}5$ events designated as main shocks by the declustering model to construct a Gardner-Knopoff filter. According to UCERF2, appendix I (Felzer, 2008*)*, the total number of $M{\geq}5$ events per year in the UCERF region is 7.50 for the full catalog, compared with 4.17 for a Gardner-Knopoff declustered catalog, which implies that 56 percent of these events are Gardner-Knopoff main shocks. The corresponding GR MFDs for both full and declustered catalogs are compared in *figure 17A*. The UCERF3 Gardner-Knopoff aftershock filter is simply the ratio of the decustered MFD to total MFD in *figure 17A*, capped at 1.0 above the point where the two MFDs cross over. This filter compares well with binned data values from table 16 in appendix L (this report), as shown here in *figure 17B*.

In applying this Gardner-Knopoff aftershock filter, the rate of each UCERF3 rupture can be scaled by the value on the red curve in *figure 17B*. This implicitly assumes that the fraction of aftershocks is location independent, which is consistent with past NSHMP applications. Observational evidence for a systematic spatial dependence is lacking, though the available data do not exclude that possibility.

From a practical perspective, our approach is the same as applied in UCERF2 for gridded sources. For fault-based sources, however, the two applications are a bit different. In UCERF2, all fault-based sources were effectively reduced by 3 percent to account for aftershocks (independent of magnitude), whereas the fractional reduction is magnitude dependent using the Gardner-Knopoff filter. Below magnitude 6.7 (where our filter has a ~3-percent reduction) the new methodology reduces rates more than in UCERF2, and above 6.7 the new reduction is less (and zero above magnitude 6.75). While these differences are generally quite small compared to

other epistemic uncertainties in the model, there are situations where the differences may require further consideration. For example, about 30 percent of magnitude ~6 Parkfield earthquakes are aftershocks according to this new filter.

To ensure maximum consistency with UCERF2 and past NSHMP practice, the Gardner-Knopoff filter defined here is applied only to gridded-seismicity sources, whereas the rates of all supraseismogenic ruptures are reduced by 3 percent (again, the latter being the UCERF2 value). This means the Gardner-Knopoff filter is not applied for supraseismogenic ruptures.
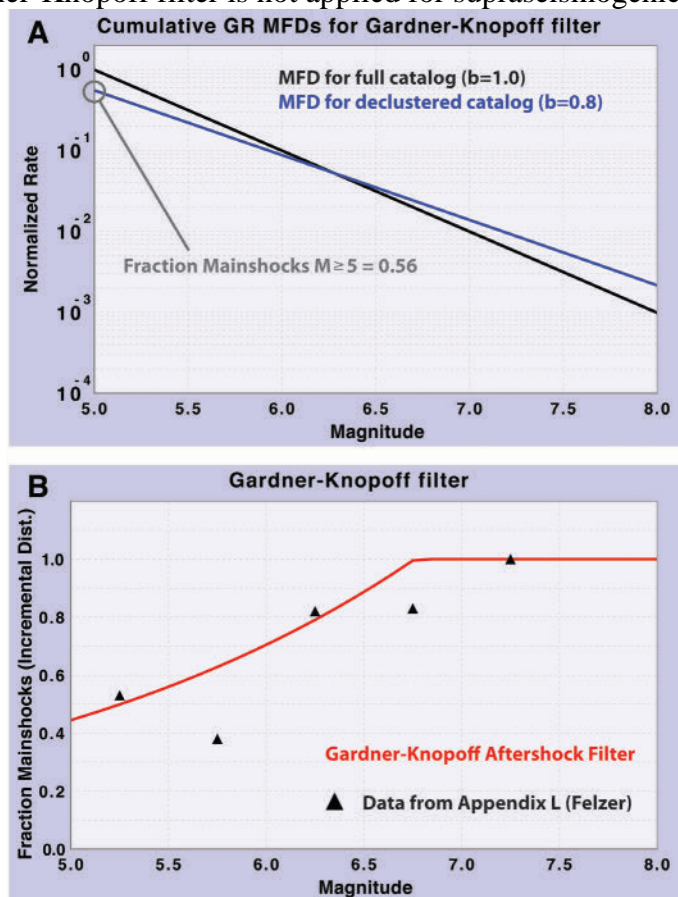
Figure 17. Plots showing application of the Gardner-Knopoff aftershock filter in UCERF3. *A*, A full-catalog cumulative magnitude-frequency distribution (MFD; black line, with b-value=1.0 and normalized by the total rate of $M{\geq}5$ events) together with the cumulative MFD implied by the Gardner-Knopoff aftershock declustering algorithm described in the text (blue line, with b-value=0.8 and a relative total rate of 0.56, meaning 56 percent of $M{\geq}5$ events are main shocks according to this algorithm). *B*, The UCERF3 Gardner-Knopoff aftershock filter (red curve), obtained by taking the ratio of incremental versions of the MFDs in A (blue divided by black) and capping values above 1.0 at 1.0 (above the crossover magnitude, which is $M6.8$ for the incremental distributions). Also shown are data (black triangles) from table 16 of appendix L (this report).

Results

This section presents UCERF3 results, postponing important sensitivity tests to the section that follows, both because those tests depend on evaluation metrics introduced here, and because interpretations here are not influenced by the test results.

Model Evaluation Challenges

One of the primary challenges in evaluating UCERF3 is the increased number of viable ruptures in the fault system—more than 250,000, compared to less than 8,000 mapped into our fault system by UCERF2. Furthermore, the rupture rates in UCERF2 were largely prescribed in terms of rupture extents and assumed MFDs, whereas these properties are derived in UCERF3 from the system-level inversion. Interpretation of UCERF3 results is therefore much more challenging. For example, a 5-second visual examination of each UCERF3 rupture would take about 350 hours for just one of the 1,440 alternative logic tree branches. We therefore have to rely on aggregate evaluation metrics.

The grand inversion approach to UCERF3 would not be feasible without access to supercomputers. In addition to the large number of ruptures in each model, we also have to contend with a large number of alternative logic tree branches (1,440). Each simulated annealing run takes about 5 hours on a typical desktop computer (appendix N, this report). Furthermore, simulated annealing finds the optimum solution by sampling the solution space somewhat randomly (using a "smart" Monte Carlo procedure based on thermodynamics). For an overdetermined problem, it is guaranteed to find the global minimum if given infinite time (Granville and others, 1994). Our computation time is limited, however, so it is important to quantify the convergence properties by examining the spread of results from repeated runs of the same problem. Multiple runs are also needed to sample underdetermined parts of the solution space. Such convergence properties, as well as the influence of alternative equation set weights, are summarized in the "Sensitivity Tests" section, and some are discussed in more detail in appendix N (this report). For the results presented here, we ran 10 separate simulated annealing inversions for each branch, which will be shown to be more than adequate in terms of quantifying hazard. Multiplying 1,440 logic tree branches by 10 runs per branch, and then by 5 hours compute time for each run, implies about 72,000 hours of total compute time (8.2 years). Consequently, most of the results presented here were computed on the Stampede cluster at the University of Texas, which can accommodate as many as 6,144 separate inversion runs at a time. We have also made extensive use of the cluster at the Center for High-Performance Computing and Communication, University of Southern California, which can accommodate as many as 60 inversions at a time.

Dealing with the large number of ruptures and logic tree branches has also necessitated the development of new evaluations metrics and visualization tools. Those currently available are listed in *table 11*, most of which are exemplified below, with most others being used in the appendixes (as noted below).

Given the many differences between UCERF2 and UCERF3, a full, step-by-step accounting of the influence of each is not feasible, especially for every site of potential interest and for every evaluation metric. Our aim here, therefore, is to identify and explain important differences with respect to UCERF2, and to characterize the influence of different UCERF3 logic tree branches as best we can.

Preliminary models (for example, UCERF3.0) included grand inversion results that used UCERF2 ingredients only (same deformation models, scaling relationships, and so forth), with the hope that this would indicate where differences are strictly methodological. Unfortunately this was not helpful, because whether or not methodological differences are important turns out to depend on which ingredients are chosen. Thus, the conclusions from such controlled experiments do not necessarily apply to the final UCERF3 model. We therefore do not present any such results here.

Table 11.   Evaluation metrics currently available in the UCERF3 framework.

Inversion data fits
Regional MFD plots
Slip rate plots (and misfits)
Paleo event rate plots (and misfits)
Tabulation of equation-set residuals and pre-inversion metrics
Simulated annealing run diagnostics
Other data fits
Event correlation between paleoseismic sites
Fault jumping statistics
Variability of average slip per event at points on faults (slip COV)
Frequency of different rupture lengths statistics
General implications
Parent-section MFDs (also tabulated)
Subregion MFDs (for example, LA and SF Boxes)
Participation rate maps
Maps showing how often other fault sections participate with a particular section
Implied segmentation (for example, on SAF)
Hazard/loss metrics
Hazard curves at sites
Tornado diagrams (showing which logic tree branches are influential)
Hazard Maps (and their ratios to UCERF2)
Risk Targeted Ground Motion (RTGM) at sites (Luco and others, 2007)
Statewide Loss Estimates (for example, Porter and others, 2012)
SCEC VDO (3D visualizations)

Model Fits To Data

Here we summarize how well final models fit the various data constraints; appendix N (this report) has further details.

Regional MFDs

Figure 18 compares the envelope of the UCERF3 branch MFDs with the mean MFDs for UCERF2 for the entire California region. The inversion successfully eliminates the apparent UCERF2 overprediction near M6.5. We also illustrate what happens if the UCERF2-like MFDs are applied strictly to all faults in UCERF3 (orange curve, obtained by giving equation set 7 infinite weight). In this case the overprediction is even greater than in UCERF2, mostly because of the addition of new fault sections. Appendix N (this report) shows that the final MFDs for a given branch match the associated pre-inversion targets very well. *Table 12* lists the cumulative

MFDs for both UCERF3 and UCERF2, averaged over all branches and including aftershocks. As expected, the rates have increased by ~42% for M≥5, gone down by ~23% at M≥6.7, and increased by ~37% for M≥8.
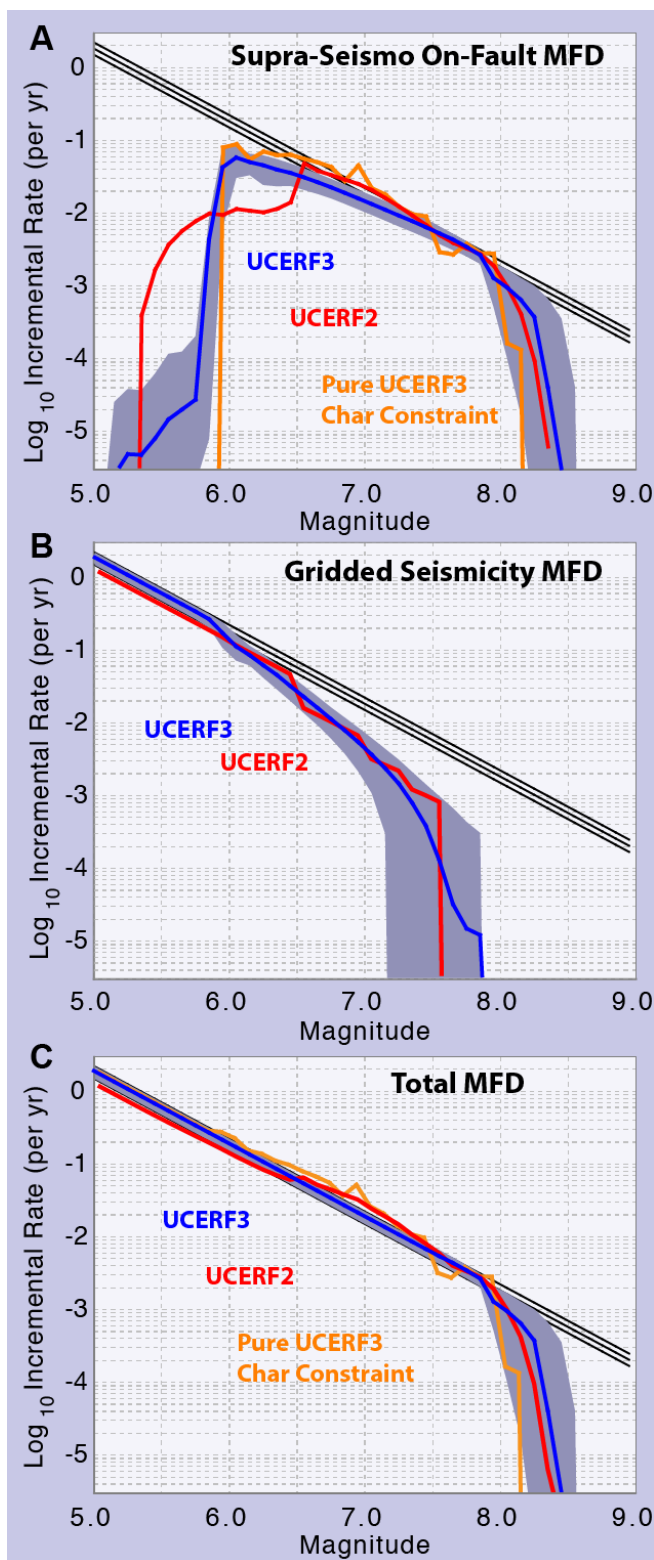
Figure 18.   Magnitude-frequency distributions (MFDs) for the entire California region for all UCERF3 logic tree branches, with comparison to mean results from UCERF2. *A,* Supraseismogenic on-fault MFDs for UCERF3 are shown in blue, with the minimum and maximum among all branches being represented by the shaded region. The average result from UCERF2 is shown in red for comparison. *B*, Same as *A*, but for gridded seismicity (subseismogenic on-fault ruptures plus truly off-fault sources). *C*, Total MFDs, representing the sum of the MFDs in *A* and *B*. The black lines in all plots represent reference Gutenberg-Richter distributions for the alternative values of the total regional *M*≥5 rate ($R_{M \geq 5}^{total}$). Also shown with orange in *A* and *C* are UCERF3 MFDs obtained by applying the Fault Section MFD Constraint (equation set 7) with infinite weight, which reveals the overprediction of regional rates when one assumes UCERF2-like MFDs for each fault. Note that the gridded seismicity MFDs for UCERF2 have had aftershocks added back in by reversing the Gardner-Knopoff filter described in the text.

Table 12. Average cumulative magnitude-frequency distributions for UCERF3 and UCERF2.

["Faults" refers to supraseismogenic on-fault ruptures; "Gridded" refers to the gridded seismicity, and "Total" includes both; each rate given in events per year. "U3/U2 Total Ratio" is the ratio of total values from UCERF3 and UCERF2. These rates include aftershocks, where those for the UCERF2 gridded seismicity were added using the Gardner-Knopoff filter described in the text. Note that UCERF2 on-fault values include aleatory variability of magnitude for given rupture area, whereas values for UCERF3 do not.]

Magnitude	UCERF3			UCERF2			U3/U2 total ratio
	Total	Faults	Gridded	Total	Faults	Gridded	
5.0	8.26E+00	4.59E-01	7.80E+00	5.80E+00	3.53E-01	5.45E+00	1.42
5.1	6.56E+00	4.59E-01	6.10E+00	4.66E+00	3.53E-01	4.31E+00	1.41
5.2	5.21E+00	4.59E-01	4.75E+00	3.76E+00	3.53E-01	3.41E+00	1.39
5.3	4.14E+00	4.59E-01	3.68E+00	3.04E+00	3.53E-01	2.69E+00	1.36
5.4	3.28E+00	4.59E-01	2.83E+00	2.46E+00	3.53E-01	2.11E+00	1.33
5.5	2.61E+00	4.59E-01	2.15E+00	2.01E+00	3.51E-01	1.66E+00	1.30
5.6	2.07E+00	4.59E-01	1.61E+00	1.64E+00	3.48E-01	1.29E+00	1.26
5.7	1.64E+00	4.59E-01	1.18E+00	1.34E+00	3.42E-01	1.00E+00	1.22
5.8	1.30E+00	4.58E-01	8.45E-01	1.10E+00	3.34E-01	7.71E-01	1.18
5.9	1.03E+00	4.54E-01	5.80E-01	9.11E-01	3.24E-01	5.87E-01	1.14
6.0	8.20E-01	4.12E-01	4.08E-01	7.55E-01	3.15E-01	4.40E-01	1.09
6.1	6.50E-01	3.54E-01	2.96E-01	6.31E-01	3.03E-01	3.27E-01	1.03
6.2	5.15E-01	3.03E-01	2.12E-01	5.30E-01	2.93E-01	2.37E-01	0.97
6.3	4.08E-01	2.58E-01	1.50E-01	4.48E-01	2.82E-01	1.65E-01	0.91
6.4	3.22E-01	2.18E-01	1.04E-01	3.79E-01	2.71E-01	1.08E-01	0.85
6.5	2.55E-01	1.82E-01	7.23E-02	3.20E-01	2.57E-01	6.30E-02	0.80
6.6	2.01E-01	1.51E-01	4.96E-02	2.56E-01	2.09E-01	4.76E-02	0.78
6.7	1.58E-01	1.25E-01	3.35E-02	2.06E-01	1.71E-01	3.52E-02	0.77
6.8	1.24E-01	1.02E-01	2.22E-02	1.62E-01	1.37E-01	2.51E-02	0.76
6.9	9.72E-02	8.29E-02	1.43E-02	1.26E-01	1.08E-01	1.71E-02	0.77
7.0	7.58E-02	6.69E-02	8.86E-03	9.40E-02	8.34E-02	1.06E-02	0.81
7.1	5.88E-02	5.36E-02	5.19E-03	7.02E-02	6.26E-02	7.56E-03	0.84
7.2	4.53E-02	4.25E-02	2.82E-03	5.16E-02	4.66E-02	5.03E-03	0.88
7.3	3.46E-02	3.32E-02	1.36E-03	3.72E-02	3.43E-02	2.92E-03	0.93
7.4	2.60E-02	2.54E-02	5.71E-04	2.68E-02	2.51E-02	1.75E-03	0.97
7.5	1.92E-02	1.90E-02	1.87E-04	1.90E-02	1.82E-02	7.87E-04	1.01
7.6	1.38E-02	1.37E-02	5.94E-05	1.32E-02	1.32E-02	0.00E+00	1.04
7.7	9.43E-03	9.40E-03	2.71E-05	9.35E-03	9.35E-03	0.00E+00	1.01
7.8	5.97E-03	5.95E-03	1.21E-05	6.08E-03	6.08E-03	0.00E+00	0.98
7.9	3.30E-03	3.30E-03	0.00E+00	3.35E-03	3.35E-03	0.00E+00	0.98
8.0	2.01E-03	2.01E-03	0.00E+00	1.47E-03	1.47E-03	0.00E+00	1.37
8.1	1.07E-03	1.07E-03	0.00E+00	5.09E-04	5.09E-04	0.00E+00	2.09
8.2	4.20E-04	4.20E-04	0.00E+00	9.99E-05	9.99E-05	0.00E+00	4.21
8.3	4.55E-05	4.55E-05	0.00E+00	7.26E-06	7.26E-06	0.00E+00	6.27
8.4	4.68E-06	4.68E-06	0.00E+00	1.08E-06	1.08E-06	0.00E+00	4.34
8.5	1.56E-06	1.56E-06	0.00E+00	0.00E+00	0.00E+00	0.00E+00	Inf

Slip Rates

The final slip rate misfits (solution over target, branch-averaged) are listed for each fault section in the "AveSolSlipRates" sheet of the *U3_FaultSectionData* file given in the "Data and Resources" section. *Figure 19* shows these misfits for FM 3.1, together with an equivalent plot for UCERF2. In general, the UCERF3 fits are better than for UCERF2, which tends to overpredict slip rates near the centers of fault sections and underpredict those near the ends. This is caused by the UCERF2 "floating" ruptures being given a uniform probability along strike, and partly by the tapered-slip distribution.

There are two prominent overprediction (red) outliers for UCERF3 (*fig. 19*). The southernmost represents the Elsinore-Glen Ivy fault section. Here the solution slip rate is pulled above the target, by a factor of 1.54, in fitting the paleoseismic event rate constraint on this section (*table 7*), which is underpredicted by a factor of 0.73; improving the match to one worsens the fit to the other, illustrating data inconsistency. The other red outlier, in central California, is in the center of the Creeping Section of the San Andreas Fault (SAF), where the mean slip rate is reduced by 80 percent to 5 mm/yr to account for creep. The inversion is unable to match this rapid slip rate change, giving a high value of 10 mm/yr. All other UCERF3 slip rate overpredictions are within 20 percent of the targets, and virtually all those greater than 10 percent can be explained by fitting relatively high paloeseismic event rates.

Overall, UCERF3 underpredicts slip rates more than it overpredicts them, particularly in southern California (where many faults are slightly blue in *figure 19*). On average, total on-fault solution moment rates are 4 percent below the targets, primarily because of limitations on total event rates by the regional MFD constraint. Although some fault sections have slip rate reductions of as much as a factor of two, all can be explained by either the paleoseismic rate constraint being incompatible with the slip rate constraint (for example, the Whittier alt 1 fault section) or by the regional MFD constraint coupled with a lack of fault connectivity needed to produce larger events (for example, the Santa Susana East (connector) fault section). Only six fault sections have final branch-averaged slip rates that fall outside the range defined by the alternative deformation models, and all of these cases fall within the Geologic bounds.

Paleo Event Rate Data

UCERF3 paleoseismic event rate misfits are also listed in the *U3_FaultSectionData* file given in the "Data and Resources" section (sheets labeled "PaleoEventRateFits" and "ProxyEventRateFits"). Results for paleoseismic sites along the SAF are compared with UCERF2 results in *figure 20* with slip rate fits, to clarify why rates vary along strike. All UCERF3 data are fit well, given uncertainties, and are generally fit better than in UCERF2.

Misfits on the North Coast, Santa Cruz, Big Bend, and Mojave North sections are dominated by inconsistencies between paleoevent rate and slip rate constraints. The average slip rate discrepancy for Parkfield, which reflects the a priori constraint on the 25-year recurrence interval of historical ~*M*6 events, is at odds with other inversion constraints, possibly a result of deficiencies in modeling the aseismic processes on this fault.

Average slip rates on the Cholame, Carrizo, and Coachella sections are also underpredicted. Paleoseismic event rates are also underpredicted on the latter two, which raises the question of why the inversion does not simply add more events to satisfy these data. Owing to the regional MFD constraint, adding earthquakes there requires subtracting such events from other areas, which degrades the slip rate fits. Both slip rates and event rates can be fit well on

these sections if the MFD constraint is removed altogether, but this leads to a significant overprediction of the regional event rates near *M*7.
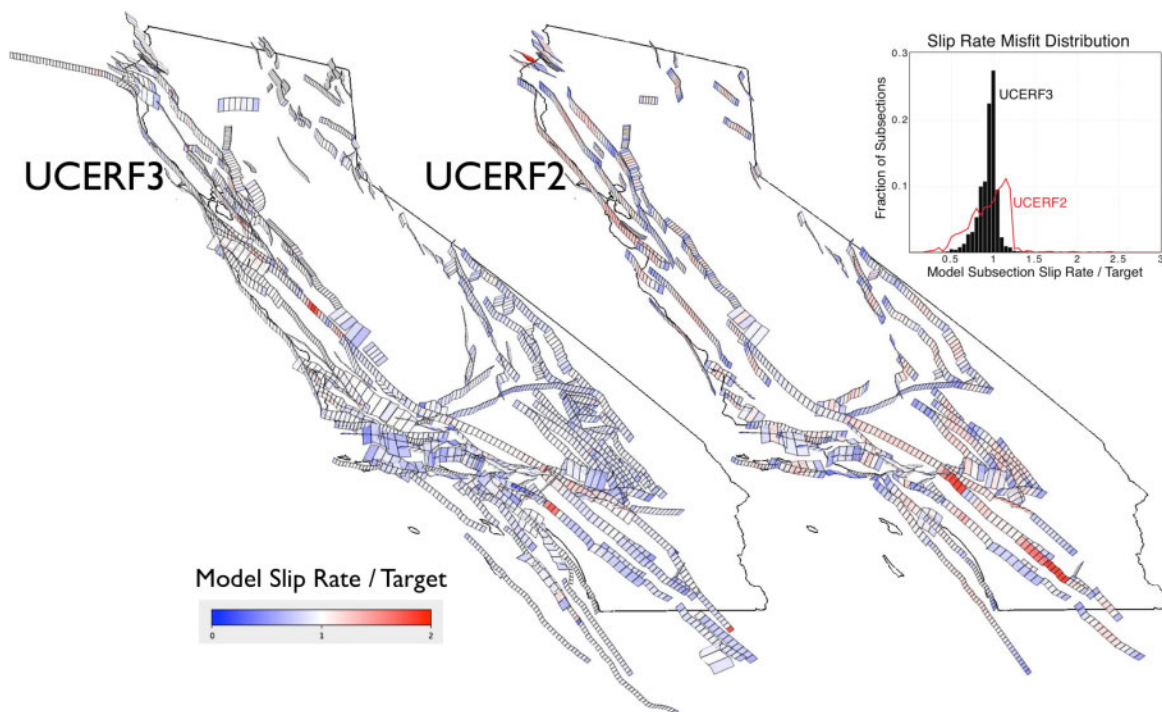

Figure 19.   Maps showing average subsection slip rate misfits for both UCERF3 (Fault Model 3.1) and UCERF2 (Fault Model 2.1), shown as ratios of final implied slip rates divided by deformation model slip rates, and averaged over all logic tree branches. Equivalent plots for each deformation model (branch subsets) are given in appendix N (this report). The distribution of subsection slip rate misfits is shown for UCERF2 and UCERF2 at the upper right.

Removing the MFD constraint also puts a high rate of smaller events at the northern end of the Cholame section. These events fill in the precipitous drop in modeled slip rates toward the north (*fig. 20*), as required by the Parkfield a priori constraint (appendix N, this report). This issue is also apparent in the UCERF2 results. From a hazard perspective, it is more important to get the total rate of events correct than to satisfy slip rates exactly, so we kept the regional MFD constraint to prevent the inflation of total event rates.

UCERF3 event rates on the southern SAF average about 25 percent below our best paleoseismic estimates (*table 7*). The worst case is Carrizo, where the mean model rate (an observable paleoevent every 193 years) is 40 percent below the best paleo-rate estimate (one every 115 years). In UCERF2, the average paleo constraint for Carrizo was an event every 225 years (*fig. 20*), so the paleo estimate has been revised by almost a factor of two. The average UCERF3 model rate is relatively consistent with the UCERF2 model average (one every 193 year versus one every 185 years, respectively); therefore, the hazard change in UCERF3 is minimal. Hazard-ratio maps, discussed later, will show that this is generally true of the entire SAF.

The misfits on the southern SAF nevertheless point to some possible inconsistencies that we should strive to understand and resolve in the future. Until we do so, however, minimizing

changes with respect to UCERF2 is appropriate, especially since matching the paleoseismic data better will increase hazard. Nevertheless, the uncertainties reflected in *figure 20* indicate general agreement, as well as the existence of some UCERF3 branches that do fit the southern SAF data better (meaning these branches could be given higher weight if users could justify doing so).

None of the UCERF3 model rates at the 31 paleoseismic sites are outside of the 95-percent confidence bounds on the data, and the reduced chi-squared value for the UCERF3 event rate fit is 0.72, indicating that, on the whole, UCERF3 over-fits the paleoseismic event rate data (appendix N, this report). Although the model systematically underpredicts event rates on the southern SAF, these sites do not represent independent data because the sites are seeing the same period of time and many of the same events. UCERF2 rates, for comparison, are outside of the (UCERF3) 95-percent confidence bounds at five of the sites.

Plots like *figure 20* are available for all the faults that have paleoseismic constraints (*Plots of Paleoseismic Data Fits Along Faults*; see the files that end with "_combined.png," for which the legend is the same as in *figure 20*). The data fits on these faults are generally better than on the SAF, with discrepancies in the mean model being attributable to conflicts between slip rate and paleoevent rate constraints.

A Posteriori Model Evaluation

Each inversion run provides quantitative metrics on how well the final model fits each data constraint (see appendix N, this report). In principal, these data could be used to adjust logic tree branch weights a posteriori (for example, using Bayes theorem with the a priori branch weights listed in *figure 3*). Likewise, some of the pre-inversion metrics, such as the implied off-fault coupling coefficients discussed above, could be used to rank models. We have not attempted any such branch-weight modifications here, however, because doing so will require more careful analysis in terms of avoiding cases where a good fit to data is actually the result of two "wrong" components canceling each other.

Fits to Data Not Used in the Inversion

One type of observation not included in the inversion is the extent to which paleoseismically inferred events are observed to corupture neighboring trench sites simultaneously (event correlation, or lack thereof). For example, such inferences are an important component of the "stringing pearls" methodology of Biasi and Weldon (2009). Appendix N (this report) demonstrates that currently available correlation data not only agree well with UCERF3 results, but also generally agree better than those implied by UCERF2. The interpretive uncertainties are admittedly large with respect to these correlation data because samples are limited, and correlation does not necessarily mean rupture in the same event because of uncertainty in the event dates.

Appendix N also compares UCERF3 results to a couple of different multifault rupture statistics, such as how often ruptures involve fault sections with different names and how many times ruptures jump across fault steps of various distance thresholds. Even considering data uncertainties and interpretive assumptions, the analysis implies that, if anything, UCERF3 has too few multifault ruptures, not too many.
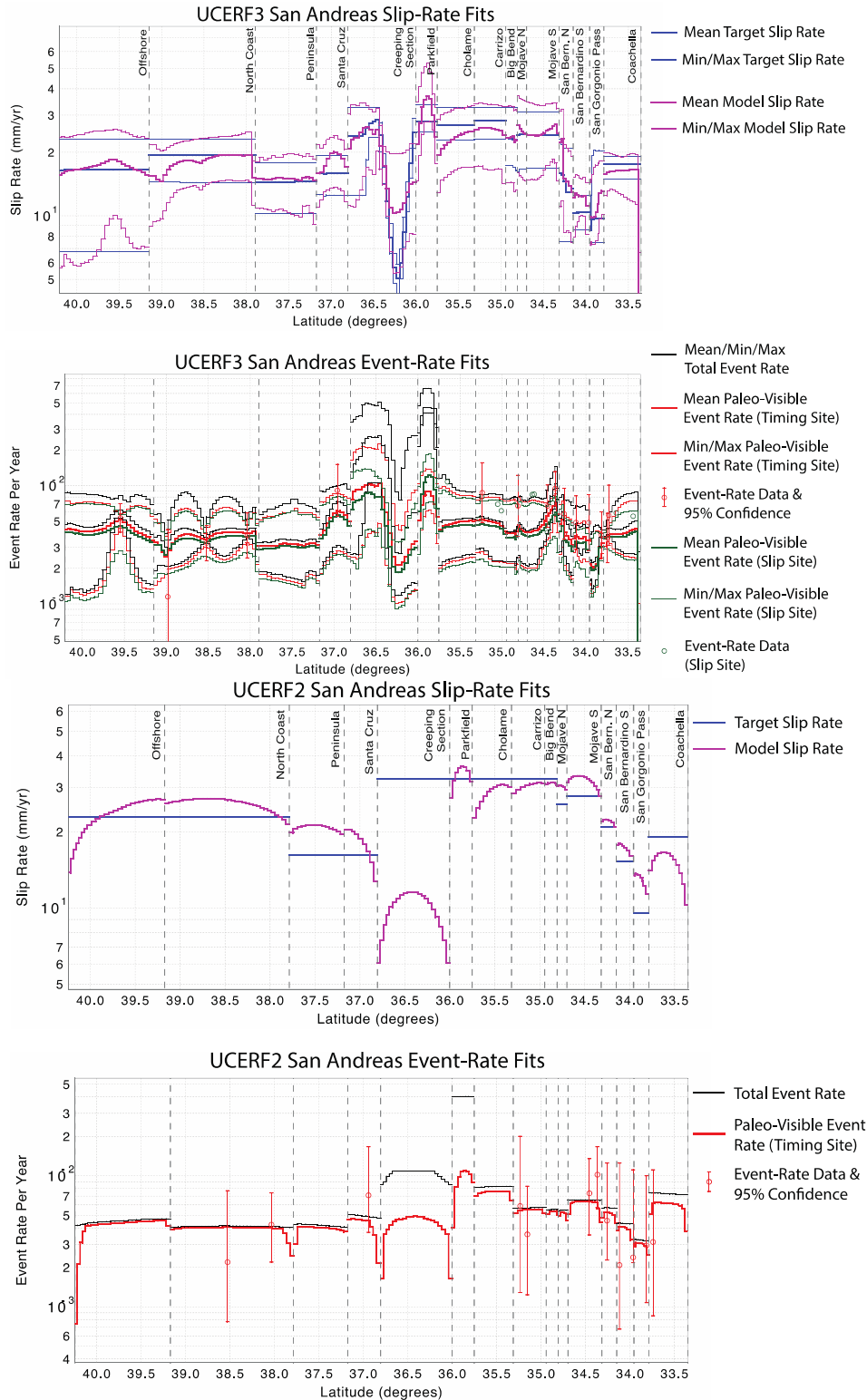
Figure 20. Latitudinal plots showing slip rate and paleoseismic data fits for the southern San Andreas Fault, for both UCERF3 (top) and UCERF2 (bottom). The paleoseismic data on the UCERF2 plot are those used in that study, whereas the version of this figure in *appendix N* (this report) compares UCERF2 results to UCERF3 data.

Wells (2013) presented a preliminary update to the Wells and Coppersmith (1994) global database, including a list of magnitude, area, length, and average slip for a number of historical ruptures. *Figure 21* compares the histogram of observed rupture lengths based on 258 events in the dataset with the frequency of rupture lengths predicted by the UCERF3 branch-averaged model, which agrees quite well. Again, if anything UCERF3 underpredicts the rate of the longest events.
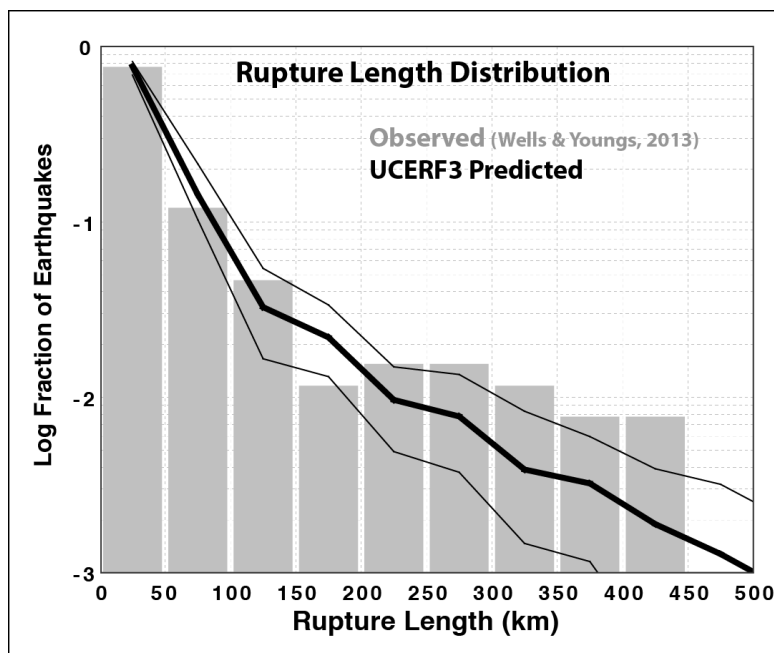

Figure 21. Histogram of observed rupture lengths from a global data compilation of 258 earthquakes (Wells, 2013), compared to the distribution implied by UCERF3 (thicker black line represents branch-averaged values, and thin lines represent the min and max among all branches). Curves have been normalized to density functions (values sum to 1) for comparison purposes.

The above analyses indicate that UCERF3 is quite reasonable with respect to multifault rupture statistics, and that our exclusion of the improbability constraint (*equation set 4*) seems to be justified. Good statewide statistics do not, however, guarantee that the data for individual faults are also well fit. The fault-by-fault review meetings (*table 3*) did not reveal egregious problems. To allow users to judge for themselves, we have generated participation rate maps that show the frequency with which other fault sections corupture (or participate) with any given section (*http://pubs.usgs.gov/of/2013/1165/data/UCERF3_SupplementalFiles/UCERF3.3/Model/FaultParticipation/*), as exemplified for the Cucamonga Fault in *figure 22*. Note that this figure does not show a rupture, but rather the combined sum of many different ruptures that connect with Cucamona in different ways.

Noda and Lapusta (2013) recently presented a "plausible physical mechanism" for ruptures passing completely through the creeping section of the SAF, which had zero probability of occurrence in UCERF2. Branch-averaged recurrence intervals for UCERF3 are as follows: 150,000 years between the center of the Offshore and Coachella sections; 2,500 years between the center of the North Coast and Mojave sections, and 900 years between the Parkfield and Santa Cruz sections. While these recurrence intervals are certainly reasonable, we caution that they have high uncertainties due to several modeling assumptions.
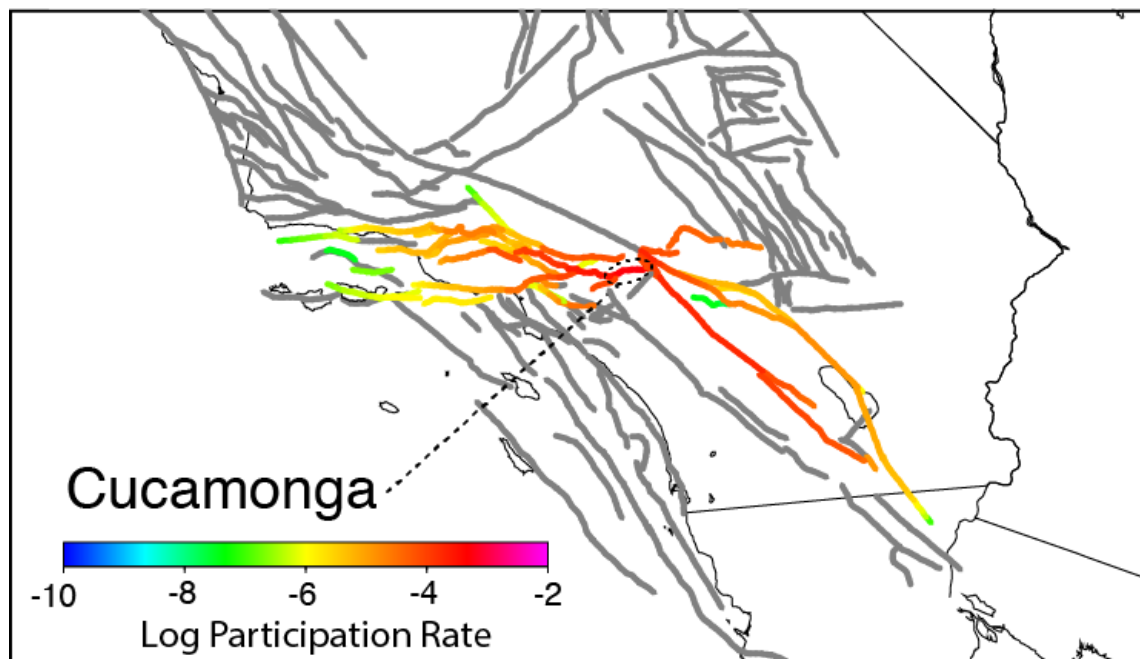
Figure 22. Map showing the rate at which the Cucamonga Fault coruptures (participates) with other fault sections for the branch-averaged UCERF3 model (for Fault Model 3.1). Such plots for other fault sections were also prepared (available at *http://pubs.usgs.gov/of/2013/1165/data/ UCERF3_SupplementalFiles/UCERF3.3/Model/FaultParticipation/*).

Another evaluation metric is the coefficient of variation (COV) for slip at a site, computed as the standard deviation of paleo-observable slip per event divided by the mean. *Figure 23* shows a histogram of subsection COVs for the reference logic tree branch. The center of the peak is about 0.42, which is a central value among alternative scaling relationships; EllsworthB produces the smallest value, about 0.33, and HanksBakun08 produces the largest, 0.47. These results are only a bit less than the values of 0.45 to 0.5 inferred by Hecker and others (2013) from a global paleoseismic data compilation. However, the latter includes intraevent variability (along-strike variability within a given observed rupture), whereas our values only include the amount of that captured by our average Tapered slip model for D_{sr} (or none for the equally weighted Boxcar branches). Our values are therefore roughly consistent. However, evaluation of this will be more relevant for any future GR logic tree branches, as the Hecker and others (2013) study concluded that their observed COVs are incompatible with a GR model.
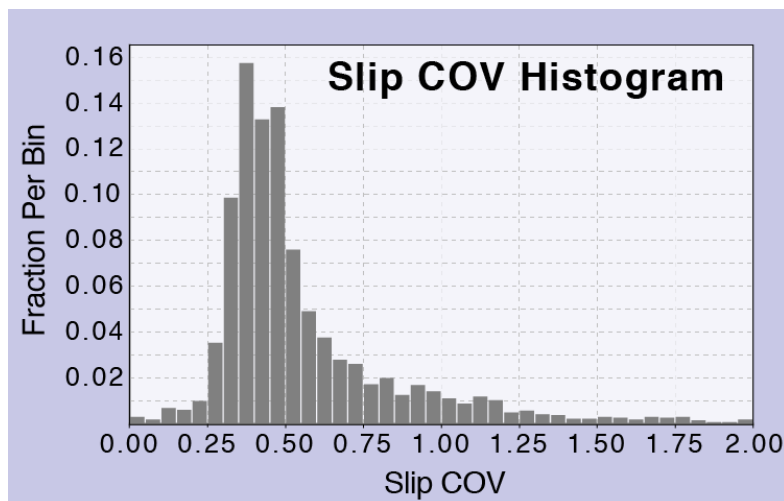
Figure 23.   Histogram of the coefficient of variation (COV) for average slip per event, where each sample is the standard deviation of slip on a subsection divided by the mean slip, taken among all subsections for the reference logic-tree branch inversion. The rates of each rupture and the probability of paleoseismic observance ($P_r^{paleo-slip-proxy}$) have been accounted for in generating this plot.

Hazard Related Metrics

This section presents evaluation metrics that are particularly relevant to hazard implications.

Total Regional Moment Rates

Figure 24 shows the regional moment rate distributions implied by the UCERF3 logic tree branches, as well as the deformation model targets listed *table 4*. The solution on-fault values are in general agreement with the targets, but the off-fault rates are well below deformation model values. As discussed above, the off-fault moment rates are not explicitly used in UCERF3, whereas the model values are implied by the choice of total regional earthquake rate, maximum magnitude off fault, and other branch choices. The reason for this off-fault discrepancy remains unresolved, although it may be associated with assumptions made in calculating the deformation model values (appendix C, this report). We also note that the coupling coefficients implied by geodetic deformation in broad regions are subject to considerable uncertainty, with values between 20 and 100 percent being cited in the literature (for example, Ward, 1998; Kagan, 2002a,b; Jenny and others, 2004; Masson and others, 2005; Pancha and others, 2006; Rontogianni, 2010). The total moment rate implied by the earthquake catalog is 2.29×10^{19} N·m/yr, in good agreement with the average model values of both UCERF3 (2.15×10^{19} N·m/yr) and UCERF2 (2.27×10^{19} N·m/yr).
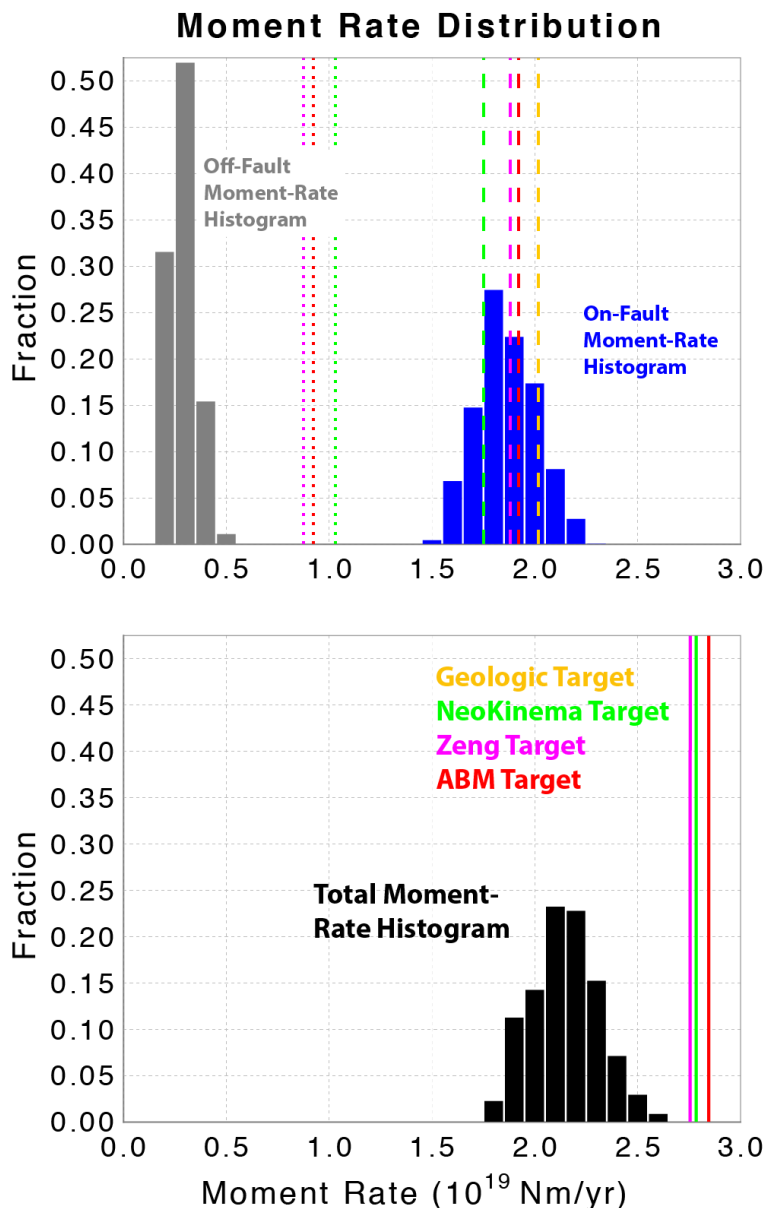
Figure 24. Graphs showing the distribution of regional moment rates implied by UCERF3 logic tree branches (including their weights), where blue represents total on-fault (including subseismogenic ruptures), gray is the off-fault, and black is the total combined rate. The vertical lines represent the various model targets as listed in *table 4* and as labeled at the bottom, where dotted is for off-fault and dashed is for on-fault values at the top.

Fault Section Participation MFDs

 Hazard at a site is often dominated by one or more nearby faults, so a particularly important metric is the participation MFD, which quantifies the rate at which ruptures occur on each fault section (even if they nucleate elsewhere). While these MFDs were prescribed in UCERF2, UCERF3 derives them by finding the range of models that fit the data. The characteristic MFD nucleation constraint (*equation set 7*) overdetermines the inversion for fault

section MFDs, so the remaining concerns are whether simulated annealing can find the global minimum and whether the results are robust with respect to equation-set weights (both of which are quantified below).

Because it is not practical to look at the participation MFDs for all ~2,600 fault subsections, we aggregate results back onto the 350 main fault sections, which also aids in making meaningful comparisons to UCERF2. Results were produced for all fault sections (available at *http://pubs.usgs.gov/of/2013/1165/data/UCERF3_SupplementalFiles/ UCERF3.3/Model/FaultMFDs/*); see the appropriate subdirectories for nucleation versus participation, and incremental versus cumulative MFDs), with *figure 25* providing a few representative examples. Participation MFDs for the two SAF sections (Peninsula and Mojave S) are very consistent between UCERF2 and UCERF3. For the two other San Francisco Bay area faults (Calaveras N and Hayward N), UCERF3 has a wider range of magnitudes and lower total rates of supraseismogenic ruptures. Of the two Los Angeles region examples (San Cayetano and Cucamonga), both have lower total UCERF3 rates because they participate in larger magnitudes. In fact, Cucamonga represents the biggest rate change that is due primarily to methodological differences (the inclusion of multifault ruptures, as depicted in *figure 22*). Both of these cases were viewed as an improvement by participants of the fault-by-fault review meetings *table 2*), and the Cucamonga multifault ruptures are supported by the static and dynamic stress modeling of Anderson and others (2003).

Note that UCERF2 fault section MFDs are generally smoother than those for UCERF3, which is only because the former have aleatory variability in magnitude for a given rupture area (a Gaussian magnitude PDF applied to each characteristic rupture, with a standard deviation of 0.12 and truncated at ±2 standard deviations). For example, there are only 10 different magnitudes for all characteristic model events on the northern SAF in UCERF2, so without this aleatory variability UCEF2 results would be spikier than those of UCERF3. Whether or not to apply such aleatory variability in UCERF3 is a hazard modeling question not addressed in this report, except to note that the option exists for users that want it. The point here is that UCERF2 fault section MFDs are not really any smoother than those of UCERF3.

Subregion MFDs

Figure 26 shows the mean and range of nucleation MFDs, for both UCERF2 and UCERF3, in rectangular regions surrounding San Francisco (SF), Los Angeles (LA), and in the vicinity of the Northridge Fault. These box regions are mapped in *figure 27*, which also shows the ratio of off-fault spatial seis PDFs (SpatialPDF) between UCERF2 and UCERF3, as well as the ratio of branch-averaged, on-fault moment rates. Note that the MFDs shown in *figure 26* are cumulative, and that aftershocks have been added back in for UCERF2 (by reversing the Gardner-Knopoff filter described above). *Table 13* lists the number of fault sections, the moment rate, and various event rates inside each of these regions.
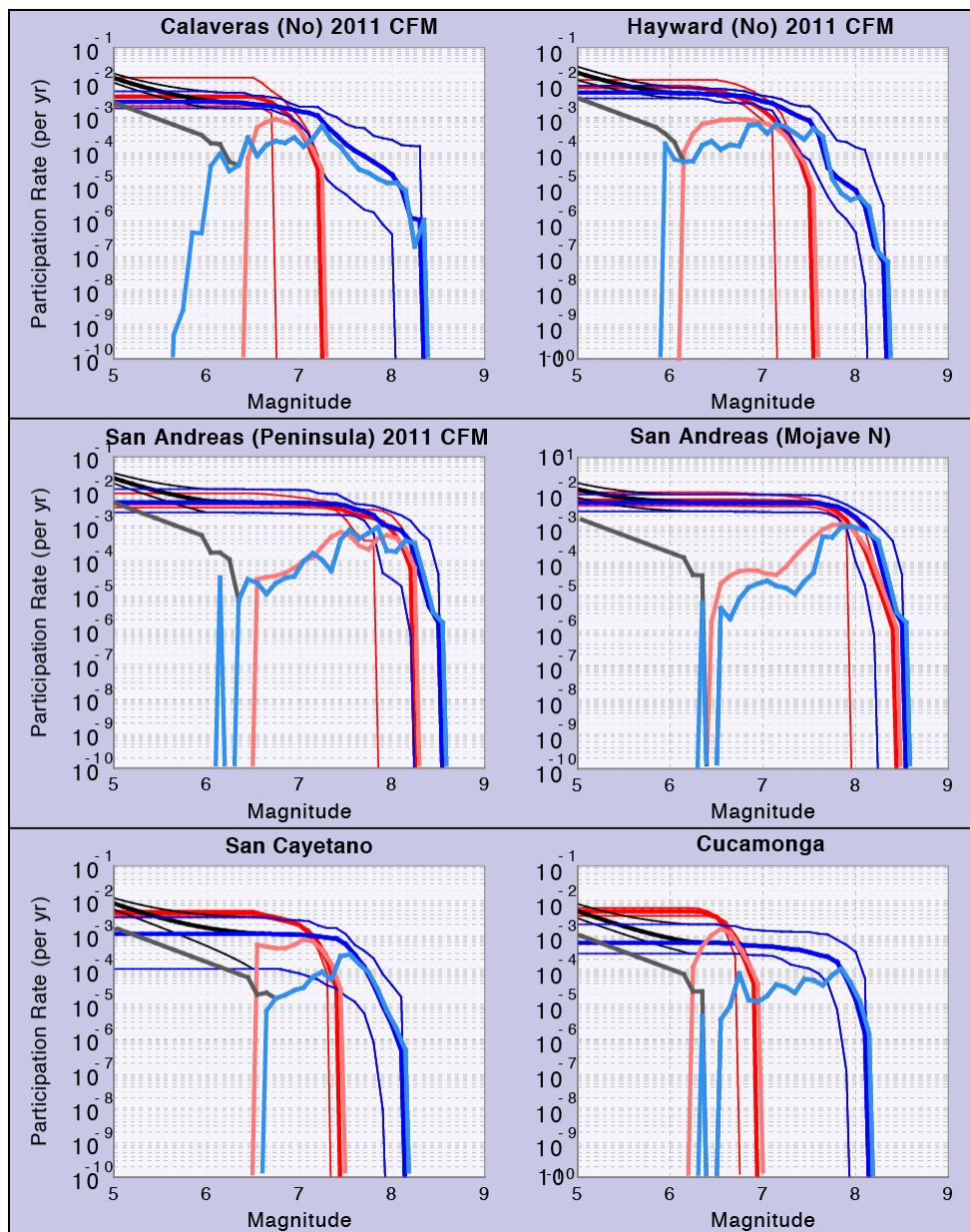
Figure 25.   Graphs showing example fault-section participation magnitude-frequency distributions (MFDs) averaged over all logic tree branches, and weighted accordingly. UCERF3 results are in blue and UCERF2 are in red. The corresponding faults sections are as labeled. The darker colored lines are cumulative distributions, and the lighter colored lines are incremental. The black/gray curves are UCERF3 MFDs with subseismogenic rupture added (total on-fault MFD). The thinner lines represent cumulative-distribution minimum and maximum among all logic tree branches. It is important to understand that "participation" includes all ruptures that touch any part of the parent fault section (even if a large rupture extends only a couple of subsections in at one end). For this reason, participation MFDs at a point on the fault (for example, a peleoseismic trench) will be less than or equal to those shown here. Results were also obtained for other fault sections (*http://pubs. usgs.gov/of/2013/1165/data/UCERF3_SupplementalFiles/UCERF3.3/Model/FaultMFDs/*).
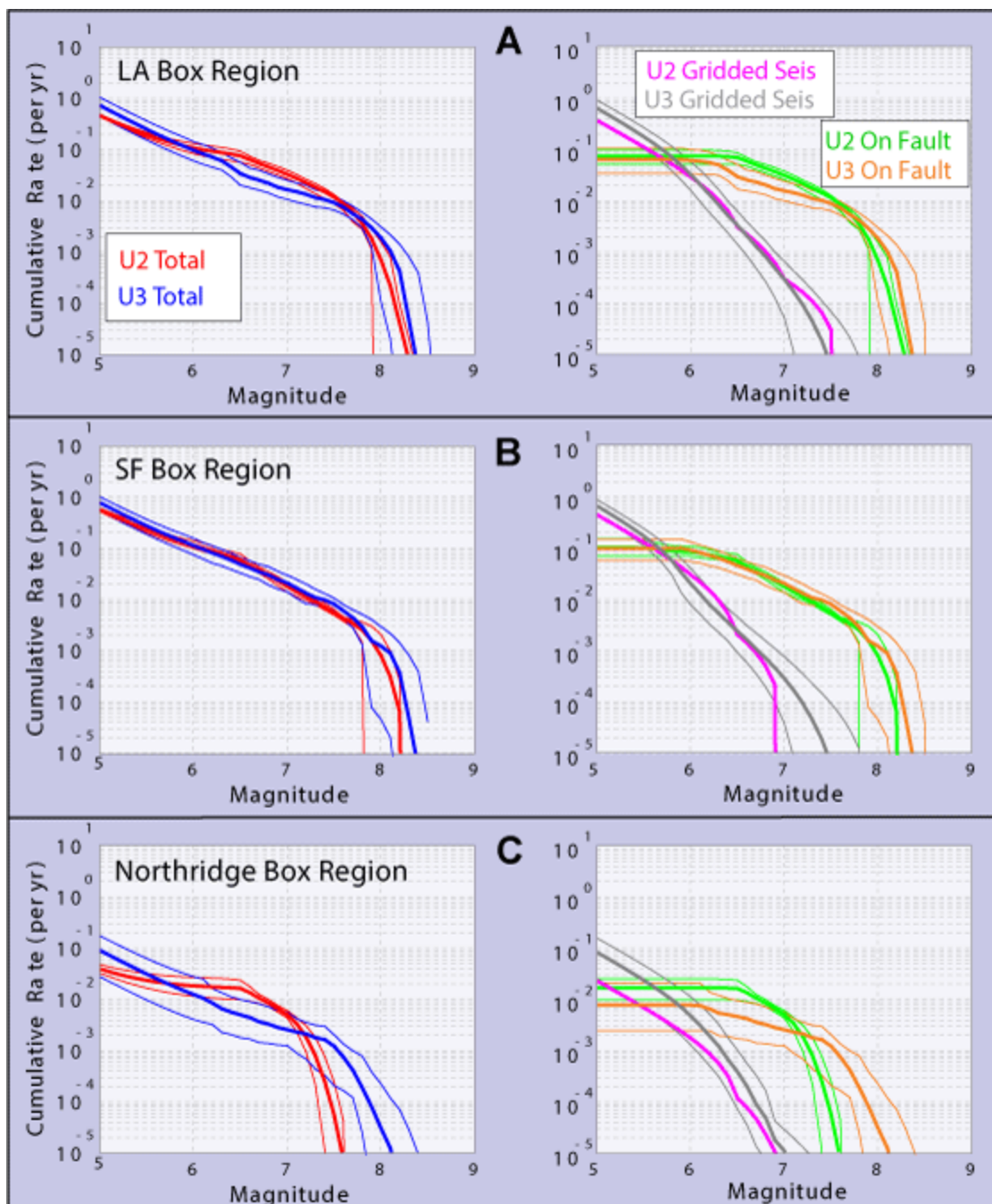
Figure 26. Plots showing cumulative magnitude-frequency distributions (MFDs) for selected regions. *A*, Total branch-averaged cumulative MFD for the Los Angeles region depicted in *figure 27*. Blue is for UCERF3, red is for UCERF2, and the thin lines represent the minimum and maximum over all branches. Note that aftershocks have been added back in for UCERF2 by reversing the Gardner-Knopoff filter described above. *B* and *C* are equivalent plots for the San Francisco and Northridge regions depicted in *figure 27*.

The UCERF3 MFDs for the Los Angeles region are more consistent with a GR distribution, with lower mean rates from $M6.0$ to $M7.7$ and higher mean rates above, as expected from the inclusion of multifault ruptures. The range of MFDs from the respective logic trees generally overlaps, except between $M6.5$ and $M7.0$ and just barely at $M5$. The UCERF3 rate of $M{\geq}5$ is about 58 percent greater than for UCERF2 (*table 13*), which is consistent with the branch-averaged 43 percent increase in $R_{M\geq5}^{total}$ discussed above. The total rate of $M{\geq}6.7$ events has gone down by a factor of two in UCERF3 because of the inclusion of multifault ruptures. Note also that while 40 new fault sections were added to the Los Angeles region in UCERF3, the new deformation models actually lowered the average total moment rate by about 7 percent (*table 13*).

The UCERF2 and UCERF3 MFDs for the San Francisco region are much more consistent. The rate of $M{\geq}5$ events has increased by 39 percent in UCERF3, which also is generally consistent with the effective 43 percent increase in $R_{M\geq5}^{total}$. The rate of $M{\geq}6.7$ events is essentially unchanged, while the rates of $M{\geq}7.5$ are about 48 percent higher, which reflects a tradeoff between the inclusion of multifault ruptures and a ~7-percent increase in moment rate from the addition of 33 new fault sections (*table 13*).

Table 13.　Number of fault sections, total moment rate (in units of 10^{18} N·m/year), and event rates (per year) inside the three subregion boxes shown in figure 27.

["U3" corresponds to UCERF3, and "U2" corresponds to UCERF2, both averaged over all logic tree branches. More rates and (or) lists of fault sections inside the regions are available upon request. Aftershocks are included as described in the *figure 26* caption]

	LA region		SF region		Northridge region	
	U3	U2	U3	U2	U3	U2
Number of fault sections	102	62	67	34	18	11
On-fault moment rate	4.18	4.51	3.12	2.91	0.43	0.36
Total rate M≥5	0.736	0.465	0.780	0.561	0.091	0.040
Total rate M≥6.7	0.025	0.053	0.035	0.037	0.0036	0.011

The UCERF3 MFD for the Northridge box (*fig. 26C*) is much more GR than that of UCERF2. In fact, we included this region here precisely because the strongly characteristic UCERF2 MFD was found to produce runaway aftershock sequences in preliminary Northridge earthquake ETAS simulations (Field, 2012). The inclusion of multifault ruptures has cut the average rate of $M{\geq}6.7$ events by a factor of three, even though UCERF3 has a 19 percent moment rate increase in this area (*table 13*). This change represents a significant improvement over UCERF2.
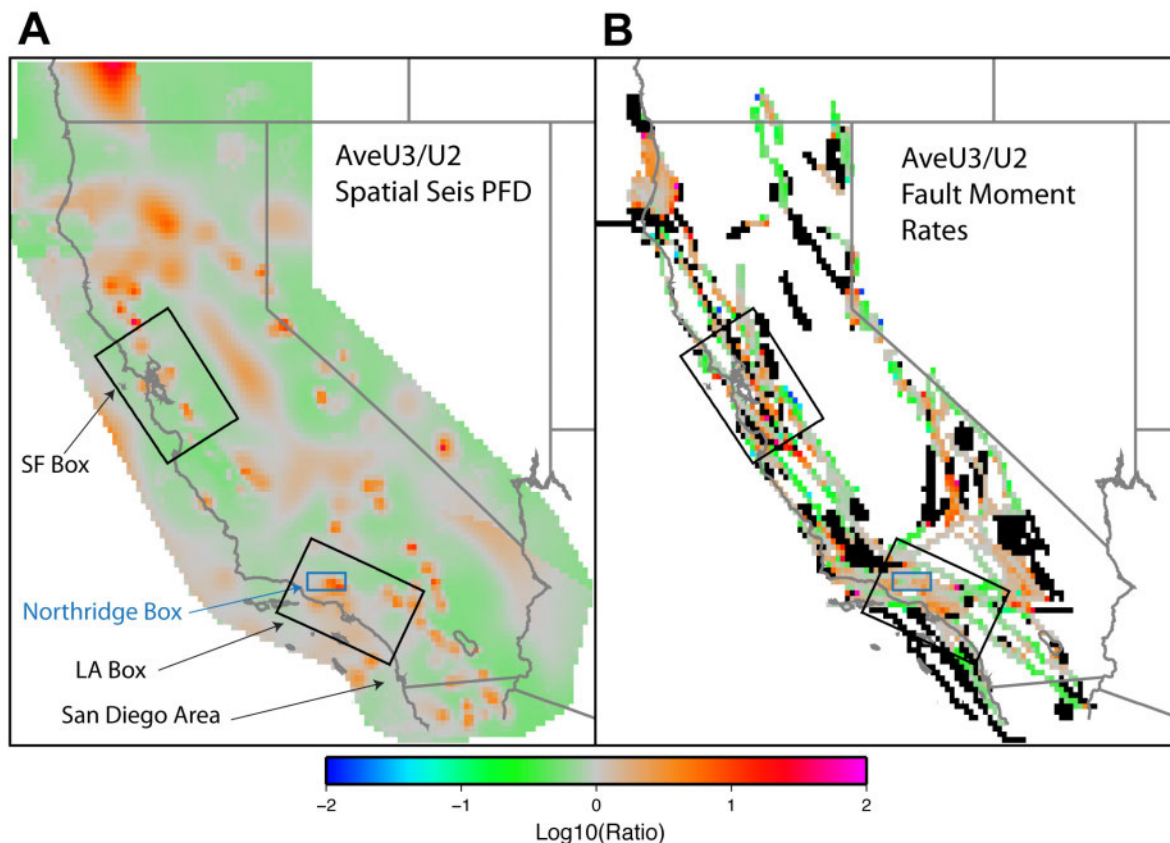
Figure 27. Maps showing ratios of UCERF2 and UCERF3 results. *A*, Ratio of the average UCERF3 to UCERF2 off-fault spatial seis PDF (equal to 0.5(U2sm+U3sm)/U2sm, where U2sm is the UCERF2 smoothed seismicity map *fig.14A*) and U3sm is the UCERF3 smoothed seismicity map (*fig. 14B*). This ratio does not include the overall regional rate increase for $R_{M \geq 5}^{total}$. *B*, Ratio of branch-averaged, on-fault moment rates between UCERF3 and UCERF2, where infinite values are shown in black (a result of new faults being added where none existed in UCERF2).

Participation Rate Maps

Figure 28 compares the mean UCERF3 participation rate maps for various magnitude thresholds with those for UCERF2. The ratio for *M*≥5 is generally high owing to the increase in $R_{M \geq 5}^{total}$, although there are some low areas near faults. The ratios for *M*≥6.7 are more extreme, including low areas near the UCERF2 Type C zones in northeastern California, high areas where new faults have been added (for example, offshore San Diego), and some low values on preexisting faults, reflecting lowered rates owing to the inclusion of multifault ruptures. More areas are capable of *M*≥7.7 events in UCERF3 because of an increase in $M_{max}^{off-fault}$, and more areas generate *M*≥8 events because of multifault ruptures. Such events on Elsinore and Death Valley are seen in UCERF2 but not UCERF3, because the former includes aleatory magnitude-area variability.
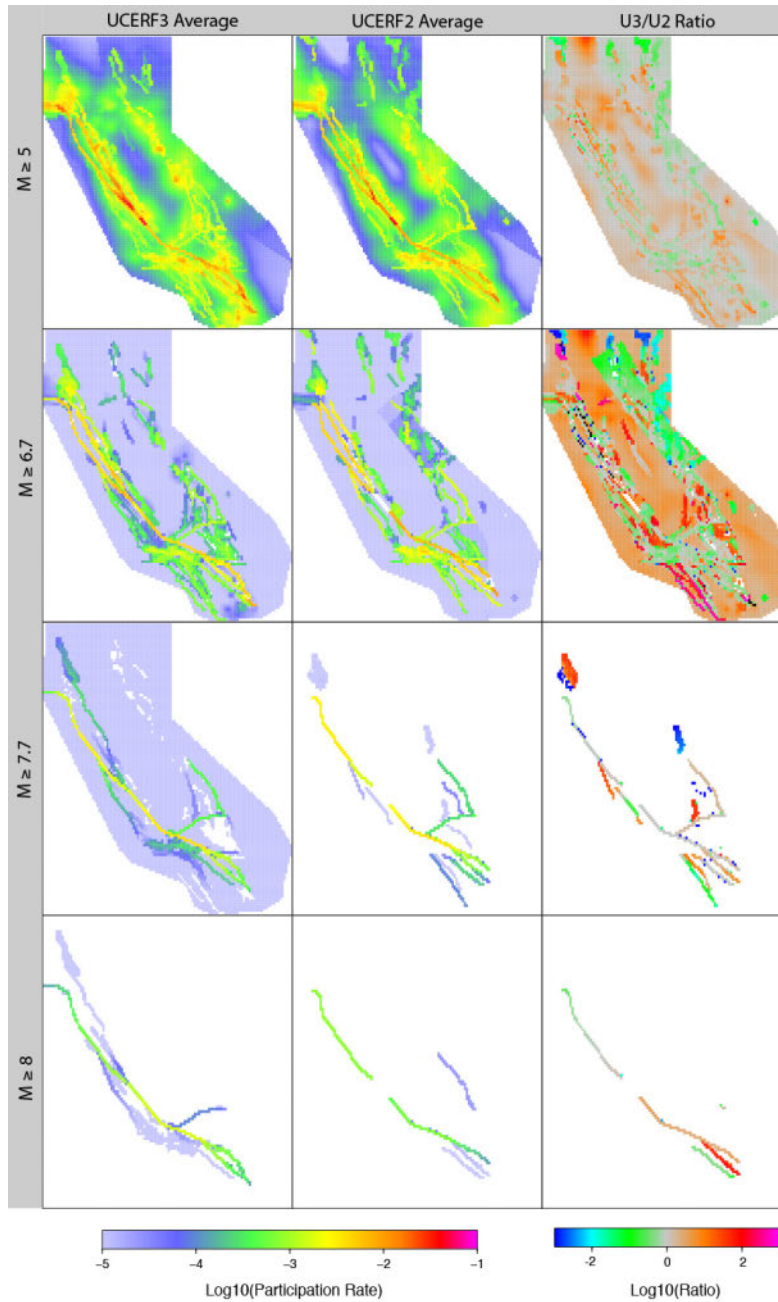
Figure 28.   Branch-averaged participation rate maps for UCERF3 and UCERF2, and for the ratio of the two (UCERF3/UCERF2). For the ratios, zero values are white, values above the color scale maximum (10^3) are black, and infinite values are white (where the UCERF2 denominator is zero). These plots have had aftershocks removed in order to make the comparison to UCERF2.

Implied Segmentation

Figure 29 (from appendix N, this report) shows model-implied segmentation along the SAF for both UCERF3 and UCERF2. As expected, segmentation is much less pronounced in the new model, which can significantly influence hazard. For example, in a strictly segmented model, a site on a segment boundary has twice as many events at zero distance, on average, than a site halfway down a segment, which is a potential factor of two difference in hazard. The effect is less when both single and multisegment ruptures are included, as with UCERF2 type A faults, but strict segmentation was effectively applied to adjacent type B faults in UCERF2. This effect partially explains a hazard reduction identified for the city of Oakland below.
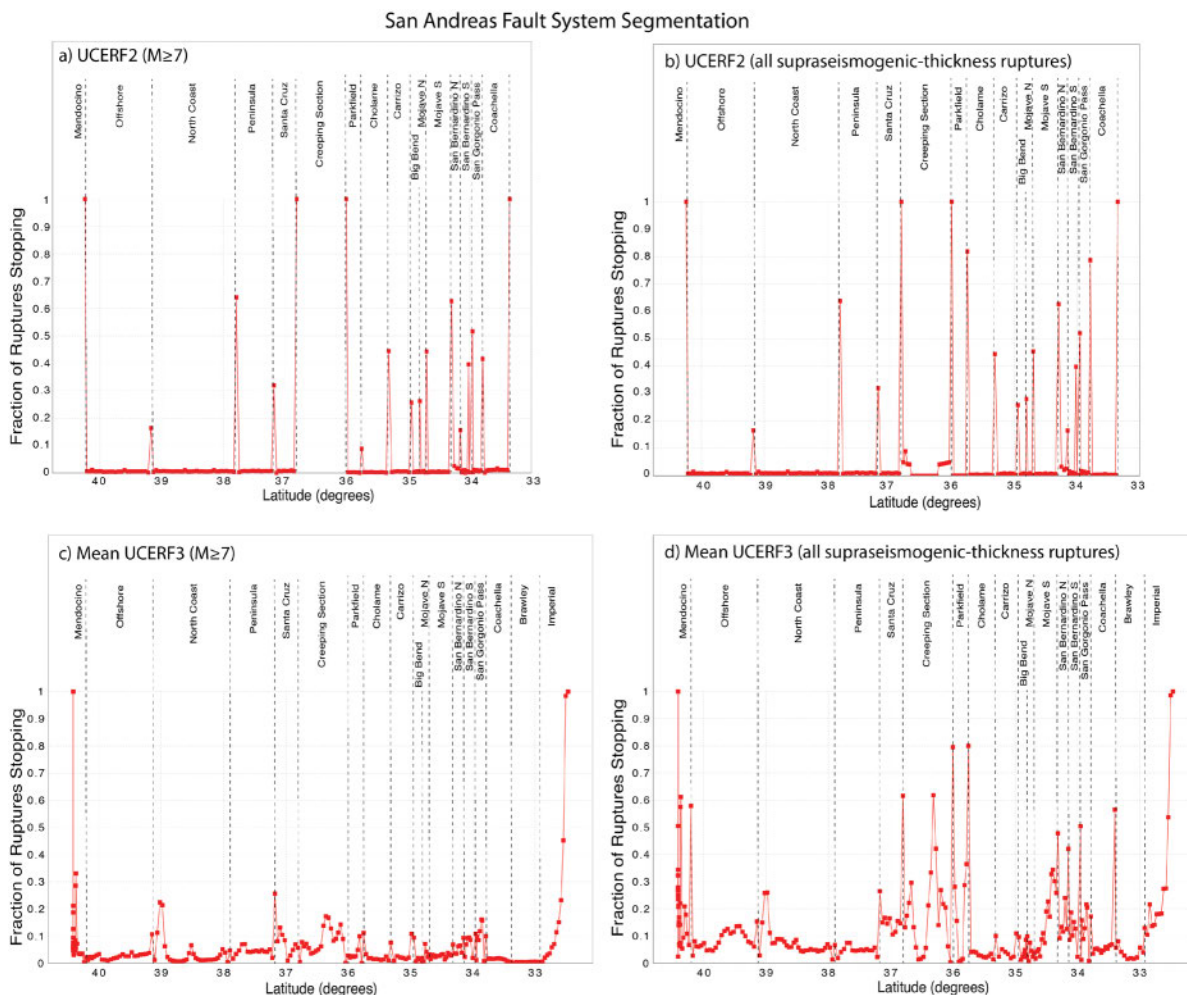
Figure 29.   Latitudinal plots showing average model-implied segmentation on the San Andreas Fault system for UCERF2 (top) and UCERF3 (bottom). The right side includes all supraseismogenic ruptures, whereas the left side is for only *M*≥7 events. The Brawley and Imperial Faults were not included in UCERF2 (and are therefore not shown for this model). Red points show the rate at which neighboring subsections do not rupture together, normalized by the total rate of ruptures involving those two subsections. Thus, when the red line reaches 1, there is strict segmentation and no ruptures break through that location.

Hazard Curves and Maps

Perhaps the most important questions for UCERF3 are: how and why have hazard estimates changed relative to UCERF2; and what are the most influential UCERF3 logic tree branches? This section addresses these questions, concluding that the dominant factors are deformation models (slip rates) and the new smoothed seismicity model, with methodological differences (multifault ruptures) being important in some places.

A seismic hazard curve gives, for a site, the probability of exceeding various earthquake-shaking levels over a specified period of time period (typically 50 years for building codes). The type of shaking is referred to as the ground motion parameter, or intensity measure type, with the most widely used including peak ground acceleration (PGA) and spectral acceleration (SA) at 3-second, 1-Hz, and 5-Hz (3s SA, 1Hz SA, and 5Hz SA, respectively). For example, the seismic design provisions recommended by the Building Seismic Safety Council (2009) use 1Hz and 5Hz SA. To support engineering design and building codes, the USGS NSHMP publishes probabilistic ground motion maps, which show the shaking levels that have a certain probability of being exceeded over a given time period (the hazard-curve x-axis value corresponding to some y-axis level, with the latter typically being the 2-percent- or 10-percent-in-50-years exceedance probability; see *figure 30* for an example).

To understand UCERF3 implications, a wide variety of hazard curves and maps have been generated using OpenSHA (www.OpenSHA.org), which was the only PSHA code that could accommodate UCERF3 (at least at that time). Doing so, however, required considerable effort in terms of implementing and verifying details needed for a precise replication of official 2008 NSHMP values (based on the NSHMP FORTRAN Code). Documentation of such implementation details will be provided in a forthcoming report, but results for all UCERF3 hazard calculations are currently available, with explanations, at *http://pubs.usgs.gov/of/2013/1165/data/UCERF3_SupplementalFiles/UCERF3.3/Hazard/*.

The results cited below come from this database. To ensure meaningful comparisons, the same set of ground motion models employed by NSHMP-2008 (for crustal faults) has been used. Although a wide array of hazard metrics are available at the above website, including the risk targeted ground motions now being considered by the BSSC (Luco and others, 2007), we focus only on those needed to make important points here.

Table 14 lists a number of sites where hazard curves have been computed, along with various UCERF3/UCERF2 hazard ratios (or more precisely, ratios of ground motions that have a certain probability of exceedance). The first 21 "NEHRP" sites are those used by the Building Seismic Safety Council (BSSC) when considering updates to seismic design provisions, and those listed as "Other" have been of particular interest to the WGCEP (for example, added during review). The full hazard-curve results for all these sites, from which the data in *table 14* were obtained, are available at *http://pubs.usgs.gov/of/2013/1165/data/UCERF3_SupplementalFiles/UCERF3.3/Hazard/HazardCurves/*. To complement these test-site calculations, we computed a variety of probabilistic ground motion maps. *Figure 31* shows the UCERF3/UCERF2 ratio map for 2-percent-in-50-year PGA (abbreviated as "2in50 PGA" hereafter).

One goal has been to understand and justify all "important" hazard differences between UCERF3 and UCERF2, which we define as greater than ten percent changes in probabilistic ground motion. Sites with such discrepancies are color coded in *table 14* and shown as non-yellow areas in *figure 31*. Although considerable effort has been put into understanding all such cases, we focus here on the more discrepant and informative examples.

The biggest change listed in *table 14* is a factor of 2.32 increase for 2in50 PGA at the Redding site, the location of which is plotted in *figure 31B*. The hazard curve for Redding is shown in *figure 30*, together with a tornado diagram and histogram revealing the influence of alternative logic tree branches, relative to a median branch. The SpatialSeisPDF logic tree branch is clearly most influential at this site; the two options (UCERF2 versus UCERF3 Smoothed Seis) create a strong bimodal distribution of ground-motion levels. This is because Redding is situated near a high seismicity area that is clearly visible in the UCERF3 Smoothed Seis model, but spreads into other regions in the UCERF2 Smoothed Seis model. Adding the new SpatialSeisPDF option has therefore increased the hazard at Redding, as well as at other sites indicated in *figure 31B* (which represents areas of correlation between *figure 27A* and *figure 31A*). However, the more focused smoothing kernels have also reduced the hazard at areas further from the seismicity clusters.

San Diego has a factor of 1.37 increase for 10in50 PGA, which is the largest change among the National Earthquake Hazards Reduction Program (NEHRP) sites in *table 14*. This increase is clearly attributable to the addition of new offshore faults, including those shown as black in *figure 27*: Carlsbad, Thirty Mile Bank, San Clemente, San Diego Trough north, San Diego Trough south, Oceanside, and half of Coronado Bank (the latter was used in only one of two UCERF2 fault models). *Figure 31C* highlights this and other areas influenced by the addition of faults, or by changes in average fault moment rates.

Cucamonga exhibits the biggest decrease among all sites in *table 14*, with a factor of 0.53 reduction for 2in50 PGA, which can also be seen in the ratio map in *figure 31D*. As noted previously in the context of *figure 25*, the rate of $M{\geq}6.7$ events on the Cucamonga Fault has dropped by a factor of three, due entirely to the inclusion of multifault ruptures (going from ~M6.7 single-segment ruptures in UCERF2 to also participating in events up to ~M8 in UCERF3). Therefore, this fault also represents the biggest methodological change with respect to hazard. Another example is the San Cayetano Fault section, as indicated in *figure 31D* and also shown in *figure 25*. We reiterate that both these cases were deemed a significant improvement at the fault-by-fault review meetings (*table 2*).

The Oakland site shows the largest reduction amongst NEHRP sites in *table 14*, a drop of 22 percent for 10in50 5Hz SA, which is more challenging in terms of parsing influences. The hazard in Oakland is dominated by the nearby North fault section, which actually had a 90 percent increase in the average moment rate. This increase is apparently countered by its now participating in more multifault ruptures; for example, the 10,000-year event has gone from ~M7.3 in UCERF2 to ~M7.7 in UCERF3 (*fig. 25*). Another significant factor, revealed by high-resolution hazard maps, is that Oakland is situated near a UCERF2 segment boundary, which gives it a higher rate of events in close proximity than at other locations along the fault. Removing the strong influence of this segment boundary in UCERF3 therefore contributed to reducing the hazard in Oakland (another methodological influence).

Other cites of interest include Los Angeles, which has only a minor reduction (<10 percent) for the location in *table 14*, and San Francisco, which also shows minor differences in *table 14*. An exception for the San Francisco site is 10in50 1Hz SA, which dropped by 11 percent. Evaluation of the tornado diagram for this location (available at *http://pubs.usgs.gov /of/2013/1165/data/UCERF3_SupplementalFiles/UCERF3.3/Hazard/HazardCurves/Sites/sites/SAN_FRANCISCO/10in50_1Hz.pdf*) implies that average slip-rate changes are responsible. Sacramento, another site of interest, exhibits an 11 percent increase for 2in50 PGA.

The associated tornado diagram (*http://pubs.usgs.gov/of/2013/1165/data/UCERF3_SupplementalFiles/UCERF3.3/Hazard/HazardCurves/Sites/sites/SACRAMENTO/2in50_PGA.pdf*) indicates that gridded seismicity is most influential, so the change can be attributed to the total regional rate increase for UCERF3.

To summarize, the following are generally found to be most influential in terms of UCERF2 to UCERF3 hazard changes (listed in descending order of importance, although this has a heavy spatial dependence):

- Addition of new faults and average moment rate changes on existing faults
- Addition of the UCERF3 Smoothed Seis option
- Inclusion of multifault ruptures in UCERF3
- The effective 43 percent increase in the total rate of $M{\geq}5$ events

This conclusion generally applies to all ground motion parameters and probability levels examined.
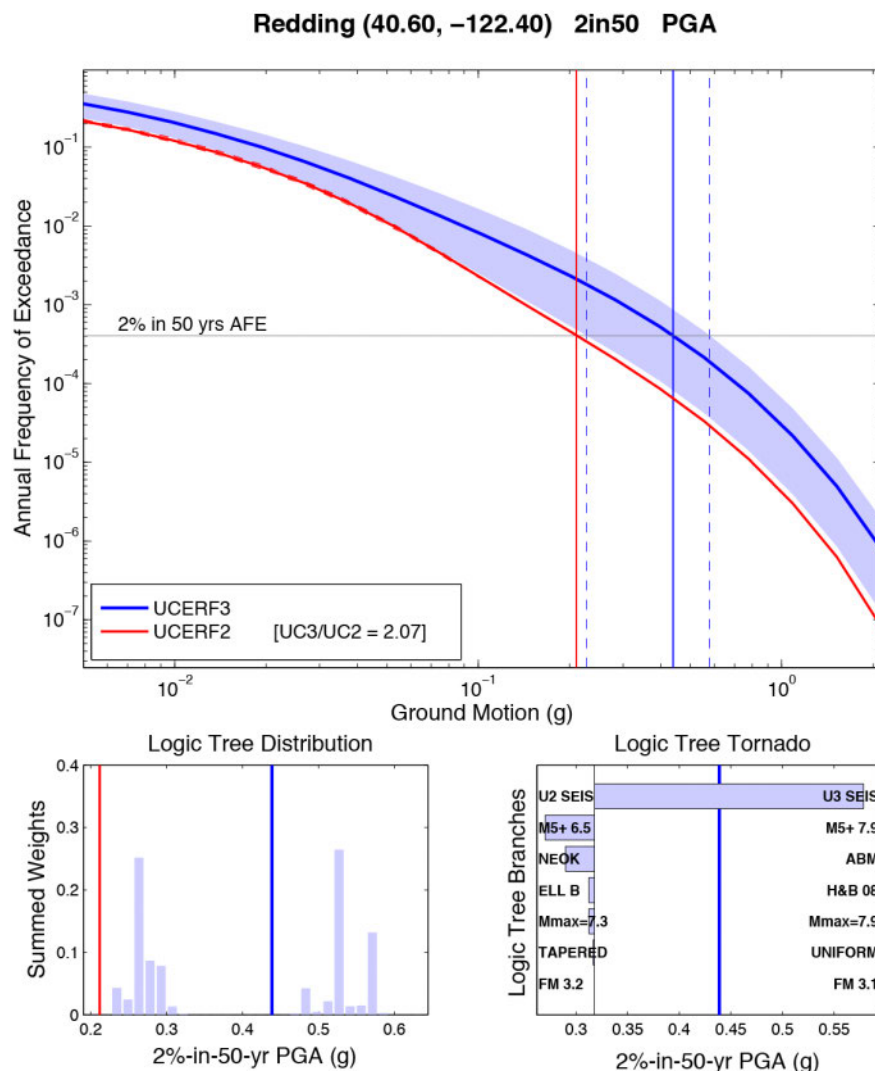
Figure 30. Graphs illustrating the hazard-curve example for PGA at the Redding site listed in _table 13_. Top, Comparison of UCERF3 and UCERF2 hazard curves. The blue and red lines mark the weighted mean hazard curve across all UCERF3 and UCERF2 (time-independent) logic tree branches, respectively. The light blue shaded region delineates the minimum and maximum hazard values among all UCERF3 branches, and the dashed red lines are the same for UCERF2 (just barely visible to the left). The horizontal grey line marks the 2-percent-in-50-year probability of exceedance level. The vertical lines mark the mean (solid) and minimum and maximum (dashed) 2-percent-in-50-year ground-motion values. Bottom left, Distribution of 2-percent-in-50-year ground motions across the UCERF3 logic tree (considering branch weights). Color coding of the vertical lines is the same as at the top. Bottom right, Tornado diagram (see, for example, Porter and others, 2012), indicating the influence of each UCERF3 logic tree branch on the overall uncertainty. The "swings" away from the thin vertical line represent the influence of changing each branch option, one at a time, relative to the branch corresponding to the median, and ignoring branch weights.

Table 14.   Ratios of UCERF3 to UCERF2 ground motion exceedance values for varios sites, intensity measures, and return periods*.

Site	Lat	Lon	Group	2% in 50 years				10% in 50 years				RTGM		Average
				PGA	5Hz SA	1Hz SA	4sec SA	PGA	5Hz SA	1Hz SA	4sec SA	5Hz	1Hz	
Century City	34.05	-118.40	NEHRP	1.07	1.07	1.04	1.04	1.07	1.05	1.02	1.00	1.06	1.02	1.04
Concord	37.95	-122.00	NEHRP	1.02	0.98	1.01	1.09	0.96	0.93	0.94	1.01	0.97	0.98	0.99
Irvine	33.65	-117.80	NEHRP	0.91	0.91	0.90	0.98	0.98	0.98	0.92	0.90	0.94	0.91	0.93
Long Beach	33.80	-118.20	NEHRP	1.15	1.13	1.11	1.06	1.13	1.11	1.04	1.00	1.12	1.07	1.09
Los Angeles	34.05	-118.25	NEHRP	0.94	0.93	0.95	1.09	0.94	0.93	0.91	0.96	0.93	0.93	0.95
Monterey	36.60	-121.90	NEHRP	0.96	0.94	0.96	0.99	0.93	0.93	0.96	0.99	0.97	0.98	0.96
Northridge	34.20	-118.55	NEHRP	1.20	1.18	1.16	1.20	1.15	1.13	1.06	1.03	1.15	1.09	1.14
Oakland	37.80	-122.25	NEHRP	0.85	0.83	0.87	0.99	0.81	0.78	0.80	0.90	0.81	0.83	0.85
Riverside	33.95	-117.40	NEHRP	1.03	1.02	0.97	1.02	0.98	0.97	0.88	0.85	0.99	0.91	0.96
Sacramento	38.60	-121.50	NEHRP	1.11	1.10	1.07	1.10	1.04	1.02	1.02	1.06	1.05	1.03	1.06
San Bernardino	34.10	-117.30	NEHRP	0.90	0.89	0.88	1.03	0.89	0.86	0.79	0.81	0.88	0.83	0.88
San Diego	32.70	-117.15	NEHRP	1.18	1.19	1.12	1.00	1.37	1.36	1.23	1.06	1.21	1.12	1.19
San Francisco	37.75	-122.40	NEHRP	0.94	0.93	0.91	0.92	0.92	0.90	0.89	0.90	0.91	0.90	0.91
San Jose	37.35	-121.90	NEHRP	1.07	1.07	1.12	1.20	1.05	1.04	1.08	1.18	1.04	1.09	1.09
San Luis Obispo	35.30	-120.65	NEHRP	1.09	1.08	1.07	1.09	1.03	1.02	1.00	0.99	1.06	1.04	1.05
San Mateo	37.55	-122.30	NEHRP	0.96	0.95	0.95	0.96	0.96	0.96	0.95	0.96	0.95	0.95	0.95
Santa Barbara	34.45	-119.70	NEHRP	0.91	0.88	0.93	1.00	0.83	0.81	0.81	0.89	0.86	0.89	0.88
Santa Cruz	36.95	-122.05	NEHRP	1.03	1.03	1.04	1.07	1.03	1.03	1.05	1.06	1.04	1.05	1.04
Santa Rosa	38.45	-122.70	NEHRP	0.88	0.88	0.87	0.93	0.87	0.85	0.82	0.85	0.88	0.86	0.87
Vallejo	38.10	-122.25	NEHRP	1.28	1.23	1.26	1.25	1.13	1.10	1.12	1.12	1.13	1.16	1.18
Ventura	34.30	-119.30	NEHRP	0.94	0.94	0.96	1.08	0.94	0.92	0.89	0.94	0.91	0.92	0.95
Bakersfield	35.35	-119.00	Other	1.06	1.06	1.06	1.07	1.02	1.02	0.99	0.97	1.04	1.01	1.03
Big Sur	36.25	-121.75	Other	1.26	1.22	1.24	1.17	0.94	0.94	0.96	0.95	1.13	1.17	1.10
Brawley	33.00	-115.55	Other	1.09	1.08	1.14	1.38	1.10	1.08	1.08	1.12	1.08	1.09	1.12
Brookings	42.05	-124.25	Other	2.06	2.12	1.98	1.81	1.67	1.66	1.52	1.54	1.91	1.80	1.81
Carson City	39.15	-119.75	Other	1.19	1.26	1.19	0.98	1.18	1.22	1.15	1.00	1.22	1.16	1.16

Site	Lat	Lon	Group	2% in 50 years				10% in 50 years				RTGM		Average
				PGA	5Hz SA	1Hz SA	4sec SA	PGA	5Hz SA	1Hz SA	4sec SA	5Hz	1Hz	
Coalinga	36.15	-120.40	Other	1.03	1.03	0.98	1.02	1.06	1.05	0.97	0.95	1.05	0.98	1.01
Cucamonga	34.20	-117.55	Other	0.53	0.53	0.67	0.98	0.57	0.57	0.60	0.77	0.57	0.64	0.64
Death Valley	36.35	-116.85	Other	0.58	0.56	0.60	0.73	0.57	0.58	0.58	0.61	0.58	0.62	0.60
Diablo Canyon	35.20	-120.85	Other	0.90	0.85	0.84	0.92	0.88	0.87	0.88	0.89	0.88	0.88	0.88
Eureka	40.80	-124.20	Other	1.05	1.02	1.07	1.04	1.17	1.16	1.10	1.02	1.06	1.08	1.08
Fresno	36.75	-119.75	Other	1.22	1.22	1.14	1.09	1.15	1.15	1.08	1.06	1.17	1.11	1.14
Malibu West	34.05	-118.95	Other	0.73	0.68	0.71	0.95	0.89	0.86	0.83	0.91	0.77	0.78	0.81
Morgan Hill	37.15	-121.65	Other	0.94	0.93	1.05	1.24	0.94	0.94	1.01	1.19	0.96	1.03	1.02
Palm Springs	33.85	-116.55	Other	0.93	0.90	0.90	0.94	0.91	0.91	0.88	0.89	0.91	0.88	0.91
Palmdale	34.50	-118.00	Other	0.95	0.93	0.93	0.97	0.92	0.92	0.87	0.86	0.93	0.91	0.92
Pasadena	34.15	-118.15	Other	0.86	0.85	0.91	1.09	0.78	0.76	0.79	0.91	0.82	0.86	0.86
Redding	40.60	-122.40	Other	2.32	2.29	1.67	1.18	2.21	2.19	1.42	1.12	2.15	1.55	1.81
Reno	39.55	-119.80	Other	0.93	0.94	0.84	0.71	1.00	1.02	0.93	0.82	0.99	0.89	0.91
San Onofre	33.40	-117.55	Other	1.05	1.04	1.03	1.02	0.99	0.99	0.95	0.92	1.04	0.99	1.00
AC01	34.42	-118.10	PBR	0.98	0.97	0.98	1.02	0.95	0.94	0.93	0.94	0.95	0.95	0.96
ACTN	34.46	-118.18	PBR	0.97	0.96	0.98	1.02	0.94	0.92	0.92	0.93	0.94	0.94	0.95
BKBU	34.56	-117.73	PBR	0.98	0.99	0.98	1.00	0.98	1.00	0.94	0.89	0.99	0.95	0.97
GLBT	33.96	-117.38	PBR	1.03	1.01	0.97	1.02	0.97	0.96	0.87	0.84	0.98	0.90	0.96
GOPH	33.90	-117.36	PBR	1.02	1.01	0.96	1.00	0.97	0.96	0.88	0.84	0.98	0.91	0.95
GV03	34.28	-117.23	PBR	0.67	0.66	0.69	0.86	0.71	0.70	0.67	0.74	0.70	0.68	0.71
LBUT2	34.59	-117.81	PBR	0.98	0.99	0.98	1.01	0.98	0.99	0.94	0.90	0.99	0.95	0.97
LMAT	33.79	-117.40	PBR	1.10	1.11	1.03	0.96	1.13	1.14	1.03	0.92	1.11	1.02	1.05
LPER	33.89	-117.16	PBR	0.82	0.78	0.77	0.88	0.77	0.76	0.68	0.68	0.79	0.74	0.77
MKBD	33.88	-117.39	PBR	1.03	1.03	0.97	1.00	0.99	0.99	0.90	0.86	1.00	0.93	0.97
MRVY	33.93	-117.17	PBR	0.83	0.80	0.82	0.95	0.76	0.74	0.66	0.69	0.79	0.75	0.78
NUEVO	33.78	-117.15	PBR	0.93	0.90	0.88	0.94	0.87	0.86	0.80	0.78	0.89	0.84	0.87
PACI2	34.39	-118.05	PBR	0.99	0.98	0.99	1.03	0.95	0.94	0.93	0.94	0.95	0.95	0.97

Site	Lat	Lon	Group	2% in 50 years				10% in 50 years				RTGM		Average
				PGA	5Hz SA	1Hz SA	4sec SA	PGA	5Hz SA	1Hz SA	4sec SA	5Hz	1Hz	
PBWL	34.41	-117.86	PBR	1.00	1.00	0.95	0.98	1.02	1.03	0.96	0.88	1.03	0.96	0.98
PEDLEY1	33.99	-117.46	PBR	1.04	1.03	0.99	1.02	0.99	0.98	0.90	0.87	0.99	0.92	0.97
PERR2	33.79	-117.24	PBR	0.97	0.95	0.91	0.96	0.93	0.93	0.86	0.83	0.95	0.89	0.92
PERRM	33.80	-117.25	PBR	0.96	0.95	0.91	0.96	0.93	0.92	0.86	0.83	0.95	0.89	0.92
PIBU	34.65	-117.85	PBR	0.99	1.00	0.99	1.01	0.98	0.99	0.94	0.91	0.99	0.95	0.98
SW01	34.30	-117.34	PBR	0.79	0.78	0.81	0.95	0.77	0.75	0.72	0.78	0.77	0.76	0.79
UCR	33.96	-117.32	PBR	0.99	0.96	0.92	1.01	0.94	0.92	0.82	0.80	0.94	0.86	0.92

 *In the "Group" column, "NEHRP" sites are from table C11.4-1 of the Recommended Seismic Provisions for New Buildings and Other Structures (2009). Those listed as "Other" are WGCEP-chosen sites, and those listed as "PBR" are locations of precariously balanced rocks (James Brune, written commun., 2012). The "RTGM" column gives ratios of the Risk Targeted Ground Motions, as described by Luco and others (2007). A digital version (Microsoft Excel file format xlsx) of this table is available *here*.

To help quantify the influence of UCERF3 epistemic uncertainties, 2in50 PGA maps were computed for all 1,440 logic tree branches. We then averaged over the options on each branch separately, and normalized by the total average, to reveal the influence of each. The process is illustrated in *figure 32* for Deformation Models, where each option is represented by an average over the associated subset of maps (360 given the four branch options in this example) divided by the average over all 1,440 maps. *Figure 32* reveals a strong influence from the block boundaries used in the ABM model (red areas), which was the basis for down-weighting this model (because some of these areas may be model artifacts).

The resultant branch ratio maps for all UCERF3 epistemic uncertainties are available as links in *table 15*. The most influential choices in descending order of overall importance are: deformation models, UCERF2 versus UCERF3 smoothed seis, and scaling relationships. Fault models and total M≥5 event rate have some influence in specific areas, while $M_{max}^{off-fault}$ and slip along rupture (Dsr) have very little influence. These conclusions are generally applicable to other return periods and ground motion parameters, although we reemphasize the spatial dependence of such conclusions.

Table 15.   Influence of different logic-tree branches.

[Clicking on the links in this table will show the relative influence of different logic tree branches (as labeled) for 2-percent-in-50-year peak ground acceleration. These are subdirectories of
http://pubs.usgs.gov/of/2013/1165/data/UCERF3_SupplementalFiles/UCERF3.3/Hazard/BranchRatios/

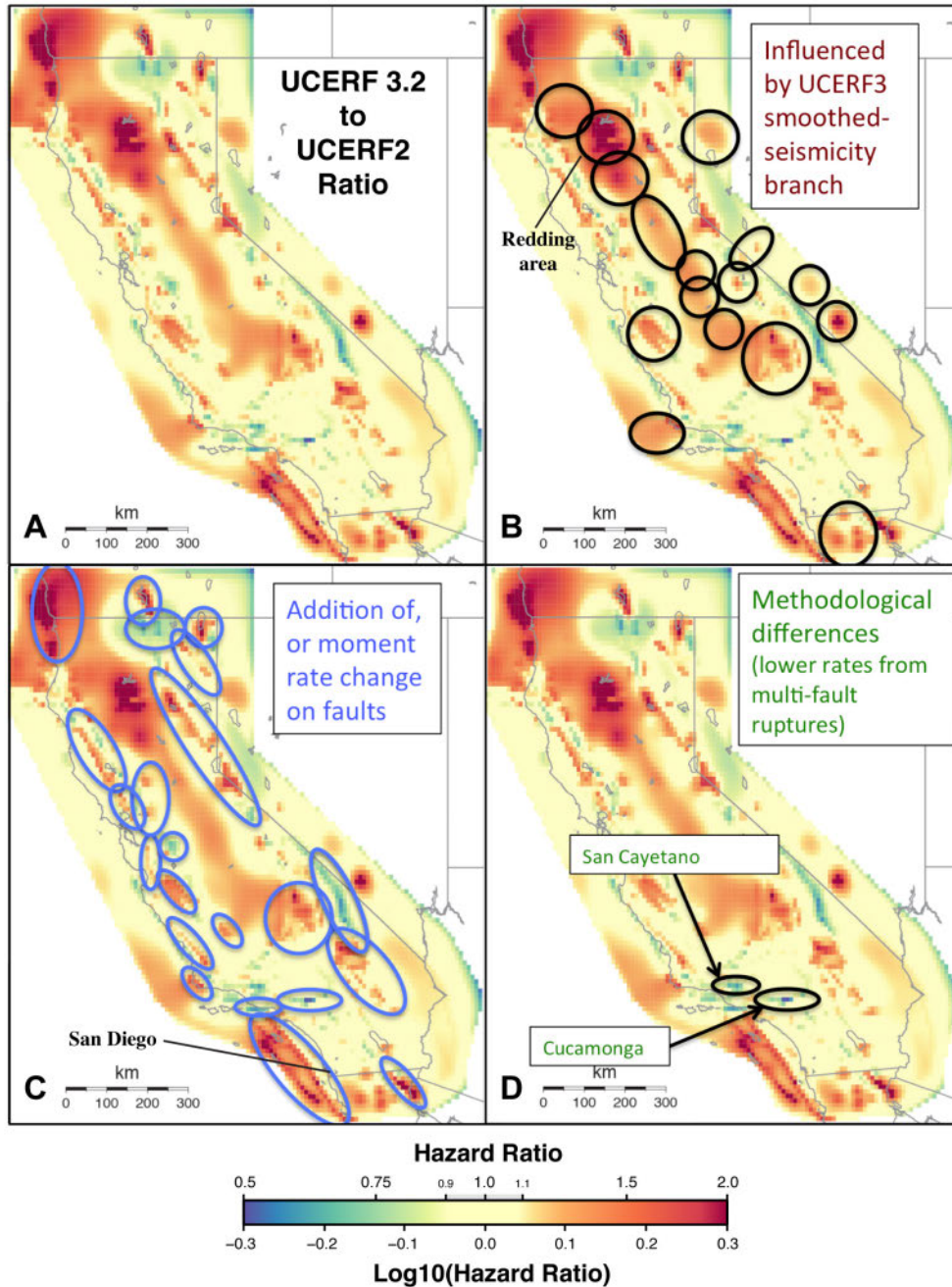| Branch Ratio Maps for Logic tree Subsets |
|---|
| *Fault Model 3.1 versus 3.2* |
| *Deformation models* |
| *Scaling relationships* |
| *Tapered versus boxcar slip along rupture (Dsr)* |
| *Total M≥5 event rate* |
| *Off-fault M_{max}* |
| *Off-fault spatial seis PDF (UCERF2 vs UCERF3 smoothed seismicity)* |
| *Total M≥5 event rate and off-fault M_{max}* |

Figure 31. Comparison of UCERF2 and UCERF3 for 2-percent-in-50-year PGA. *A*, Ratio of UCERF3 2-percent-in-50 year PGA map divided by that for UCERF2. The attenuation relationships used for these calculations are the same ones used in the NSHMP 2008 maps. In *B–D*, ovals show areas where discrepancies can be explained by (*B*) addition of the UCERF3 Smoothed Seism option, (*C*) addition of new faults or average moment-rate changes on existing faults, and (*D*) methodological changes in terms of including multifault ruptures.
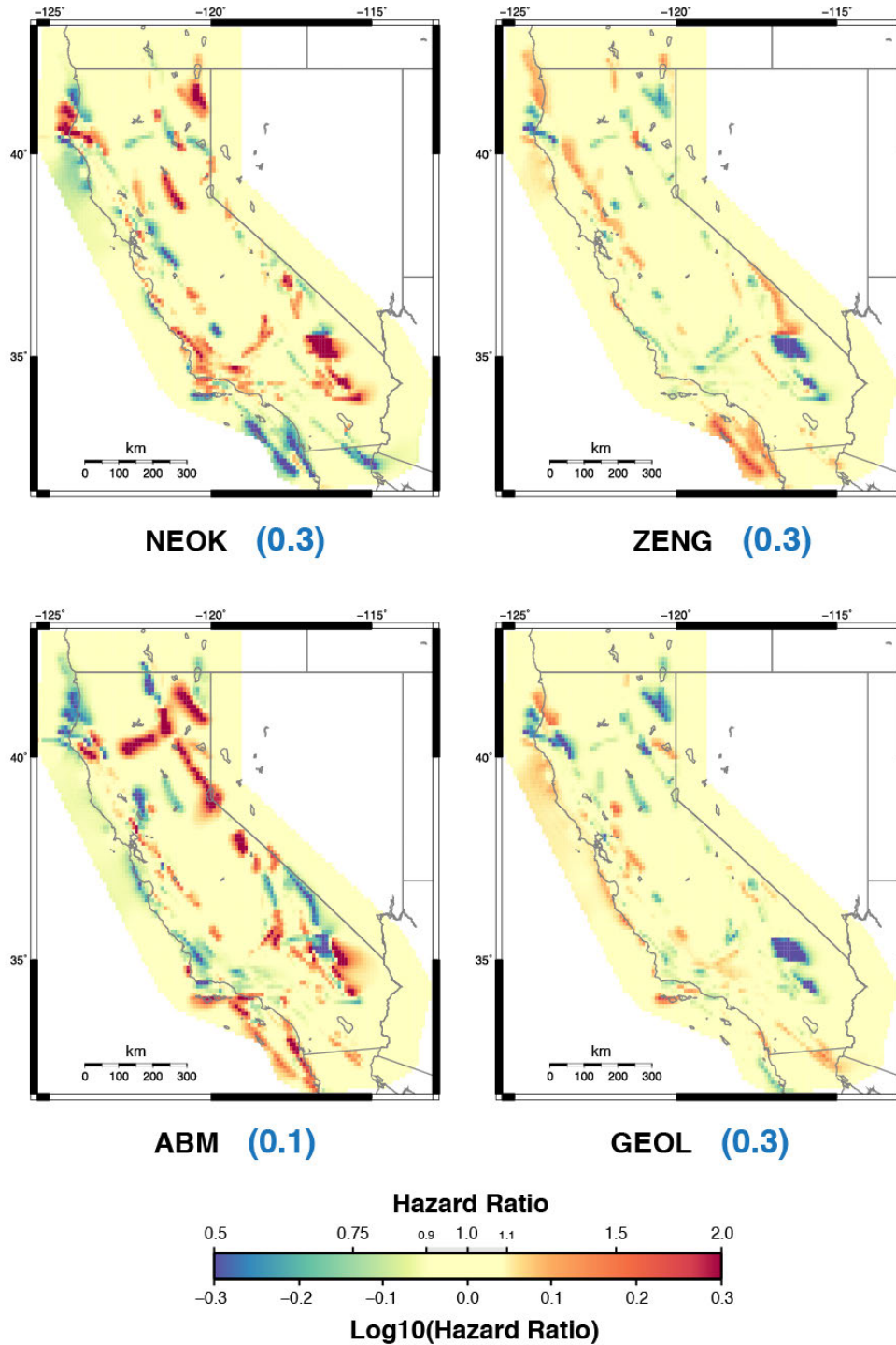
Figure 32. Branch ratio maps showing the influence of each deformation model on 2-percent-in-50 year peak ground acceleration. These ratios are obtained by averaging results over deformation-model subset branches, and then dividing by the total average. Numbers in blue indicate the weights each model is given in UCERF3.

Sensitivity Tests

Simulated Annealing Convergence and Nonuniqueness

We first consider how well the simulated annealing algorithm converges, which depends on the problem and how long the inversion algorithm is run. We also consider the problem of nonuniqueness, in particular how the simulated annealing samples the null space. Given that there can be an infinite, yet bounded, number of viable models in this situation, the more appropriate question is how many runs are needed to get stable averages of individual solutions. We refer to both of these issues as convergence because the convergence and nonuniqueness problems cannot be separated in our tests.

Whether the inversion is over-, under-, or mixed-determined depends on the evaluation metric of interested. We are solving for more than 250,000 unknown rupture rates (f_r) with about 37,000 equality constraints (appendix N, this report), so clearly individual solutions are not unique. But what about metrics that are more relevant to seismic hazard, such as fault section participation MFDs and hazard curves? And what about branch-averaged results versus what is resolved on individual branches? We quantify sensitivity to each of these here, and conclude that convergence is not an issue for hazard-related metrics.

Individual Logic Tree Branches

To test convergence for individual branches, we ran 200 simulated annealing inversions for the reference model (bold typeface options in *figure 3*). About 10,000 nonzero-rate (or above-water-level) ruptures are needed to "fit" the data on a single run, which is only ~4 percent of all ruptures. *Figure 33* shows how this number varies as a function of the number of runs averaged. For example, averaging 10 runs, as done for each branch in UCERF3, increases the number to ~38,000 (~15 percent of ruptures), and averaging 200 runs increases the number to ~115,000 (~46 percent). This indicates that each solution samples a different set of ruptures in satisfying the data, as expected for an underdetermined problem. The roll off in *figure 33* suggests that an infinite number of runs would yield 50 to 60 percent ruptures above water level, implying that half the ruptures are excluded on this particular branch.

We attempted to quantify the number of runs needed to resolve mean rupture rates to some level of precision. However, interpretations were complicated by the fact that most rates are at water level (producing a bimodal distribution with a relatively high spike at the water level). Therefore the mean rupture rates are difficult to resolve on individual branches, although we did find that those with higher rates are also better resolved.

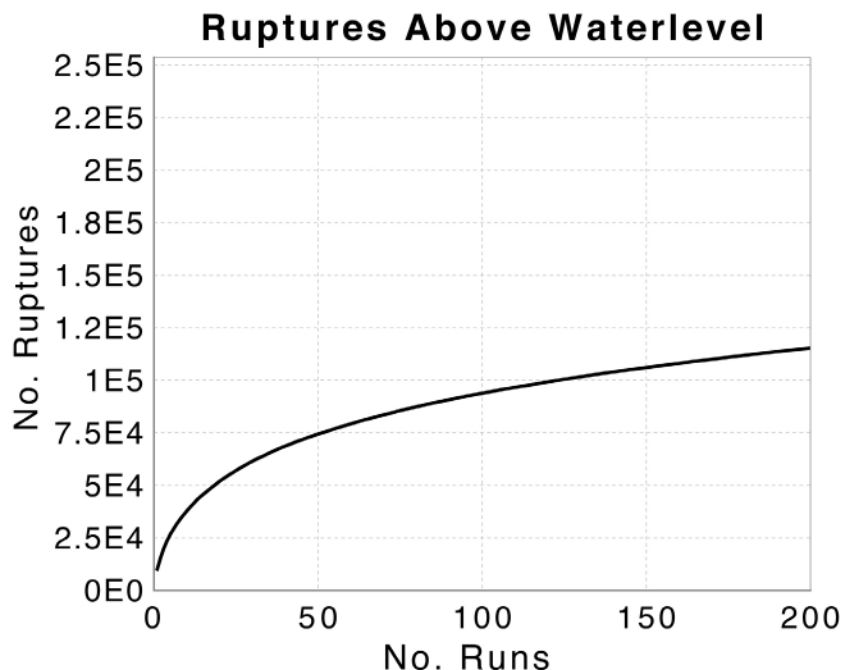**Ruptures Above Waterlevel**

Figure 33.   Graph showing number of above-water-level ruptures as a function of the number of simulated annealing runs averaged (for the reference branch). The maximum value on the y-axis is the total number of ruptures (~250,000 = 2.5×10⁵ = 2.5E5).

Fault section participation MFDs represents a more appropriate metric for hazard. For a given magnitude event, standard PSHA for a site is relatively insensitive to rupture-endpoint differences, and completely so if the closest point to the rupture surface is the same. _Figure 34_ shows three participation MFDs obtained from the 200 reference branch runs. In terms of $M>6.7$ rate variability among the 200 solutions, defined as the sample standard deviation (s) divided by the sample mean (μ), these represent the worst, median, and best cases among all fault sections. The number of inversion runs (N) needed to get "well resolved" average estimates (those with the upper 95-percent confidence bound ($\mu + 1.96s/\sqrt{N}$) within 10 percent of the mean) is:

$$\mu + 1.96s/\sqrt{N} \leq 1.1\mu$$

where $s/\sqrt{N}$ is the sample standard deviation of the mean. Solving for N we obtain:

$$N = (19.6s/\mu)^2$$

With the sample statistics shown in _figure 34_, the implied number of runs needed for well-resolved $M{\geq}6.7$ event rates is 1,294 for the worst case (Richfield), 9 for the median case (Puente Hills), and 1 for the best case (San Jacinto-Anza). The median is near the number of runs chosen for each branch in UCERF3 (10), which implies that roughly half our fault sections have "well resolved" rates on individual branches. The worst case implies that, for some fault sections, many more runs would be needed to get well-resolved rates on individual branches. However, these turn out to be the least hazardous faults, because there is anticorrelation between variability and mean rate. For example, the worst case in _figure 34_ also has the lowest rate of $M{\geq}6.7$ events among all fault sections (with an average repeat time exceeding 1,000,000 years). All fault sections that have average $M{\geq}6.7$ repeat times less than 1,000 years are well resolved,

and the mean fractional uncertainty for all faults, weighted by the mean rate of each section, is 1.04.

We have also conducted this same analysis with respect to hazard curves. Specifically, from the 200 reference branch runs, and for all test locations in *table 14*, we computed sample means and standard deviations for 2in50 and 1in100 ground motion levels for PGA, 5Hz SA, 1Hz SA, and 4sec SA. Note that the 1in100 case, representing a 10,000-year return period, and 4-sec SA were added to test more extreme circumstances (where more uncertainty might be expected). In terms of variability (s/μ), the worst case is 2in50 5Hz SA at Brookings (located just north of California on the Oregon coast). The fractional uncertainty for this worst case, $(\mu + 1.96s/\sqrt{N})/\mu$, is 1.03 for N=10, meaning the upper 95- percent confidence bound is 3 percent above the mean with 10 runs. The median and best cases among this test had fractional uncertainties of 1.004 and 1.0001. These results imply that all customary hazard metrics are well resolved on individual branches given the 10 simulated annealing runs on each in UCERF3. The same conclusions can be drawn by examining the mean and range of hazard curves obtained among the 200 reference branch runs, which are available for each site at *http://pubs.usgs.gov/of/2013/1165/data/UCERF3_SupplementalFiles/UCERF3.3/Hazard/InversionTests/Convergence/* (note that the range plotted is the minimum and maximum among all branches, not a standard-deviation-based confidence or range, which would require very thin lines to discern from the mean).
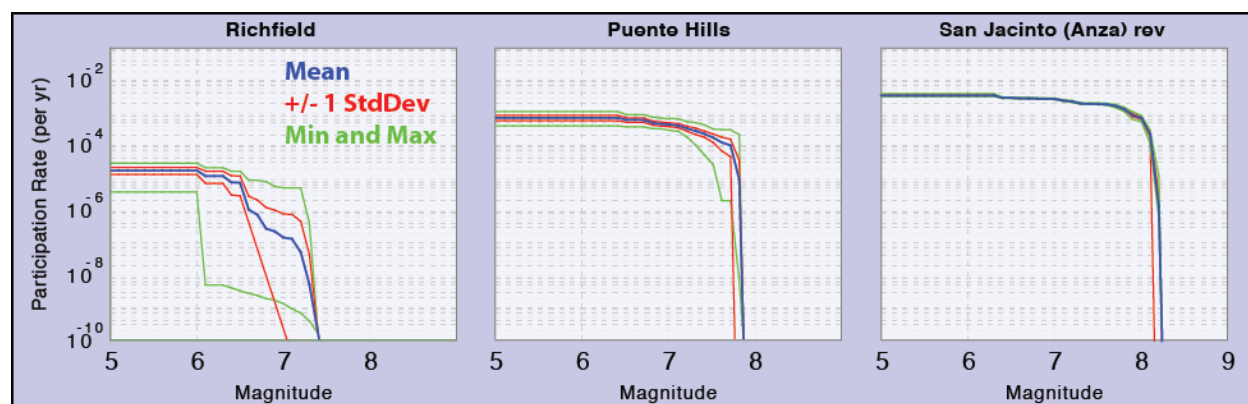

Figure 34.   Graphs showing cumulative participation magnitude-frequency distribution statistics for 200 simulated annealing runs on the reference branch. The fault-section examples shown here represent the worst case (Richfield), median case (Puente Hils), and best case (San Jacinto-Anza) in terms of fractional uncertainty described in the test (which is proportional to the standard deviation divided by the mean).

Branch-Averaged Results

The 1,440 different logic tree branches provide a great deal of additional averaging with respect to mean hazard, and we can use the 10 different runs for each branch to quantify how well such metrics are resolved for branch-averaged results. *Figure 35* shows the number of ruptures above water level for branch-averaged results, as a function of how many runs on each branch are included. If only one simulated annealing run is used for each branch, about 176,000 events (76 percent) are above water level in the branch-averaged model. After averaging over all 10 runs, the full UCERF3 branch-averaged model has about 236,000 ruptures above water level

(94 percent). Mean rupture rates are also much better resolved, but they are still difficult to interpret given bimodal distributions with respect to water levels.
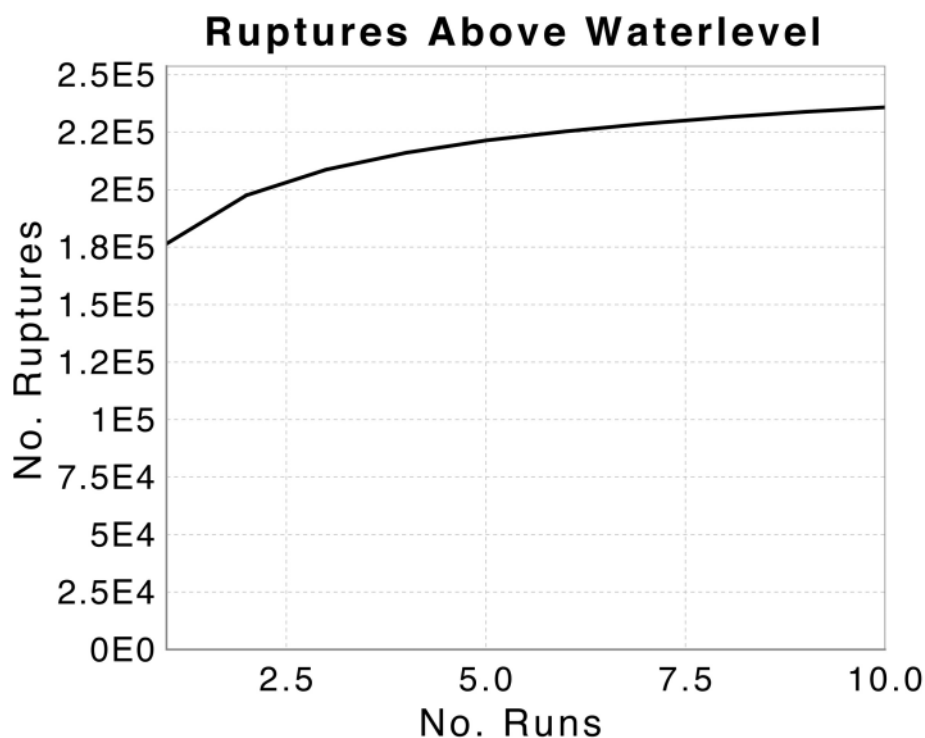
Ruptures Above Waterlevel

Figure 35.   Number of above-water-level ruptures for branch-averaged solutions as a function of the number of simulated annealing runs on each branch (for Fault Model 3.1). The maximum value on the y-axis is the total number of ruptures (~250,000=2.5×10^5 =2.5E5).

Fault-section-participation MFDs are also much better resolved for branch average results. Sample means and standard deviations were computed from the 10 different sets, and fractional uncertainties for $M{\geq}6.7$ event rates were computed for all fault sections. The worst case found is the Fitzhugh Creek section, which has a fractional uncertainty of 1.07 (meaning the upper 95-percent confidence bound is 7 percent above the mean and not visually discernable as plotted in *figure 34*. The median case implies that half the fault sections have upper 95-percent confidence bounds that are less than 0.5 percent above the mean. This implies that branch-averaged participation MFDs are well resolved on all fault sections in UCERF3.

Hazard metrics are extremely well resolved for branch averages. We generated a 2in50 PGA map for each of the 10 branch-averaged models, computed a sample mean and standard deviation from these 10, and then computed the fractional mean uncertainty at each map location. We then repeated this process for 1in100 PGA, 2in50 3-sec SA, and 1in100 3-secHz SA. Among all the map sites, probability levels and ground motion parameters, the largest fractional uncertainty found was 1.004 (for a site near the northwest corner of California). This implies that for branch-averaged probabilistic ground motion maps, including all those released by the USGS NSHMP, inversion nonuniqueness is negligible, and even one simulated annealing run on each branch would be adequate (because the 1,440 logic tree branches provide sufficient averaging on their own).

These conclusions apply not only to mean hazard, but to logic tree-implied percentiles as well. For each site listed in _table 14_, we computed 2-, 16-, 84-, and 98-percent fractiles among the 10 sets of runs, for both PGA and 3-sec SA, and for 2in50 and 1in100 probability levels. The worst case found was a fractional uncertainty of 1.006, meaning an upper 95-percent confidence bound that is just 0.6 percent above the mean percentile.

Equation-Set Weights

A thorough discussion of how the inversion equation-set weights were applied is given in appendix N (this report), which includes sensitivity tests conducted on the reference branch, where each equation-set weight was scaled up and down by a factor of 10. It is important to note that this range of weights is considered extreme in that fits to the other data are generally degraded to the point of model rejection. Example hazard curves from these tests are shown in _figure 36_ (and more results are available at _http://pubs.usgs.gov/of/2013/1165/data/ UCERF3_SupplementalFiles/UCERF3.3/Hazard/InversionTests/EquationSetWeights/_), where it can be seen that the range of values from alternative equation-set weights is small compared to that implied by alternative logic tree branches. We therefore conclude that accommodating a range of equation-set weights for each branch, which would need to be narrower than that tested, would not significantly change UCERF3 results.
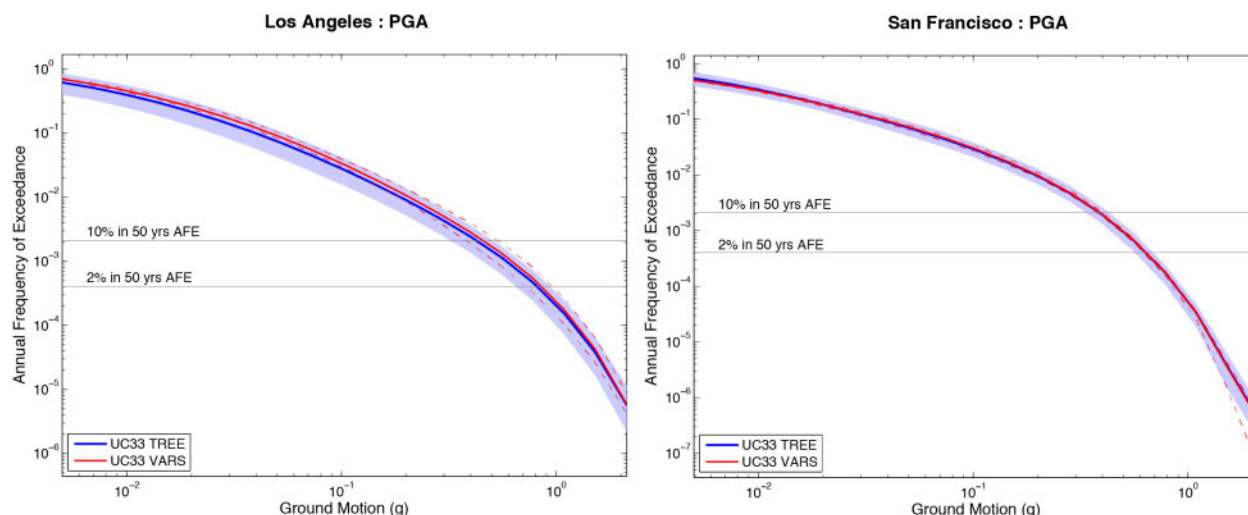

Figure 36.   Peak ground acceleration (PGA) hazard curves for the Los Angeles and San Francisco sites listed in _table 14_, obtained by varying equation-set weights on the UCERF3 reference branch, as summarized in the main text and detailed in appendix N (this report). The minimum and maximum curves among these tests are plotted with the red dashed lines, which can be compared with the range implied by alternative logic tree branches (blue shaded region). The difference between the mean curves (red and blue solid lines) is not meaningful in this comparison. Results for other sites are available _here_.

Discussion

We begin this section with a summary of UCERF3 advantages (relative to UCERF2) and then discuss model limitations, both of which are important from a user's perspective. _Table 15_

lists some of the key assumptions underlying UCERF3, and we finish this section with possible future improvements.

Improvements Over UCERF2

The UCERF3 long-term model appears largely successful in terms of the original project goals—relaxing segmentation assumptions; incorporating multifault ruptures; fitting a broader range of data better; and sampling a wider range of epistemic uncertainties. This has been accomplished by implementing a system-level, "grand inversion" framework, which has the following advantages over previous approaches:

- The rate of all earthquakes is solved for simultaneously
- A wider range of viable solutions is provided (all those consistent with data)
- The inversion is conceptually simple (summarized in *table 5*)
- Results are relatively reproducible (in terms of the influence of expert opinion)
- The framework is extensible (other constraints can easily be added)

UCERF2 and previous models were largely prescriptive in terms of making assumptions about magnitude-frequency distributions and in treating different seismic sources separately (for example, via segmentation assumptions). Although elegantly simple, this approach produces an overprediction of regional *M*6.5-7 event rates and ignores the potential influence of multifault ruptures. The UCERF3 approach, in contrast, is more derivative in that fault MFDs are not assumed, but rather derived from a system-level inversion.

Results from the derivative approach are more difficult to understand, especially given a large increase in the number of possible fault-based ruptures (form ~8,000 to 250,000). Whereas previous efforts had only to verify that assumed MFDs and rupture extents were correctly implemented, the grand inversion required the development of new tools for exploring the nature of solutions and their implications. UCERF3 also posed considerable computational challenges with respect to solving the large inverse problem thousands of times, and extensive hazard calculations were required to understand the potential influence of solution nonuniqueness. All of these challenges were new to UCERF3, and not fully appreciated at the beginning of the project.

Although the grand-inversion approach is not free of subjectivity, it does provide a more comprehensive framework for checking overall consistency between, and therefore balancing the influence of, different experts. Opinions of the latter were solicited through an unprecedented set of technical, consensus-building workshops (*table 2*), with a particularly good example being the series of fault-by-fault review meetings. These not only provided an important reality check for individual faults (not needed in the prescriptive approach taken previously), but also allowed comparisons with new, unpublished data and provided a record of faults needing further scrutiny in future efforts (see the "ReviewComments" sheet of the *U3_FaultSectionData* file given in the "Data and Resources" section).

UCERF3 also constitutes an improvement in terms of epistemic uncertainty representation. For example, UCERF2 had only a single logic tree branch in areas dominated by gridded seismicity (for example, Sacramento). UCERF3 now has 18 such branches given the new alternatives for off-fault maximum magnitude, the spatial distribution of seismicity, and the total regional rate of events. Epistemic uncertainties have also been added for fault-based ruptures, including a wider range of slip rates (deformation models), new scaling relationships that represent the possibility that larger ruptures extend below the depth of microseismicity, and alternatives for how average slip varies along strike.

The geologic databases have been substantially revised and expanded, including statewide fault models (appendix A, this report), geologic slip data (appendix B), and paleoseismic recurrence rates (appendix G). Fault polygons have been introduced to associate fault surfaces with deformation volumes (appendix O). New datasets have been compiled, including GPS velocities (appendix C) and displacement-per-event data (appendix R). Geologic and geodetic data have been jointly inverted for a suite of statewide deformation models (appendix C).

The data on fault creep rates have been greatly enlarged using InSAR measurements, and a new approach has been introduced for extrapolating surface creep rates to average creep rates across the fault surface (appendix D, this report). The probability of detecting ground ruptures at paleoseismic sites has been estimated (appendix I), and the interpretation of paleoseismic interevent times has been updated (appendix H). A revised earthquake catalog (appendix K) has been used to constrain magnitude-frequency distributions (appendix L), to develop a new model of smoothed seismicity (appendix M), and to reconsider the issue of empirically adjusted seismicity rates (appendix Q). Scaling relationships for magnitude and depth of rupture have been reexamined (appendix E), and a dataset relating rupture length to displacement has been developed (appendix F).

The new deformation models are particularly noteworthy. In addition to a relatively pure geologic model (appendix B, this report), we have three that are based on kinematically consistent inversions of geodetic and geologic data (appendix C). This is in contrast to the previous approach, which relied on expert opinion to broker discrepancies between geologic and geodetic observations. The geodetic signal is persistently "flat" across the southern SAF system, causing models that use these data to seek slip in places other than the SAF. The signal expected from geology and paleoseismology, on the other hand, would have a sharper change in observed velocity across the southern SAF (as it is in northern California, although the signal is muted compared to geology there too). This is a data-driven result, but we do not know how well the short-term GPS data reflect the long-term slip rates; the geologic and paleoseismic constraints suggest that they may not be representative of 10^3 to 10^5 year time scales. Finally, the kinematically consistent deformation models have also provided estimates of off-fault deformation, allowing us to retire the less refined type C zones used in previous models.

Observations have been compiled to constrain fault-to-fault rupture probabilities (appendix J, this report), which not only guided the development of our rupture plausibility filter (appendix T) but will also constitute an important resource for further testing of, and improving upon, UCERF3. With respect to the grand inversion, appendix N documents the simulated annealing algorithm, including parallelization; sensitivity tests, including some based on synthetic datasets; the tuning and testing of final constraint weights; and how well each type of data is fit by final models. Appendix N also provides additional implementation details, such as the treatment of creep and how multifault rupture statistics compare with various types of observations.

The system-level aspect of the grand inversion makes it well suited for hypothesis testing. Perhaps the best and most important example of this is with respect to the Gutenberg-Richter (GR) branches, where the hypothesis that each fault nucleates such a distribution of events cannot match all data—not even close. The inversion implies that doing so would require one or more of the following to fall outside the current bounds of consensus-level acceptability: (1) a higher degree of creep both on and off faults; (2) higher long-term rate of earthquakes over the

whole region (and significant temporal variability on faults such as the SAF); (3) more fault connectivity throughout the state (for example, ~*M*8 anywhere); and (or) (4) lower shear rigidity.

The obvious alternative is that the GR hypothesis does not apply at the local scale of individual faults, which would make reports of the death of the Characteristic Model (Kagan and others, 2012) greatly exaggerated. Either way, the GR hypothesis is clearly inconsistent with the current UCERF3 modeling framework, which is why it was given zero weight on the logic tree. If the GR hypothesis turns out to be correct, then the explanation for current discrepancies will be equally profound scientifically, and quite consequential with respect to hazard. The main point here is that the grand inversion provides an ideal framework for testing this and other such hypotheses, which will not only further our scientific understanding, but will also allow us to identify and focus resources on the questions that matter. Eliminating model options will also reduce epistemic uncertainties, and thereby improve hazard and loss assessments.

Finally, the entire UCERF3 development has been followed closely by a participatory scientific review panel, from reviewing original project plans, attending the various meetings and workshops (*table 2*), reviewing all appendixes (*table 1*), and scrutinizing four different versions of UCERF3. We also hosted two workshops where results were presented to the broader scientific and engineering communities (*table 2*). Furthermore, UCERF3 was evaluated by an NSHMP steering committee, which recommended that it be used in the 2014 national maps.

Model Limitations

In spite of improvements, UCERF3 is still an approximation of the system. For example, we continue to divide between "on-fault" and "off-fault" ruptures, whereas nature will surely violate these model boundaries. Our plausibility filter for multifault ruptures also has arbitrary cutoffs, such as the 5-km jumping threshold between faults, and we currently lack any improbability constraint. These limitations, coupled with the fact that the relative geometry of neighboring faults is poorly known at depth, imply we have most certainly included some unlikely ruptures, and excluded some that are plausible. In addition, the multifault rupture rates coming out of the grand inversion depend both on how average slip is distributed along such ruptures (D_{sr}), and how slip rates transition between faults, neither of which is well known.

Some reviewers expressed dissatisfaction with the nonuniqueness of UCERF3 solutions, exemplified by the fact that single inversions leave only about 4 percent of ruptures above water-level rates. In an attempt to remedy this, we tried applying an additional constraint to, in essence, make the rate of similar ruptures equal. However, doing so effectively made the inversion nonlinear and therefore prohibitively slow in comparison to simply averaging more inversion runs. Each simulated annealing solution can be thought of as one sample among an infinite population of viable models, or even as a realization of events for some time period. We do not see this as a problem, but rather an improvement in terms of acknowledging nonuniqueness and sampling a wider range of models; the problem is inherently underdetermined unless you impose segmentation. Fortunately, solution nonuniqueness has a negligible impact on hazard estimates, because results depend more on the participation MFD of faults, and much less so on rupture-endpoint details.

Concerns were voiced regularly that our large number of fault-based ruptures was going to be a problem in terms of PSHA computation time. Not only have those concerns turned out to be unfounded (OpenSHA calculation time is about the same as it was for UCERF2, in part because of the increased speed of computers), but our analysis also demonstrates that use of a single inversion solution might be a legitimate way of down-sampling the entire event set. Doing

so properly, however, will vary between different types of hazard and loss studies, so we do not attempt any generic down-sampling advice here.

Another concern raised during review is whether relaxing segmentation has reduced epistemic uncertainty. For example, the Cucamonga Fault section has gone from a relatively high rate of moderate sized events (~M6.7) to a lower and relatively uniform rate of events out to M8 (*fig. 25*). Technically speaking, this has not reduced epistemic uncertainty, but rather changed the behavior from one extreme to perhaps another. And while all such cases that have had a perceptible influence on hazard were deemed an improvement at our fault-by-fault review meetings, we acknowledge that there may be some areas where UCERF3 lacks an adequate characteristic alternative. For example, and in spite of the theoretical modeling of Anderson and others (2003), it is possible that Cucamonga never ruptures with neighboring faults.

To address this possibility, we were asked to explore an inversion that imposes UCERF2 segmentation throughout the system. While we know this would not be correct everywhere, it might be more correct on certain faults. BSSC deadlines prevented us from doing this for UCERF3. Furthermore, one does not need the grand inversion to implement a characteristic model (that would be overkill), and there is no guarantee that UCERF2 is correct with respect to segmentation details anyway. Potential cases like Cucamonga should therefore be handled on a case-by-case basis (for example, through site-specific analysis). That being said, *figure 21* implies that we are not grossly overpredicting the rate of multifault ruptures (see also the multifault evaluation metrics in appendix N (this report), so we believe UCERF3 is doing better overall, and that UCERF2 is a relatively poor approximation in more areas of California.

There is also the possibility that UCERF3 lacks connectivity in areas where it exists, which is another form of epistemic uncertainty left out of the model. Given all these limitations and assumptions, one might deem the grand inversion overly sophisticated or premature. However, we currently lack any alternative for relaxing segmentation and including multifault ruptures. Physics-based earthquake simulators (Ward, 2000; Rundle and others, 2006; Dieterich and Richards-Dinger, 2010; Tullis and others, 2012) are a promising solution. However, they currently suffer even more from some uncertainties, such as the unknown proximity of faults at depth. Simulator tuning procedures are also needed to match data (for example, paleoseismic event rates; fault-jumping statistics), and the propagation of epistemic uncertainties poses considerable computational challenges.

We also emphasize that UCERF3 is heavily weighted toward UCERF2, most notably in terms of the characteristic Fault Section MFD Constraint, but also in terms of the various limits on multifault ruptures. For example, both slip along rupture (D_{sr}) models put high amounts of slip at the mid-point along strike, as compared to the characteristic-slip model (Working Group on California Earthquake Probabilities, 1995), so rupture rates are consequently more limited by the slip rate constraint. These impositions explain why UCERF3 underestimates the observed frequency of multifault ruptures. Analysis in appendix N (this report) also implies that we are overfitting much of our data (as did UCERF2 and previous models). All of these factors further limit the range of UCERF3 models.

A final UCERF3 limitation is with respect to fitting some of the paleoseismic data and slip rates on the southern SAF (*fig. 20*). As noted, these constraints can be fit perfectly well if the regional MFD constraint is relaxed. Doing so, however, brings back the overprediction of moderate event rates. This tradeoff exemplifies the potential long reach of inversion constraints, where the rate in one location can be influenced by conditions far away. While some reviewers regarded this as physically problematic, others saw it as an appropriate way to achieve system-

level balance. With respect to the SAF, some branches do fit the data better, but on average our rates are about 25 percent low compared to paleoseismic rates. Therefore, while the hazard implied by the SAF has changed little since UCERF2, it is currently underestimated if the latest paleoseismic interpretations are correct.

Table 16.   Key assumptions made in UCERF3, most of which have at least implicit or partial representation on our logic tree.

Key Assumptions
1. Simplified faults models derived from synthesized data (for example, geologic mapping, microseismicity, well logs) provide an adequate approximation of fault structure and connectivity at depth.
2. Approximate 20-year GPS observations reflect long-term deformation rates.
3. Model-based transient corrections made to GPS data for past earthquakes and seasonal hydrologic processes are correct, and apparent outliers removed represent measurement error and not real signals.
4. "Backslip" methods used in deformation models (Zeng, ABM) are adequate.
5. Faults that lack slip rate constraints can reliably be assigned a categorical value based on recency of activity.
6. Depth extent of large ruptures is appropriately modeled by our scaling relationships.
7. Surface slip observations can be used to estimate slip at depth.
8. Surface creep mostly manifests as a seismogenic area reduction (rather than slip rate reduction)
9. Tapered and (or) boxcar models of D_{sr} represents average slip along rupture, even for multifault events.
10. A generic model for the probability of seeing events in a paleoseismic trench applies to all sites (as opposed to site-specific models).
11. Large regions honor the Gutenberg-Richter magnitude-frequency distribution.
12. Magnitude completeness thresholds as function of time, space, and magnitude have been correctly estimated.
13. Seismicity rates vary with time over the course of historical and instrumental observations.
14. Higher-resolution smoothed seismicity maps are applicable to large, damaging earthquakes and for approximately 50-year time periods.
15. Our plausibility filter provides an adequate set of ruptures in terms of quantifying hazard and risk at all locations.

Future Improvements

The extensibility of the grand-inversion platform will lend itself to several potential improvements. For example, quantification of multifault rupture statistics via observations, dynamic rupture modeling, and physics-based simulations could allow us to improve upon the UCERF3 plausibility filter, both in terms of representing epistemic uncertainties and the addition of improbability constraints. Some other possible improvements include the following (in no particular order):

- Apply deformation-model based options for off-fault spatial seis PDF.
- Explore inversions with UCERF2 segmentation imposed.
- Explore a wider range of models by relaxing the UCERF2 fault section MFD constraint.
- Explore a wider range of models by not over-fitting data as much.
- Explore use of inversion data fits for a posteriori adjustment of logic tree branch weights.
- Try to implement an inversion constraint that will achieve more equality among rupture rates (fewer water level ruptures).

- Further explore possibility that points on faults nucleate a Gutenberg-Richter distribution of events.
- Apply more customized/targeted inversion-constraint weights in order to fit certain data better (for example, on the southern SAF).
- Investigate the discrepancy between off-fault moment rates predicted by the deformation models and those implied by the grand-inversion models.
- Address issues identified for particular faults at the fault-by-fault review meetings (see the "ReviewComments" sheet of the *U3_FaultSectionData* file given in the "Data and Resources" section).
- Study creep manifestation and implications further, especially given the discrepancy between off-fault seismic moment rates between UCERF3 and those predicted by the deformation models (*fig. 24*).
- Coordinate/integrate fault zone polygon definitions with future deformation model developments.
- Investigate how the characteristic slip model (for example, Hecker and others, 2013) could be incorporated into the inversion framework given we lack observed estimates on most faults.
- Explore model-based inferences that average slip, for a given length rupture, goes down with increasing number of fault-to-fault jumps (appendix F, this report)
- Develop and use site-specific models for the probability of seeing events in a paleoseismic trench.
- Explore the applicability of recent seismicity to 50-year forecasts.
- Explore the applicability of different smoothed seismicity algorithms in forecasting large, damaging events and for different forecast durations.

Conclusions and Recommendations

We believe UCERF3 represents a considerable improvement over UCERF2. In addition to the methodological enhancements represented by the grand inversion, we have expanded the range of epistemic uncertainty representation. Hazard calculations allow us to conclude that the most influential uncertainties are deformation models (slip rates), the smoothed seismicity algorithm, the total regional rate of events, and scaling relationships. All of these new branches have produced significant and important changes in mean hazard estimates. New faults have also been added to the model, which produce some of the biggest hazard differences relative to UCERF2. The apparent overprediction of *M*6.5-7 event rates in UCERF2 has been removed, and UCERF3 includes multifault ruptures like those seen in nature.

The added epistemic uncertainties are generally more influential than the inclusion of multifault ruptures, with at least two notable exceptions identified. However, these conclusions are with respect to traditional NSHMP hazard metrics, and may not apply to, for example, statewide loss estimates (where large, rare events may be more influential). It will therefore be important that practitioners carefully assess the applicability of this model in the context of their particular applications, as results may be sensitive to aspects of the model that differ from the influential factors inferred here. This is particularly true for site-specific studies, where the nearby influential fault(s) may not have adequate epistemic uncertainty representation in UCERF3.

While the addition of epistemic uncertainties in UCERF3 is mentioned as an accomplishment, this also means we have not yet reached the point where further study is reducing the range of viable models. In fact, we have argued that UCERF3 may still be too limited, implying that a broader range of models could be forthcoming. That this conclusion is being made for one of the most data-rich areas on Earth implies that epistemic uncertainties are likely underestimated elsewhere.

Although the inversion is conceptually simple and extensible, the overall framework and implementation is far more involved than for previous models. UCERF3 relies on an extensive object-oriented programming framework, versus an Excel spreadsheet for Working Group on California Earthquake Probabilities (1995). However, this will be true of any system-level model, and the only consolation we can provide is the fact that everything is open-source and freely available.

The grand inversion has proven to be a powerful tool for quantifying the influence and consistency of various constraints, for exploring a range of models, and for testing hypotheses. There is considerable interactive complexity in the system, however, and further study will be needed to fully understand tradeoffs between the various inversion constraints. Such analyses may support applying a posteriori weights to UCERF3 branches in the future.

Acknowledgments

References

Algermissen, S.T., Perkins, D.M., Thenhaus, P.C., Hanson, S.L., and Bender, B.L., 1982, Probabilistic estimates of maximum acceleration and velocity in rock in the contiguous United States: U.S. Geological Survey Open-File Report 82–1033. 99 p.

Anderson, G., Aagaard, B., and Hudnut, K., 2003, Fault interactions and large complex earthquakes in the Los Angeles area: Science, v. 203, p. 1946–1949, doi:10.1126/science.1090747.

Andrews, D.J., and Schwerer, E., 2000, Probability of rupture of multiple fault segments: Bulletin of the Seismological Society of America, v. 90, p. 1498–1506.

Biasi, G.P., and Weldon, R.J., 2009, San Andreas fault rupture scenarios from multiple paleoseismic records—stringing pearls: Bulletin of the Seismological Society of America, v. 99, p. 471–498, doi:10.1785/0120080287.

Bird, P., 2009, Long-term fault slip rates, distributed deformation rates, and forecast of seismicity in the western United States from joint fitting of community geologic, geodetic, and stress direction data sets: Journal of Geophysical Research, v. 114, B11403, doi:10.1029/2009JB006317.

Box, G.E.P., 1979, Robustness in the strategy of scientific model building, *in* Launer, R.L., and Wilkinson, G.N., eds., Robustness in statistics: Proceedings of a Workshop (1979).

Brune, J.N., Anooshehpoor, A., Purvance, M.D., and Brune, R.J., 2006, Band of precariously balanced rocks between the Elsinore and San Jacinto, California, fault zones—constraints on ground motion for large earthquakes: Geology, v. 34, p. 137–140.

Building Seismic Safety Council, 2009—NEHRP recommended seismic provisions for new building and other structures, 2009 edition: Federal Emergency Management Agency, publication number P-750, *http://www.fema.gov/media-library/assets/documents/18152/*.

Cornell, C.A., 1968, Engineering seismic risk analysis: Bulletin of the Seismological Society of America, v. 58, p. 1583–1606.

Cua, G., Fischer, M., Heaton, T., and Wiemer, S., 2009, Real–time performance of the Virtual Seismologist earthquake early warning algorithm in Southern California: Seismological Research Letters, v. 80, p. 740–747, doi:10.1785/gssrl.80.5.740.

Dieterich, J.H., and Richards-Dinger, K.B., 2010, Earthquake recurrence in simulated fault systems: Pure and Applied Geophysics, v. 167, p. 1087–1184.

Felzer, K.R., 2008, Calculating California seismicity rates, appendix I *of* the Uniform California Earthquake Rupture Forecast, Version 2 (UCERF2): U.S. Geological Survey Open-File Report 2007–1437–I.

Felzer, K.R., Abercrombie, R.E., and Ekström, G., 2004, A common origin for aftershocks, foreshocks, and multiplets: Bulletin of the Seismological Society of America, v. 94, p. 88–99.

Field, E.H., 2007, Overview of the Working Group for the Development of Regional Earthquake Likelihood Models (RELM): Seismological Research Letters, v. 78, p. 7–16.

Field, E.H., 2012, Aftershock statistics constitute the strongest evidence for elastic relaxation in large earthquakes—take 2 [abs.]: 2012 annual meeting of the Seismological Society of America, April 17–19, San Diego, Calif., *http://www.seismosoc.org/meetings/2012/.*

Field, E.H., Dawson, T.E., Felzer, K.R., Frankel, A.D., Gupta, V., Jordan, T.H., Parsons, T., Petersen, M.D., Stein, R.S., Weldon, R.J., II, and Wills, C.J., 2009, Uniform California Earthquake Rupture Forecast, Version 2 (UCERF 2): Bulletin of the Seismological Society of America, v. 99, p. 2053–2107, doi:10.1785/0120080049.

Field, E.H., Jordan, T.H., and Cornell, C.A., 2003, OpenSHA; a developing community-modeling environment for seismic hazard analysis: Seismological Research Letter, v. 74, p. 406–419.

Field, E.H., and Page, M.T., 2011, Estimating earthquake-rupture rates on a fault or fault system: Bulletin of the Seismological Society of America, v. 101, p. 79–92, doi:10.1785/0120100004.

Frankel, A., 1995, Mapping seismic hazard in the Central and Eastern United States: Seismological Research Letters, v. 66, p. 8–21.

Frankel, A., Mueller, C., Barnhard, T., Perkins, D., Leyendecker, E., Dickman, N., Hanson, S., and Hopper, M., 1996, National seismic-hazard maps; documentation June 1996: U.S. Geological Survey Open-File Report 96–532, 69 p.

Frankel, A.D., Petersen, M.D., Mueller, C.S., Haller, K.M., Wheeler, R.L., Leyendecker, E.V., Wesson, R.L., Harmsen, S.C., Cramer, C.H., Perkins, D.M., and Rukstales, K.S., 2002, Documentation for the 2002 update of the national seismic hazard map: U.S. Geological Survey Open-File Report 2002–420, 34 p.

Gardner, J K., and Knopoff, L., 1974, Is the sequence of earthquakes in southern California with aftershocks removed Poissonian?: Bulletin of the Seismological Society of America, v. 64, p. 1363–1367.

Granville, V., Krivanek, M., and Rasson, J.-P., 1994, Simulated annealing; a proof of convergence: IEEE Transactions on Pattern Analysis and Machine Intelligence, v. 16, p. 652–656, doi:10.1109/34.295910.

Hammond, W.C., Blewitt, G., and Kreemer, C., 2011, Block modeling of crustal deformation of the northern Walker Lane and Basin and Range from GPS velocities: Journal of Geophysical Research, v. 166, B04402.

Hanks, T.C., and Bakun, W.H., 2008, M-log A observations of recent large earthquakes: Bulletin of the Seismological Society of America, v. 98, p. 490.

Harris, R.A., and Day, S.M., 1993, Dynamics of fault interaction–parallel strike-slip faults: Journal of Geophysical Reearch, v. 98, p. 4461–4472.

Hauksson, E., Stock, J., Hutton, K., Wenzheng, Y., J. Antonio Vidal-Villegas, J., and Kanamori, H., 2011, The 2010 Mw 7.2 El Mayor-Cucapah earthquake sequence, Baja California, Mexico and southernmost California, USA; active seismotectonics along the Mexican Pacific margin: Pageoph, v. 168, p. 1255–1277, doi:10.1007/s00024-010-0209-7.

Hecker, S., Abrahamson, N.A., and Wooddell, K.E., 2013, Variability of displacement at a point; implications for earthquake-size distribution and rupture hazard on faults: Bulletin of the Seismological Society of America, v. 103, p. 651–674, doi:10.1785/0120120159.

Helmstetter, A., Kagan, Y.Y., and Jackson, D.D., 2007, High-resolution time-independent grid-based forecast for M≥5 earthquakes in California: Seismological Research Letters, v. 78, p. 78–86.

Holmes, R.R., Jr., Jones, L.M., Eidenshink, J.C., Godt, J.W., Kirby, S.H., Love, J.J., Neal, C.A., Plant, N.G., Plunkett, M.L., Weaver, C.S., Wein, A., and Perry, S.C., 2013, U.S. Geological Survey natural hazards science strategy—promoting the safety, security, and economic well-being of the Nation: U.S. Geological Survey Circular 1383–F, 79 p. http://pubs.usgs.gov/circ/1383f/.

Jenny, S., Goes, S., Giardini, D., and Kahle, H.-G., 2004, Earthquake recurrence parameters from seismic and geodetic strain rates in the eastern Mediterranean: Geophysical Journal International, v. 157, p. 1331–1347, doi:10.1111/j.1365-246X.2004.02261.x.

Johnson, K.M., and Fukuda, J., 2010, New methods for estimating the spatial distribution of locked asperities and stress-driven interseismic creep on faults with application to the San Francisco Bay Area, California: Journal of Geophysical Research, v. 115, B12408, doi:10.1029/2010JB007703.

Jordan, T.H., Chen, Y.-T., Gasparini, P., Madariaga, R., Main, I., Marzocchi, W., Papadopoulos, G., Sobolev, G., Yamaoka, K., and Zschau, J., 2011, Operational earthquake forecasting; state of knowledge and guidelines for implementation—Final Report of the International Commission on Earthquake Forecasting for Civil Protection: Annals of Geophyics., v. 54, no. 4, p. 315–391, doi:10.4401/ag-5350.

Kagan, Y.Y., 2002a, Seismic moment distribution revisited; I. Statistical results: Geophysical Journal International, v. 148, p. 520–541.

Kagan, Y.Y., 2002b, Seismic moment distribution revisited; II. Moment conservation principle, Geophysical Journal International, v. 149, p. 731–754.

Kagan, Y.Y., and Jackson, D.D., 2013, Tohoku earthquake—a surprise?: Bulletin of the Seismological Society of America, v. 103, p. 1181–1194.

Kagan, Y.Y., Jackson, D.D., and Geller, R.J., 2012, Characteristic earthquake model, 1884–2011, RIP: Seismological Research Letters, v. 83, p. 951–953, doi:10.1785/0220120107.

Kaiser, A., Holden, C., Beavan, J., Beetham, D., Benites, R., Celentano, A., Collett, D., Cousins, J., Cubrinovski, M., Dellow, G., Denys, P., Fielding, E., Fry, B., Gerstenberger, M., Landgridge, R., Massey, C., Motagh, M., Pondard, N., McVerry, G., Ristau, J., Stirling, M., Thomas, J., Uma, S.R., and Zhao, J., 2012, The Mw 6.2 Christchurch earthquake of February, 2011—preliminary report: New Zealand Journal of Geology and Geophysics, v. 55, p. 67–90, doi:10.1080/00288306.2011.641182.

Lawson, C.L., and Hanson, D.J., 1974, Solving least squares problems: Englewood Cliffs, New Jersey, Prentice-Hall, 337 p.

Luco, N., Ellingwood, B.R., Hamburger, R.O., Hooper, J.D., Kimball, J.K., and Kircher, C., 2007, Risk-targeted versus current seismic design maps for the conterminous United States: Structural Engineers Association of California, Proceedings of SEAOC 2007 Convention, Sacramento, California.

Machette, M., Haller, K., and Wald. L., 2004, Quaternary fault and fold database for the nation: U.S. Geological Survey Fact Sheet 2004-3033, 2 p., http://pubs.usgs.gov/fs/2004/3033/.

Masson, F., Chéry, J., Hatzfeld, D., Martinod, J., Vernant, P., Tavakoli, F., and Ghafory-Ashtiani, M., 2005, Seismic versus aseismic deformation in Iran inferred from earthquakes and geodetic data: Geophysical Journal International, v. 160, p. 217–226, doi:10.1111/j.1365-246X.2004.02465.x.

McCaffrey, R., 2002, Crustal block rotations and plate coupling, in Stein, S., and Freymueller, J., eds, Plate boundary zones: American Geophysical Union, Geodynamics Series, v. 30, p. 101–122.

McCaffrey, R., 2005, Block kinematics of the Pacific-North America plate boundary in the southwestern United States from inversion of GPS, seismological, and geologic data: Journal of Geophysical Research, v. 110, B07401, doi:10.1029/2004JB003307.

Meng, L., Ampuero, J.-P., Stock, J., Duputel, Z., Luo, Y., and Tsai, V.C., 2012, Earthquake in a maze—Compressional rupture branching during the 2012 Mw 8.6 Sumatra earthquake: Science, v. 337, p. 724–726, doi:10.1126/science.1224030.

National Research Council, 2011, National earthquake resilience—Research, implementation, and outreach: Washington, D.C., National Academies Press, 264 p.

Noda, H., and Lapusta, N., 2013, Stable creeping fault segments can become destructive as a result of dynamic weakening: Nature, v. 493, p. 518–521, doi:10.1038/nature11703.

Ogata, Y., 1988, Statistical models of point occurrences and residual analysis for point processes: Journal of the American Statistical Association, v. 83, p. 9–27.

Page, M.T., Alderson, D., and Doyle, J., 2011, The magnitude distribution of earthquakes near southern California faults: Journal of Geophysical Research, v. 116, B12309, doi:10.1029/2010JB007933.

Pancha, A., Anderson, J.G., and Kreemer, C., 2006, Comparison of seismic and geodetic scalar moment rates across the Basin and Range Province: Bulletin of the Seismological Society of America, v. 96, p. 11–32, doi:10.1785/0120040166.

Parsons, T., and Geist, E.L., 2009, Is there basis for preferring characteristic earthquakes over Gutenberg-Richter distributions on individual faults in probabilistic earthquake forecasting?: Bulletin of the Seismological Society of America, v. 99, p. 2012–2019, doi:10.1785/0120080069.

Petersen, M.D., Cao, T., Campbell, K.W., and A. D. Frankel, A.D., 2007, Time-independent and time-dependent seismic hazard assessment for the State of California—Uniform California Earthquake Rupture Forecast Model 1.0: Seismological Research Letters, v. 78, p. 99–109.

Petersen, M.D., Frankel, A.D., Harmsen, S.C., Mueller, C.S., Haller, K.M., Wheeler, R.L., Wesson, R.L., Zeng, Y., Boyd, O.S., Perkins, D.M., Luco, N., Field, E.H., Wills, C.J., and Rukstales, K.S., 2008a, Documentation for the 2008 update of the United States National Seismic Hazard Maps: U.S. Geological Survey Open-File Report 2008–1128.

Petersen, M.D., Mueller, C.S., Frankel, A., and Zeng, Y., 2008b, Spatial seismicity rates and maximum magnitudes for background earthquakes, appendix J of the Uniform California Earthquake Rupture Forecast, Version 2 (UCERF2): U.S. Geological Survey Open-File Report 2007–1437–J.

Plesch, A., Shaw, J., Benson, C., Bryant, W., Carena, S., Cooke, M., Dolan, J., Fuis, G., Gath, E., Grant, L., Hauksson, E., Jordan, T., Kamerling, M., Legg, M., Lindvall, S., Magistrale, H., Nicholson, C., Niemi, N., Oskin, M., Perry, S., Planansky, G., Rockwell, T., Shearer, P., Sorlien, C., Süss, M., Suppe, J., Treiman, J., and Yeats, R., 2007, Community fault model (CFM) for southern California: Bulletin of the Seismological Society of America, v. 97, p. 1793–1802, doi:10.1785/0120050211.

Porter. K.A., Field, E.H., and Milner. K., 2012, Trimming the UCERF2 hazard logic tree: Seismological Research Letters, v. 83, p. 815–828, doi:10.1785/0220120012.

Reasenberg, P.A., Hanks, T.C., and Bakun. W.H., 2003, An empirical model for earthquake probabilities in the San Francisco Bay region, California, 2002–2031: Bulletin of the Seismological Society of America, v. 93, p. 1–13.

Reid, H.F., 1911, The elastic-rebound theory of earthquakes: University of California Publications, Bulletin of the Department of Geological Sciences, v. 6, p. 413–444.

Rontogianni, S., 2010, Comparison of geodetic and seismic strain rates in Greece by using a uniform processing approach to campaign GPS measurements over the interval 1994–2000: Journal of Geodynamics, v. 50, no. 10, doi:10.1016/j.jog.2010.04.008.

Rundle, P.B., Rundle, J.B., Tiampo, K.F., Donnellan A., and Turcotte, D.L., 2006, Virtual California—fault model, frictional parameters, applications: Pure and Applied Geophysics, v. 163, no. 9, p. 1819–1846.

Savage, J.C., and Lisowski, M., 1993, Inferred depth of creep on the Hayward Fault, central California: Journal of Geophysical Research, v. 98, no. B1, p. 787–793.

Senior Seismic Hazard Analysis Committee, 1997, Recommendations for probabilistic seismic hazard analysis; guidance on uncertainty and use of experts: U.S. Nuclear Regulatory Commission, U.S. Dept. of Energy, Electric Power Research Institute; Report NUREG/CR-6372, UCRL-ID-122160, 2 v. [Includes a 73-p. review of the document by the National Academy of Science, Washington, D.C.]

Shaw, B.E., 2009, Constant stress drop from small to great earthquakes in magnitude-area scaling: Bulletin of the Seismological Society of America, v. 99, p. 871, doi:10.1785/0120080006.

Shaw, B.E., 2013, Earthquake surface slip-length data is fit by constant stress drop and is useful for seismic hazard analysis: Bulletin of the Seismological Society of America, v. 103, p. 876, doi:10.1785/0120110258.

Schorlemmer, D., Gerstenberger, M.C., Wiemer, S., Jackson, D.D., and Rhoades, D.A., 2007, Earthquake likelihood model testing: Seismological Research Letters, v. 78, p. 17–29.

Tullis, T.E., Richards-Dinger, K., Barall, M., Dieterich, J.H., Field, E.H., Heien, E.M., Kellogg, L.H., Pollitz, F.F., Rundle, J.B., Sachs, M.K., Turcotte, D.L., Ward, S.N. and Yikilmaz, M.B., 2012, A Comparison among Observations and Earthquake Simulator Results for the allcal2 California Fault Model, Seismological Research Letters, v. 83, no. 6, p. 994–1006.

U.S. Geological Survey, 2013, Quaternary Fault and Fold Database of the United States: U.S. Geological Survey Web site, accessed January 1, 2013, at *http://earthquake.usgs.gov/hazards/qfaults/*.

van Stiphout, T., Wiemer, S., and Marzocchi, W., 2010, Are short-term evacuations warranted? Case of the 2009 L'Aquila earthquake: Geophysical Research Letters, v. 37, doi:10.1029/2009gl042352.

Wald, D.J., Worden, B.C., Lin, K., and Pankow, K., 2005, ShakeMap manual—Technical manual, user's guide, and software guide: U.S. Geological Survey, Techniques and Methods 12-A1, 132 p.

Ward, S.N., 1998, On the consistency of earthquake moment release and space geodetic strain rates—Europe: Geophysical Journal International, v. 135, p. 1011–1018, doi:10.1046/j.1365-246X.1998.t01-2-00658.x.

Ward, S.N., 2000, San Francisco Bay area earthquake simulations—A step toward a standard physical earthquake model: Bulletin of the Seismological Society of America, v. 90, p. 370–386.

Weichert, D.H., 1980, Estimation of the earthquake recurrence parameters for unequal observation periods for different magnitudes: Bulletin of the Seismological Society of America, v. 70, p. 1337–1346.

Weldon, R.J., II, Biasi, G.P., Wills, C.J., and Dawson, T.E., 2008, Overview of the southern San Andreas fault model, appendix E *of* The Uniform California Earthquake Rupture Forecast, version 2 (UCERF 2): U.S. Geological Survey Open-File Report 2007–1437–E, and California Geological Survey Special Report 203-E.

Wells, D., 2013, Updated empirical relationships among magnitude, rupture area, rupture length, and surface displacement [abs.]: Seismological Research Letters, v. 84, p. 309.

Wells, D.L., and Coppersmith, K.J., 1994, New empirical relationships among magnitude, rupture length, rupture width, rupture area and surface displacement: Bulletin of the Seismological Society of America, v. 84, p. 974–1002.

Wesnousky, S.G., 2006, Predicting the endpoints of earthquake ruptures: Nature, v. 444, p. 358–360, doi:10.1038/nature05275.

Working Group on California Earthquake Probabilities, 1988, Probabilities of large earthquakes occurring in California on the San Andreas fault: U.S. Geological Survey Open-File Report 88–398, p. 62.

Working Group on California Earthquake Probabilities, 1990, Probabilities of large earthquakes in the San Francisco Bay Region, California: U.S. Geological Survey Circular 1053, 51 p.

Working Group on California Earthquake Probabilities, 1995, Seismic hazards in southern California; probable earthquakes, 1994–2024: Bulletin of the Seismological Society of America, v. 85, p. 379–439.

Working Group on California Earthquake Probabilities, 2003, Earthquake probabilities in the San Francisco Bay region; 2002–2031: U.S. Geological Survey Open-File Report 2003–214.

Working Group on California Earthquake Probabilities, 2008, The uniform California earthquake rupture forecast, version 2 (UCERF 2): U.S. Geological Survey Open-File Report 2007–1437.

Zechar, J.D., Schorlemmer, D., Liukis, M., Yu, J., Euchner, F., Maechling, P.J., and Jordan, T.H., 2010, The Collaboratory for the Study of Earthquake Predictability perspectives on computational earth science: Concurrency and Computation; Practice and Experience, v. 22, p. 1836–1847, doi:10.1002/cpe.1519.

Zechar, J.D., Schorlemmer, D., Werner, M.J., Gerstenberger, M.C., Rhoades, D.A., and T. H. Jordan, T.H., 2013, Regional earthquake likelihood models, I. First-order results: Bulletin of the Seismological Society of America, v. 103, p. 787–798.

Data and Resources

U3_FaultSectionData:

http://pubs.usgs.gov/of/2013/1165/data/ofr2013-1165_FaultSectionData.xlsx (800 KB)

U3_PreInversionAnalysisTable:

http://pubs.usgs.gov/of/2013/1165/data/ofr2013-1165_PreInversionAnalysisTable.xlsx (810 KB)

U3 Supplementary Figures:

http://pubs.usgs.gov/of/2013/1165/data/UCERF3_SupplementalFiles/